THE UNIVERSITY
of EDINBURGH

Mitochondrial and metabolic alterations are an early adaptation for pre-neoplastic cells during tumour initiation in a zebrafish model.

Lisa Kelly

PhD Inflammation
The University of Edinburgh
2019

Abstract

Altered metabolism is a well-defined characteristic of established cancers. Metabolic changes have been observed in various pathways, including glycolysis, oxidative phosphorylation, lipid metabolism and amino acid metabolism. Alterations can also be seen in cancer cell mitochondria, where many of these metabolic processes take place. Mitochondrial fission above normal levels has been shown to be important for the proliferation of transformed cells. While these phenotypes are described in established cancers, their role in tumour initiation and development is less well understood. The aim of this project is to begin to describe the metabolic phenotype of developing pre-neoplastic cells (PNCs) and investigate how metabolic adaptations may act synergistically with host inflammatory responses to regulate the developing tumour microenvironment at the very earliest stages of tumour initiation.

Recently, the zebrafish (*D. rerio*) has become an important and dynamic model for *in vivo* investigations. Our group has used the genetic tractability and *in vivo* imaging potential of zebrafish to develop a novel model in which tumour development can be monitored in real time. This model allows for precise spatial and temporal induction of epithelial cellular transformation in larval zebrafish, giving rise to mosaic PNCs which can be monitored *in vivo* as they develop over time. Early work for this project involved characterisation of this model under the control of the superficial skin epithelial layer specific keratin 4 promoter driven human $HRAS^{G12V}$ induced PNC initiation.

The project then began to define the metabolic phenotype for human $HRAS^{G12V}$ driven PNCs at the earliest stages of development. Data reveal that PNCs acquire a hyper-fragmented mitochondrial phenotype, which appears to be associated with altered mitochondrial function and enhanced proliferative capacity. Interestingly, while PNC bearing embryos display enhanced glycolytic flux, PNCs themselves do not show such alterations in glycolytic intermediates or end-products. This suggests that complex metabolic adaptations are taking place at early stages of PNC development and that broad spectrum, unbiased approaches are required to fully understand the complexity of metabolic adaptations in PNCs.

Here, I present data which point to an altered metabolic phenotype in PNCs during tumour initiation and development. These findings, as well as a number of new tools and techniques developed during the project, will help to enhance our understanding of cancer initiation and development and provides a basis for further studies of PNC metabolism and cross-talk with the developing PNC niche.

Lay Abstract

Cancer is a progressive disease that affects millions worldwide each year. While our understanding of cancer has vastly increased in recent times, our knowledge of the earliest stages of cancer development remains relatively limited. Metabolism is the complex process by which cells in the body break down various energy inputs, such as sugar, protein and fat in the food we eat, to generate the energy and building blocks they need to grow. Research has shown that these processes change in cancer cells, though our understanding of when and how these changes occur remains relatively limited. The aim of this project is to identify when and how changes to metabolic processes occur at the very earliest stages of cancer development.

In recent times, the zebrafish has become an important model for studies of various human diseases. These freshwater fish are easily genetically engineered and, as they are transparent, can be used for monitoring cells interacting in a realistic environment as they grow. Our group has developed a new zebrafish model which allows monitoring and manipulation of the development of cancer from very early stages.

The primary aim of this project was to identify changes to the complex metabolic processes that occur at early stages of cancer development. A number of the chemical reactions of metabolism take place in a specific part of the cell called the mitochondria, which is often referred to as the powerhouse of the cell. Data shows that early cancer cells have altered the shape and function of mitochondria, which in turn alters the ability of these early cancer cells to grow. Complex changes have also been detected in specific metabolic processes occurring very early in cancer development, suggesting that alterations to these chemical reactions could be an important event for cancer development.

Here, I present data which begins to define how metabolism is altered during the earliest stages of cancer development and provide a basis for further studies of cancer cell metabolism.

Acknowledgements

Firstly, I would like to thank my primary supervisor, Dr. Yi Feng, for giving me the opportunity to complete my PhD in her group and for her continued guidance and support throughout the project. I would also like to thank my second supervisor, Dr. Nicholas Morton for his valued input and advice, and the members of The Feng Group, both past and present, for being a sounding board for ideas and for technical support.

I would like to acknowledge the help of the staff of the CALM Imaging Facility, particularly Dr. Trudi Gillespie, for her help with microscopy, Shonna Johnston, Will Ramsay and Mari Pattison at the QMRI Flow Cytometry Facility for their help with FACS and analysis, Dr. Steven Mitchell at the COIL facility at the Wellcome Trust Centre for Cell Biology for assisting with electron microscopy, Dr. Marc Vendrell and Sam Benson for collaborating with glucose uptake experiments and Dr. Rod Carter for assisting and collaborating with Seahorse experiments. Thank you to the staff of the QMRI zebrafish facility, past and present, and the technical staff at the Centre for Inflammation Research for making all of my experiments possible. Also, many thanks to Prof. Paul Martin and his group members, particularly Lucy MacCarthy-Morrogh, at University of Bristol for hosting me for a research trip and help with electron microscopy.

To Dr. Derek Laux, who started me off, Dr. Nikolay Ogryzko, who helped me over the line, and Miss. Isabel Riberio Bravo, who was with me all alone; my sincere thanks and gratitude for all they have done for me, both as colleagues and friends. Thank you to Dyana Markose, Ross Mills, Jordan Portman, David Taggart and Francesco Vacca for necessary distractions and an ever-listening ear. Special thank you to Tess McCann, whose unwavering support and friendship helped me from start to finish. Finally, thank you to my parents, Mary and PJ, my sister, Joyce, and my extended family and friends for their continued confidence and encouragement.

Signed Declaration

I declare that this thesis has been composed solely by myself and that it has not been submitted, in whole or in part, in any previous application for a degree. Except where otherwise by reference or acknowledgment, the work presented is entirely my own.

Lisa Kelly

Table of Contents

List of Figures and Tables

Abbreviations:

2-DG: 2-Deoxyglucose
2-NBDG: 2-(N-(7-Nitrobenz-2-oxa-1,3-diazol-4-yl)Amino)-2-Deoxyglucose
3D: 3 dimensions
4-OHT: 4-Hydroxytamoxifen
aa: Amino acid(s)
Acetyl-CoA: Acetyl-coenzyme A
ADP: Adenosine diphosphate
AMPK: Adenosine monophosphate-activated protein kinase
ANOVA: Analysis of variance
APC: Adenomatous polyposis coli gene
AREG: Amphiregulin
ATP: Adenosine triphosphate
BAD: BCL-2 associated agonist of cell death
BAK1: BCL-2 antagonist/killer 1
CXCL1: C-X-C motif chemokine ligand 1
DHE: Dihydroethidium
DMSO: Dimethyl sulfoxide
(c)DNA: (complimentary) Deoxyribonucleic acid
Dnm1l: Dynamin-1 like protein
dpf: days post fertilisation
Drp1: Dynamin-related protein 1
ECAR: Extracellular acidification rate
ECM: Extracellular matrix
EdU: 5-ethynyl-2'-deoxyuridine
EMT: epithelial-to-mesenchymal transition
ERK: Extracellular signalling-related kinase (also called MAPK1)
ER^{T2}: modified ligand binding domain of the human estrogen receptor α
ETC: Electron transport chain
FACS: Fluorescence activated cell sorting
$FADH_2$: Flavin adenine dinucleotide (reduced)
FCCP: Carbonyl cyanide-4-(trifluoromethoxy)phenylhydrazone
FdG: ^{18}fluorodeoxyglucose
FET: ^{18}F-fluoro- ethyl-tyrosine
FLT: ^{18}F-flurothymidine
FRET: Forster resonance energy transfer
FSC-A: Forward Scatter-Area
GAPs: GTPase-activating proteins
GC-MS: Gas chromatography-mass spectrometry

GDP: Guanosine diphosphate
GEFs: Guanine nucleotide exchange factors
GFP: green fluorescent protein
GI tract: Gastrointestinal tract
GLUT2: Glucose transporter, type 2
GLUT5: Glucose transporter, type 5
GTP: Guanosine triphosphate
GTPase: Guanosine triphosphatase
HBEGF: Heparin binding epidermal growth factor-like growth factor
HBV: Hepatitis B virus
HER-2: Human epidermal growth factor receptor 2
hpi: hours post induction
hpf: hours post fertilization
hpt: hours post treatment
HPV: Human papillomavirus
hpw: hours post wounding
hr: hour
IFN-β: Interferon β
IL-(6)(8)(10): Interleukin (6)(8)(10)
IMS: Imaging mass spectroscopy
Krt4: *keratin 4* promoter
LC-MS: Liquid chromatography-mass spectrometry
LDH: Lactate dehydrogenase A
MAPK: Mitogen-activated protein kinase
MCT4: Monocarboxylate transporter 4
mDIVI-1: Mitochondrial Division Inhibitor-1
Mfn 1: Mitofusin 1
Mfn 2: Mitofusin 2
MMP: Matrix metalloproteinase
mtDNA: Mitochondrial deoxyribonucleic acid
NAD^+: Nicotinamide adenine dinucleotide (oxidised)
NADH: Nicotinamide adenine dinucleotide (reduced)
NF-κB: Nuclear factor kappa-light-chain-enhancer of activated B cells
NK Cell (s): Natural killer cell (s)
NMR: Nuclear magnetic resonance spectroscopy
NOS: Nitric oxide species
OCR: Oxygen consumption rate
OIS: Oncogene-induced senescence
Opa1: Optic atrophy 1
P_i: Inorganic phosphate

PBS: Phosphate buffered saline
PCNA: Proliferating cell nuclear antigen
PDH: Pyruvate dehydrogenase
PET: Positron emission tomography
PFA: Paraformaldehyde
PFK: Phosphofructokinase
PI3K: Phosphoinositide 3-kinase
PNC(s): Pre-neoplastic cell(s)
PS: Phosphatidylserine
qRT-PCR: Quantitative reverse transcription polymerase chain reaction
(H)(K)(N) RAS: (Harvey)(Kirsten)(Neuroblastoma) Rat Sarcoma Viral proto-oncogene
Rb: Retinoblastoma gene
RNA: Ribonuclease acid
ROS: Reactive oxygen species
rpm: rotation per minute
RT-PCR: Reverse transcription polymerase chain reaction
SEM: Standard Error of the Mean
SOD (s) (2): Superoxide dismutase (s) (2)
STAT3: Signal transducer and activator of transcription 3
TAM: Tumour associated macrophage
TAN: Tumour associated neutrophil
TFP: Teal Fluorescent Protein
TGF-(α)(β): Transforming growth factor (α)(β)
TILLING: Targeting-induced local lesions in genes
TNF-(α): Tumour necrosis factor α
TP53: Tumour protein p53
TUNEL: Terminal deoxynucleotidyl transferase dUTP nick end labelling
UAS: Upstream activating sequence
Ubi: *Ubiquitin* promoter
VEGF: Vascular endothelial growth factor
YFP: yellow fluorescent protein

1. Introduction

1.1 Cancer: The Basics

Cancer is a group of diseases characterised by uncontrolled proliferation, leading to metastasis of abnormal cells to distant organs of the body. The development of cancer is a multi-step process referred to as carcinogenesis and results from the accumulation of genetic mutations. Initially, mutations arise in a single cell, giving that cell a proliferative and survival advantage. The cell proceeds to proliferate in an uncontrolled manner, acquiring additional genetic mutations over time and ultimately giving rise to a heterogenous mass of cells called a tumour (**Figure 1.1**). As cellular proliferation and genetic mutation continues tumours are infiltrated by cells of other types, including inflammatory cells, while some cancer cells may acquire invasive properties and leave the tumour mass, disseminating and metastasizing to distant areas of the body [1].

While the mechanistic cause of all cancers is known to be genetic mutation, a variety of risk factors are known to play a role in initiating these genetic lesions. Only a small proportion of cancers are strongly hereditary [2], with the vast majority caused by acquired mutations. There are many risk factors associated with cancer development. As disease results from accumulation of mutations over time, the risk of developing cancer increases with age, with 36% of all newly diagnosed patients in the UK over the age of 75 [3] and 87% of all newly diagnosed patients in the United States over the age of 50 [2]. Other risk factors include smoking, excessive sun exposure, physical inactivity, obesity and poor diet. Some infectious agents are also associated with cancers, such as the human papillomavirus (HPV) associated with cervical cancer, hepatitis B virus (HBV) associated with liver cancer and *Helicobacter pylori* infection is associated with gastric cancers [4]. In fact, it is estimated that approximately 40% of cancers in both the UK [5] and the United States [2] are potentially preventable, should risk factors be controlled.

Cancers can arise in many organs of the body, but some tissues are more susceptible to cancer development than others. While organ prevalence differs in

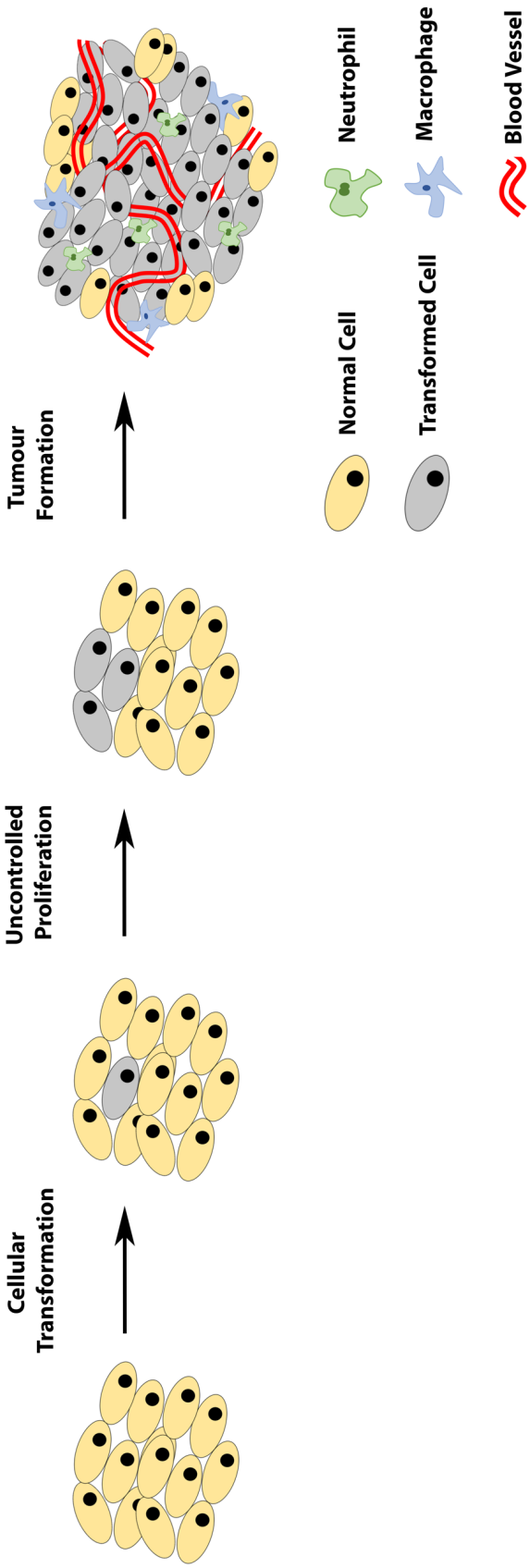

Figure 1.1: Cancer development is a multi-step process. Cancer initiation begins when a single cell acquires genetic mutation leading to cellular transformation (grey cell). This cell gains a proliferative and survival advantage over its neighbours and begins to proliferate excessively. As transformed cells continue to proliferate they acquire further mutations, ultimately leading to a heterogenous mass of cells called a tumour. Vascularisation by endothelial cells and infiltration by inflammatory cells aids tumour growth and helps to establish metastatic disease.

males and females [3], cancers of epithelial origin are most common in both sexes, accounting for approximately 80% of total human cancer cases [6][7]. Cancer survival varies depending on the combination of genetic mutations and tissue type involved. Cancer outlook is often assessed by the five-year survival rate, this reaching as high as 90% for breast cancer [2] and 98% for testicular cancer [8] but remains at just 1% for pancreatic cancer [8]. These figures highlight the diverse complexity associated with cancer and the necessity for continued research. Early detection is vital for increasing survival rates [9]. Screening programs have been developed for a number of cancer types, including breast [10], cervical [11] and bowel cancers [12], meanwhile cancer vaccines have been developed to protect against cancers caused by some infectious agents [13]. However, early detection of cancer remains a challenge as our understanding of the very earliest stages of initiation and development remains relatively limited [9]. Typically, by the time patients present to the clinic the tumour is already well established. While scientific research has excelled in recent times, issues detecting and monitoring very early oncogenic processes *in vivo* persist.

As genetic mutations accumulate, cells acquire a number of phenotypic characteristics which confer a proliferative and survival advantage on mutated cells. These features were famously described as “The Hallmarks of Cancer” in a seminal paper by Hanahan and Weinberg [14], who then updated their analysis in 2011 to reflect ongoing research by including additional “Enabling Characteristics” [15], and these are now commonly discussed under the same title as the original features. The phenotypic hallmarks of cancer described are “evading growth suppressors, activating invasion and metastasis, enabling replicative immortality, inducing angiogenesis, resisting cell death, sustaining proliferative signalling, deregulating cellular energetics, evading immune destruction, tumour promoting inflammation and genome instability and mutation” [14][15] (**Figure 1.2**). Considerable research has been completed on each of these features and work continues in an effort to further our understanding of cancer and develop effective therapies. Research has revealed the sheer complexity of cancer development and progression, with these

hallmarks of cancer working both independently and synergistically to enable disease. While it is known that these features are present and necessary in established tumours, when they arise and how they contribute to the early stages of disease development is less well understood.

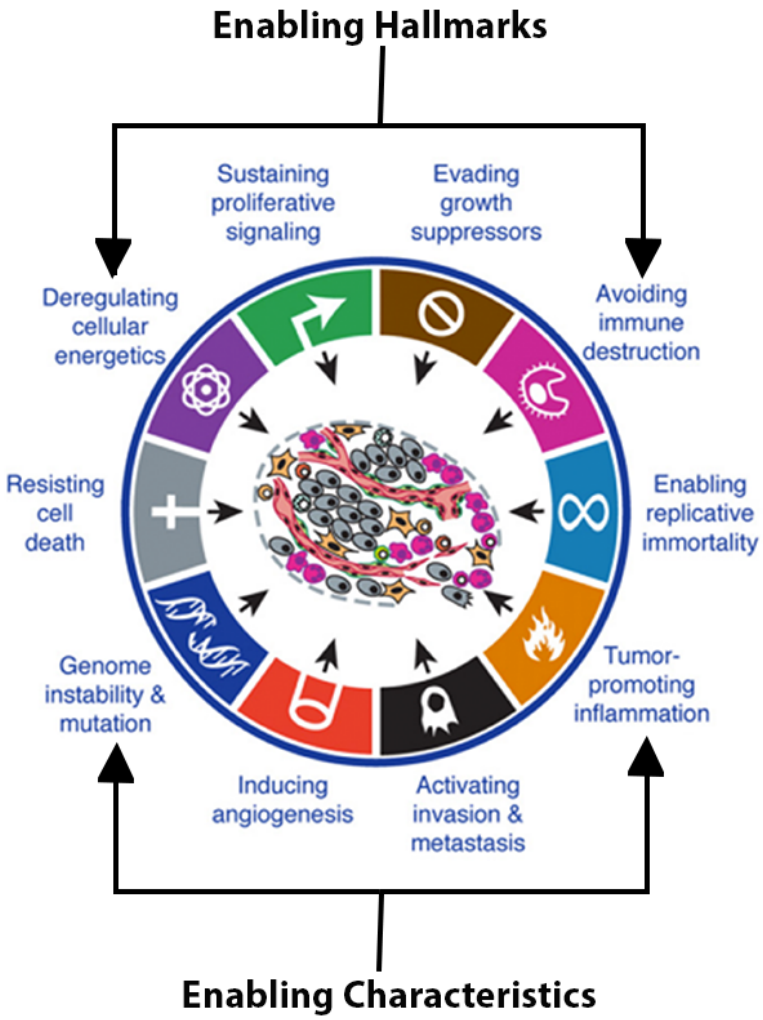

Figure 1.2: The Hallmarks of Cancer. Established cancers have a number of defining features that were famously summarised as "The Hallmarks of Cancer" by Hanahan and Weinberg. These features aid tumour growth and help establish metastatic disease. Figure adapted from [15]

1.2 Cancer Initiation and Development

The multi-stage process of cancer development is initiated when a genetic lesion arises in a cell and is not sufficiently repaired. Cancer-causing mutations generally arise in genes that control processes essential for cellular homeostasis, such as DNA repair, the cell cycle, proliferation and cell death pathways [1]. Some genetic mutations are commonly seen in a variety of cancers, while others are characteristic to certain tissues. For instance, the cell cycle regulator TP53 is mutated in many cancer types, but mutations in the receptor tyrosine kinase HER-2 gene are characteristic of breast cancer and are seen in over 25% of cases [7].

There are two classes of commonly mutated genes in cancer; oncogenes and tumour suppressor genes. Oncogenes typically control pro-tumourigenic processes such as cell growth and proliferation, with activating gain-of-function mutations leading to constitutive activation of downstream signalling processes. There are over 60 known oncogenes including RAS, c-MYC, v-SRC and HER-2 [1]. Tumour suppressor genes govern anti-tumourigenic functions such as cellular repair, growth and proliferation inhibition and cell death; processes which are often down-regulated due to loss-of-function mutations. Common examples of tumour suppressors include TP53, Rb and APC [1]. The examples provided here represent prototypical, well defined cancer-causing genes and while there are a great number of oncogenes and tumour suppressor genes [16], the functions they control generally converge to regulate a much smaller number of key pathways within a cell [17]. These pathways include the Myc, PI3K, Ras, Notch and Hippo pathways, all of which are frequently altered in cancer and have been shown to play vital roles in regulation of the cell cycle, apoptosis, growth and proliferation [18]. Due to the importance of these genes in regulating cancer initiation processes, they are often referred to as cancer “driver genes” [16].

It has been known for a long time that cancers develop from a single cell which expands clonally to generate a heterogenous population with mutations accumulating over time [19]. Mutation in one of the driver genes is insufficient to cause cancer. In fact, up to seven independent genetic mutations are thought to be

required for progression to metastatic disease [20][21]. Mutation events initiate pre-neoplastic processes such as enhanced proliferation and evasion of growth controls, conferring a selective advantage on the mutant cell. Acquisition of subsequent mutations is coupled with emergence of further features of tumourigenesis and ultimately leads to the establishment of a tumour [19]. The specific mechanisms of tumour development and order of hallmark acquisition varies depending on the combination of genetic mutations and tissue type involved. Consequently, our knowledge of the very early interactions of oncogenesis following spontaneous cellular transformation *in vivo* remains relatively limited. Intensive research on how each of the oncogenes and tumour suppressor genes, and the pathways they control, contribute to oncogenic processes, both independently and synergistically, has vastly enhanced our understanding. Recent advances in lineage tracing confirms that clonal expansion of mutated cells leads to tumour formation and gives indications of how cellular transformation occurs *in situ* [22][23]. However, difficulty detecting these very early stages of cellular transformation *in vivo* remains a limiting factor for full elucidation of cancer initiation processes.

Transformed cells continue to acquire genetic mutations as a tumour develops leading to considerable heterogeneity among tumour cells. Heterogeneity increases further as the developing tumour is infiltrated by other cell types [24]. Interactions between transformed cells and their developing microenvironment have been shown to be vital for tumour progression [25][26]. Developing tumours release a variety of factors that alter the surrounding extracellular matrix (ECM) to promote further development [27]. Fibroblasts and endothelial cells have active roles during tumour initiation, providing pro-tumourigenic signals and forming new blood vessels to supply the growing tumour with oxygen and nutrients [28]–[31]. Meanwhile, links between inflammatory cells and cancers have been proposed since the mid 19th century and have since been shown to be important for providing signalling molecules for a developing tumour (for further details see Section 1.7). Growth factors, MMPs, cytokine and chemokines are all produced by both the tumour cells and the cells of the developing tumour microenvironment to promote tumour

progression and help establish metastatic disease [26]. Again, the exact signalling molecules involved is dependent on tumour genotype and tissue involved, highlighting the complexity of cancer signalling.

1.3 RAS Signalling and Its Role in Cancer

The RAS family of proteins are a set of membrane-associated GTPases that act as molecular switches for several intracellular signalling pathways that regulate a wide variety of cellular functions. In humans, there are three RAS genes; HRAS, NRAS and KRAS which encode four protein isoforms [32].

The activation state of RAS is regulated by two classes of proteins called GEFs and GAPs, which determine the binding of GTP and GDP, respectively. RAS proteins are active when GTP is bound and inactive when GDP is bound [33][34]. The extent and duration of RAS activation has drastic downstream effects on cellular fate and function, so the balance of GEF and GAP activity is vital for regulation of cellular homeostasis [35].

Given that it is a relatively simple molecule that merely cycles between GTP- and GDP-bound states, RAS controls a remarkable variety of cellular processes and is considered a focal point for signal transduction. Different RAS isoforms have different cellular function [36], but all are involved in signal transduction for pathways that control cell growth, proliferation, survival and differentiation [32]. The best described RAS interaction is with the MAPK pathway, where RAS acts as the first intracellular effector of the pathway by recruiting Raf-1 to the plasma membrane. Signal transduction ultimately leads to ERK activation and nuclear translocation causing activation of transcription factors that regulate a vast number of cellular processes including proliferation and the cell cycle [37]. While this may be the most established RAS signalling pathway, it is by no means the only. Other RAS effector pathways include the phosphoinositide 3-kinase (PI3K) pathway [38]–[40], phospholipase Cε pathway [41] and the RAS-related Ral protein pathway [42] (**Figure 1.3**), to name a few. This broad range of effector pathways

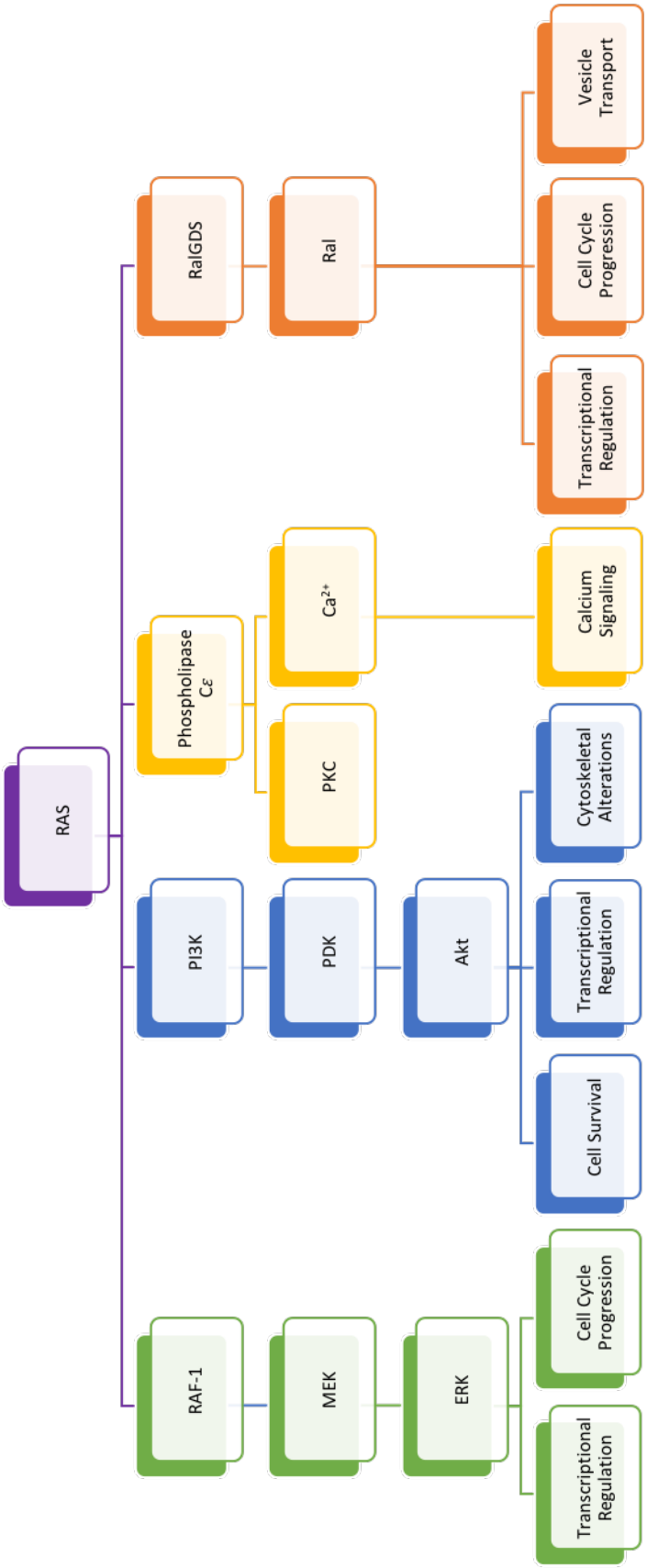

Figure 1.3 RAS effector signalling pathways RAS proteins have a number of effector signalling pathways that control a vast number of cellular processes. The best characterised is the MAPK pathway (green), which is important for proliferation and control of the cell cycle. Other effector pathways include the PI3K pathway (blue), the RAL protein pathway (orange) and the phospholipase Cε pathway (yellow). These combined effector functions mean RAS plays vital roles in regulation of proliferation, the cell cycle, apoptosis, gene expression, and cell migration.

means that RAS plays important regulatory roles in a vast number of processes, from proliferation and the cell cycle, to apoptosis and cell migration.

The RAS genes are the most frequently mutated genes in human cancers [43], with approximately 20% of all human tumours showing activating RAS mutations [44]. RAS isoforms appear to show tissue variation, with some isoforms more likely to be mutated in certain tissues. KRAS mutations, the most common of the RAS mutations in cancer[45], are commonly seen in colorectal, lung and pancreatic cancers [45][46]. NRAS mutations are associated with haematological malignancies [45][47], while HRAS mutations frequently occur in skin and head and neck cancers [45][48]. Common oncogenic alterations are seen in the G12, G13 and Q61 residues of all isoforms [45]–[48], which retain the protein in the GTP-bound active state causing continuous activation of downstream effectors [32].

Given the wide array of functions that are downstream of RAS, constitutive protein activation has significant impact on cellular function and results in several features characteristic of cancer cells [32]. RAS signalling has been shown to enhance proliferative capacity through a number of mechanisms, including driving cells into the cell cycle; upregulating growth factors including TGF-α, HBEGF and AREG and enhancing expression of growth factor receptors [49]–[51]. Oncogenic RAS initiates pro-survival mechanisms by activating RAF and PI3K pathways to down-regulate pro-apoptotic molecules such as BAK1 and BAD [52]–[54] and upregulate anti-apoptosis mediators [55][56]. RAS can also have non-cell-autonomous functions to influence cancer development. Expression of endothelial growth factors, including VEGF [57]–[59], is enhanced to promote angiogenesis, increased expression of pro-inflammatory cytokines, including IL-8, IL-6 and CXCL1, leads to inflammatory cell recruitment [60]–[63], while upregulation of MMPs promotes vascularisation and cell migration [64][59]. This vast array of cellular alterations places oncogenic RAS as a major signalling junction in a cell, with great potential to direct cellular transformation.

As research continues to further our understanding of this oncogene and how its downstream effectors coordinate cancer initiation, development and progression,

a number of oncogenic RAS models have been developed. These include *in vivo* transgenic mouse and fish models, which allow in-depth studies of Ras oncogenes and the processes they control. In mice, RAS models have been used for decades as a leading system to help understand all stages of cancer development, progression, regression and response to treatment [65], by primarily expressing mutant forms of HRAS or KRAS to induce neoplasms in tissues including lung [66], pancreas [67], skin [68] and breast [69]. Meanwhile, zebrafish RAS systems have been developed to model melanoma [70], rhabdomyosarcoma [71] and pancreatic cancer [72], as well as inducible systems that can be used in different tissue types [73][74]. These *in vivo* models have greatly enhanced our understanding of oncogenic RAS signalling and, as they continue to evolve, allow targeted and specific studies of the role of RAS in tumourigenic processes.

1.4 Glucose Metabolism

Cellular metabolism involves a remarkably complex series of interconnected pathways that break down organic molecules to produce energy and metabolic intermediates for cellular processes. Broadly speaking, carbohydrates, fatty acids and amino acids are the primary fuel sources in a cell [7], and each of these are utilised in a variety of highly regulated mechanisms to ensure cellular homeostasis.

Glucose is the central carbohydrate in cellular metabolism, acting both as a vital fuel source and a versatile supplier of a vast array of biosynthetic intermediates[75]. Within a cell, glucose can have four fates; storage as polysaccharides, synthesis of complex polysaccharides for structural functions, oxidation via the pentose phosphate pathway to generate nucleic acids, or oxidation via glycolysis to generate pyruvate for energy production [76]. Cells generate energy in the form of ATP via the complete oxidation of glucose to carbon dioxide and water via the glycolytic and oxidative phosphorylation pathways [76].

The glycolytic pathway (**Figure 1.4**) is a series of chemical reactions that take place in the cytoplasm of a cell to breakdown a single glucose molecule into two three-carbon pyruvate molecules, with the concomitant production of ATP [77]. The

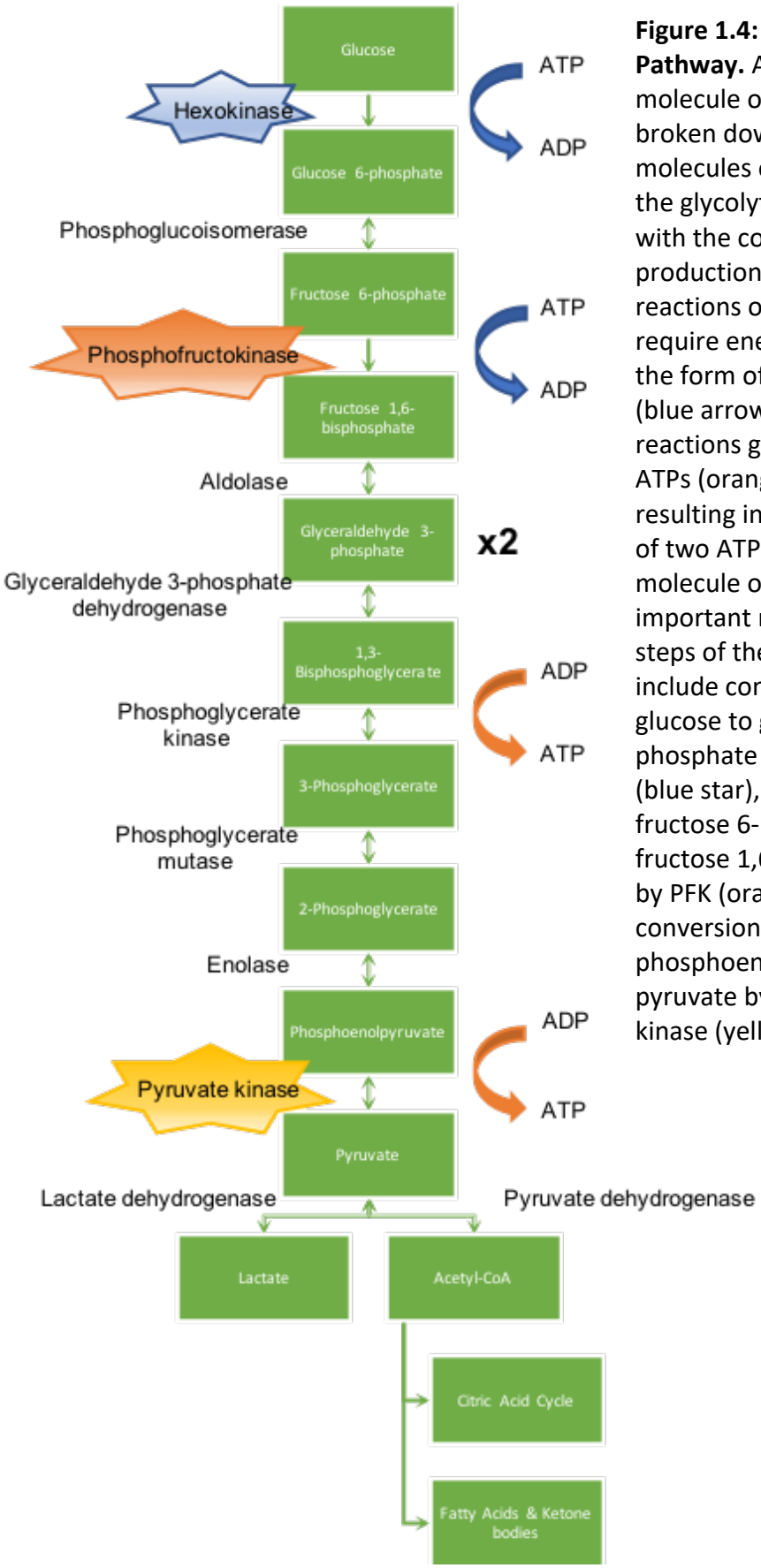

Figure 1.4: The Glycolytic Pathway. A single molecule of glucose is broken down into two molecules of pyruvate via the glycolytic pathway with the concomitant production of ATP. Early reactions of the pathway require energy input in the form of two ATPs (blue arrows), but later reactions generate four ATPs (orange arrows), resulting in net generation of two ATP molecules per molecule of glucose. The important regulatory steps of the pathway include conversion of glucose to glucose-6-phosphate by hexokinase (blue star), conversion of fructose 6-phosphate to fructose 1,6-bisphosphate by PFK (orange star) and conversion of phosphoenolpyruvate to pyruvate by pyruvate kinase (yellow star).

pathway involves 10 tightly regulated enzymatic reactions (**Figure 1.4**), resulting in the net production of two ATP molecules and multiple biosynthetic intermediates. Glycolysis requires energy investment at the early stages, with ATP acting as a phosphoryl group donor for the conversion of glucose to glucose-6-phosphate and fructose-6-phosphate to fructose 1,6-bisphosphate (**Figure 1.4, blue arrows**). However, later stages of the pathway release four ATP molecules as two molecules of 1,3-bisphosphoglycerate are converted to two molecules of pyruvate (**Figure 1.4, orange arrows**), leading to the net production of two molecules of ATP per molecule of glucose [76]. The later reactions of glycolysis also involve the generation of two molecules of the co-enzyme NADH, which are subsequently utilised in the oxidative phosphorylation pathway (discussed below). Therefore, the overall equation for the glycolytic pathway under aerobic conditions is: [76]

$$\textbf{Glucose} + 2\,\textbf{NAD}^+ + 2\,\textbf{ADP} + 2\,\textbf{P}_i \rightarrow 2\,\textbf{Pyruvate} + 2\,\textbf{NADH} + 2\,\textbf{H}^+ + 2\,\textbf{ATP} + 2\,\textbf{H}_2\textbf{O}$$

In order to maintain homeostasis, the reactions of glycolysis are tightly regulated. While all of the reactions of the pathway are controlled, there are three regulation points of particular importance. Hexokinase irreversibly catalyses the conversion of glucose to glucose-6-phosphate as the first glycolytic reaction (**Figure 1.4, blue star**). Hexokinase is inhibited by its product, glucose-6-phosphate. Should glucose-6-phosphate rise above equilibrium levels, inhibition of hexokinase will reduce production to allow the cell to return to homeostasis. [78] Arguably the most important regulatory step of the glycolytic pathway is the irreversible conversion of fructose-6-phosphate to fructose 1,6-bisphosphate by phosphofructokinase (PFK) (**Figure 1.4, orange star**) as it commits glucose utilisation to the glycolytic pathway. Given its importance, PFK has multiple regulatory sites. PFK is reversibly inhibited by ATP and citrate [79], allowing the pathway to remain responsive to cellular energy requirements. H^+ ions inhibit PFK, preventing acidosis as a result of excessive lactate production in anaerobic conditions (see below). PFK is regulated by fructose 2,6-

bisphosphate [80], a metabolic intermediate involved in the reciprocal regulation of glycolysis and gluconeogenesis. Finally, pyruvate kinase, which catalyses the conversion of phosphoenolpyruvate to pyruvate at the final stage of glycolysis (**Figure 1.4, yellow star**), is inhibited by ATP, acetyl-CoA, fatty acids and certain amino acids [81]. This, again, ensures responsiveness to the energy requirements of the cell as glycolysis is inhibited when energy levels are sufficient.

The glycolytic pathway generates two molecules of pyruvate per molecule of glucose. Under aerobic conditions, pyruvate is primarily converted to acetyl-CoA by pyruvate dehydrogenase (PDH) [82]. Acetyl-CoA then enters the citric acid cycle for further oxidation and ATP production (discussed below). However, if ATP levels are in excess, acetyl-CoA can be utilised for fatty acid or ketone body synthesis [83]. Under anaerobic conditions, pyruvate can be converted to lactate by lactate dehydrogenase (LDH) with concomitant regeneration of NAD^+ to allow glycolysis to continue [84]. This is a reversible reaction and is an important metabolic process for varying oxygen conditions and energy requirements.

In order to complete the breakdown of glucose into CO_2 and H_2O the pyruvate generated from glycolysis is converted to acetyl-CoA by PDH which then enters the citric acid cycle (**Figure 1.5**). This cycle, also known as the tricarboxylic acid cycle and the Krebs cycle, takes place in the mitochondria and is also used for the oxidation of acetyl-CoA from the breakdown of fatty acids and amino acids [76]. The eight stages of the citric acid cycle (**Figure 1.5**) result in the generation of three NADH and one $FADH_2$ [85], which are subsequently re-oxidised by oxidative phosphorylation for energy production (discussed below). In addition to cellular energy production, the citric acid cycle is of central importance to provide pre-cursors for a variety of cellular pathways, including synthesis of fatty acids, amino acids and nucleotides as well as replenishing glucose by gluconeogenesis [76].

The oxidation of glucose and other fuel sources that feed into the citric acid cycle to CO_2 and H_2O is completed by the oxidative phosphorylation pathway (**Figure 1.6**), which is the process of ATP synthesis coupled to the oxidation of NADH

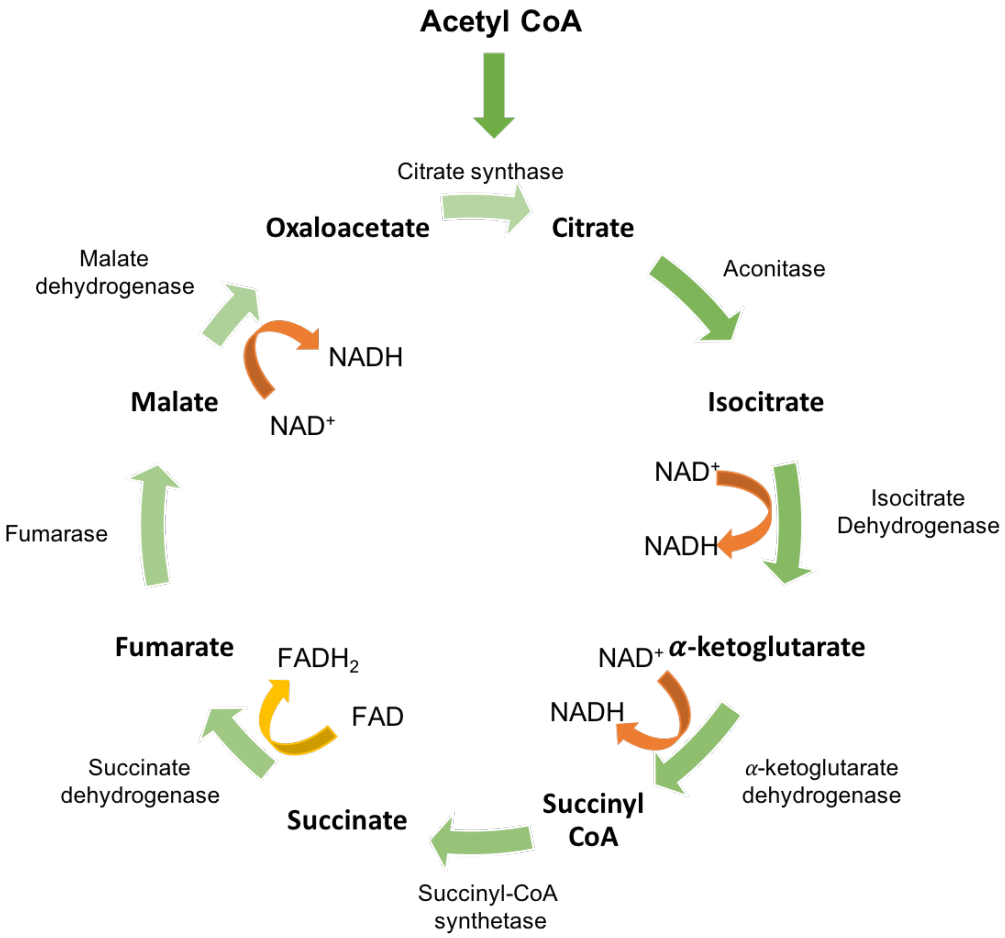

Figure 1.5: The Citric Acid Cycle. Pyruvate from glycolysis can be converted to acetyl-CoA which enters the citric acid cycle for further oxidation. The eight steps of the citric acid cycle generate three NADH (orange arrows) and one $FADH_2$ (yellow arrow) which are subsequently re-oxidised by oxidative phosphorylation.

and $FADH_2$ [76]. Transfer of electrons from NADH and $FADH_2$ to oxygen occurs via a series of electron carriers in the mitochondrial inner membrane referred to as the electron transport chain (ETC). This chain consists of four large electron carriers, referred to as complex I – IV, linked by two smaller electron carriers [76][86]. The flow of electrons through this chain also results in the generation of a proton gradient, as H^+ is pumped from the mitochondrial matrix across the mitochondrial inner membrane to the intermembrane space [87][88] (**Figure 1.6**). This proton gradient links electron transport to ATP synthesis. The protons in the intermembrane space flow back to the mitochondrial matrix through the ATP

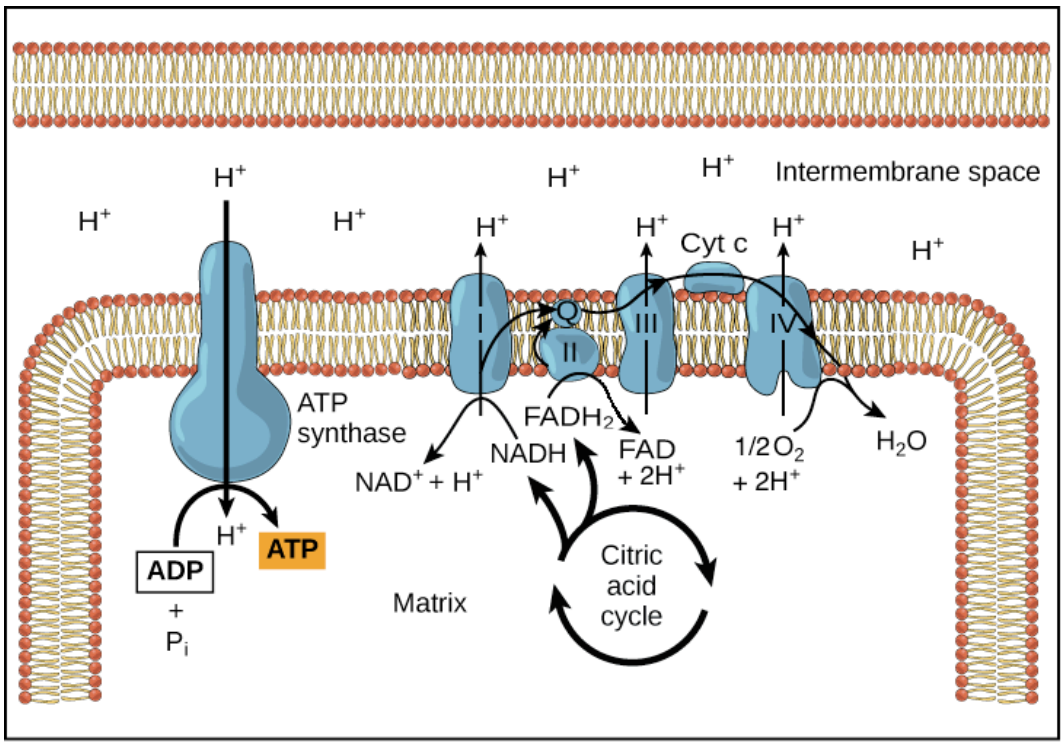

Figure 1.6: Oxidative Phosphorylation. Electrons flow from NADH and $FADH_2$ through the four complexes of the electron transport chain to form H_2O which generates a proton gradient across the mitochondrial inner membrane. Protons flow back into the mitochondrial matrix via the ATP synthase complex with concomitant generation of ATP. Figure Adapted from [88]

synthase complex in the mitochondrial inner membrane, which drives the synthesis of ATP [89]. This process results in the generation of three ATP molecules per molecule of NADH and two ATP molecules per molecule of $FADH_2$ [76].

The flow of electrons through the ETC is also associated with the generation of reactive oxygen species (ROS). Electron transfer through complex I and complex III involves a partially reduced ubiquinone radical ($^{\bullet}Q^{-}$) which can donate an electron to molecular oxygen (O_2) to generate the superoxide free radical ($^{\bullet}O_2^{-}$) [90]. Up to 4% of oxygen used for respiration forms superoxide radicals [76] and this can be damaging to the cell if not dealt with appropriately. Cells have various mechanisms for ROS detoxification, including the conversion of superoxide to hydrogen peroxide via the action of superoxide dismutases (SODs), which is subsequently reduced to H_2O via glutathione peroxidase [91].

The complete oxidation of glucose via glycolysis, the citric acid cycle and oxidative phosphorylation to CO_2 and H_2O generates approximately 30 - 32 molecules of ATP per molecule of glucose, depending on cytosolic NADH shuttle systems [76]. Additionally, numerous important biosynthetic intermediates are generated. By comparison, under anaerobic conditions just two ATP molecules per molecule of glucose are generated via glycolysis [76]. Therefore, complete oxidation of glucose via cellular respiration is vital for providing sufficient energy and biosynthetic precursors to meet cellular requirements.

Given the central importance of these metabolic processes in a cell, perturbation of pathways can be harmful. A myriad of human diseases are now recognised to include metabolic components, including type 2 diabetes, obesity and cardiovascular disease, in addition to cancers, as discussed below.

1.5 Metabolic Alterations in Cancer.

In 1956 Otto Warburg put forward a model of aerobic glycolysis in transformed cells [92]. Since termed "The Warburg Effect", this model proposes a metabolic switch from oxidative phosphorylation to glycolysis for ATP production, even in the absence of a hypoxic environment, leading to increased uptake of glucose and excessive lactate production. This led Warburg to conclude that cancers arise as a result of mitochondrial dysfunction. While this conclusion has since been disproven, many aspects of Warburg's original theory have been verified and "The Warburg Effect" is now a well-established feature of cancers [93].

In the late 20th century interest in cancer metabolism faded. However, a recent resurgence and realisation of its central role in cancer has led to an explosion of research into the metabolic features of cancer and how they could potentially be targeted for cancer treatment. Increased glycolytic metabolism in established tumours has been co-opted for diagnosis and monitoring purposes. Positron emission tomography (PET) involves uptake of ^{18}fluorodeoxyglucose (FdG), a glucose analogue used as a tracer and allows quantifiable imaging of tumours in patients [94]. This technique has permitted verification of enhanced glucose uptake in human

tumours and enabled both diagnosis and monitoring of tumour development and response to treatment [95]–[99]. It has repeatedly been reported that increased glucose uptake correlates with increased aggressiveness and metastasis and is associated with poor prognosis for patients [100]–[103]. It is now accepted that cancer cells alter glucose utilisation by channelling pyruvate towards lactate production both as a response to hypoxia as the tumour develops and as a mechanism to generate biosynthetic intermediates to fuel proliferation [104], as discussed further below. Also, it is now recognised that The Warburg Effect is not the only means of metabolic alteration in cancers. Change is also seen in a number of other metabolic pathways including the citric acid cycle, oxidative phosphorylation, the pentose phosphate pathway, glutaminolysis and β-oxidation of fatty acids [105]. Functional alterations in these pathways are commonly the result of a genetic mutation in vital enzymes, leading to altered enzyme activity. Oncogenic processes, including oncogene and/or tumour suppressor gene activation, have been shown to alter activity of hexokinase [106]–[108], pyruvate kinase [109], pyruvate dehydrogenase [110], lactate dehydrogenase [111][112], fumarate hydratase [113], succinate dehydrogenase [114] and isocitrate dehydrogenase 1 and 2 [115]–[119] in various contexts leading to dysregulation of normal metabolic processes. These changes can manifest in a variety of ways which often converge to provide increased energy and biosynthetic intermediates for cell growth and ultimately aid tumour progression [105][118]. Downstream of these changes, acidosis, hypoxia, increased reactive oxygen species (ROS) and altered metabolic end-products are all features that arise in the tumour microenvironment [120], often in conjunction with other hallmarks of cancer [14][15]. These features can have profound effects on surrounding cells, from decreasing survival potential to allow the tumour cells to thrive, to changing cellular signalling to aid tumour growth.

The purpose of metabolic switching was not understood for some time. Aerobic glycolysis is approximately 18-fold less efficient at ATP production than oxidative respiration [15]. Furthermore, metabolic pathways are intrinsically linked to maintain adequate supply of metabolic intermediates by a process called

anaplerosis. Disruption to these processes alters flux between these pathways and leads to metabolic imbalance and increased ROS production. However, while less efficient for energy production, the metabolic alterations seen in cancers are highly efficient for generating biosynthetic intermediates [121]. For example, altered regulation of hexokinase funnels glucose-6-phosphate into the pentose phosphate pathway for generation of ribose-5-phosphate, required for the synthesis of nucleic acids for cellular proliferation [76]. This increased generation of biosynthetic intermediates allows for the highly increased growth, proliferation and survival of tumour cells and drives tumour progression. While tumour cells are required to increase consumption of fuels such as glucose and glutamate to sustain these processes [122], they also generate sufficient energy to survive and drive increased proliferative processes, despite the reduced efficiency.

As previously mentioned, oncogenic RAS can alter cellular metabolism in cancer cells. Through the upregulation of HIF-1α via MAPK-PI3K-mTOR signalling, RAS can stimulate the metabolic switch to aerobic glycolysis and enhance glucose uptake by upregulating expression of glucose transporters [123]–[125]. RAS also upregulates expression of glycolytic enzymes including hexokinase and lactate dehydrogenase [126][32]. Therefore, RAS signalling drives the cell towards glycolytic metabolism and contributes to the metabolic signature that is characteristic of established cancer cells.

While our knowledge of altered metabolism in cancer has vastly increased as a result of the recent resurgence in attention, the complexity of cancer mechanisms intertwined with metabolic intricacies still leaves many unanswered questions. It remains to be determined how and why some of these changes occur and mechanisms of how they contribute to tumour progression remain poorly understood. Further insights into when these features arise during tumour development and how they interact with tumourigenic processes could enhance our understanding of established tumours and provide potential targets for cancer prevention and/or therapy.

1.6 Mitochondrial Dynamics in Health and Disease

Mitochondria are double-membraned cellular organelles that are specialised for energy production [127] (**Figure 1.7**). The smooth outer mitochondrial membrane encases the organelle and is freely permeable to small molecules and ions. The inner mitochondrial membrane forms extensive convolutions called cristae which hold the four electron carriers of the electron transport chain and the ATP synthase complex for ATP production by oxidative phosphorylation. These cristae provide a large surface area on which oxidative phosphorylation can occur and the degree of convolution is linked to the bioenergetic requirements of the tissue. The mitochondrial matrix encased within the inner membrane is the site of numerous metabolic reactions including the citric acid cycle, β-oxidation of fatty acids and amino acid oxidation [76]. Given this vital role for generation of cellular energy, the mitochondria are often referred to as "The Powerhouse of the Cell". However, in addition to energy generation, mitochondria also have important functions in calcium homeostasis, regulation of the cell cycle, regulation of apoptosis and control of ROS signalling [128]–[130]. Mitochondria also contain their own genome, referred to as mtDNA, which primarily encodes components of the respiratory network [131].

Within a cell, mitochondria form dynamic networks that are in constant flux depending on the requirements of the cell. This mitochondrial network undergoes continuous cycles of fusion and fission (**Figure 1.8**) that are inextricably linked to functional requirements [132][133]. These cycles are vital for maintenance of a healthy mitochondrial population in the cell [132] and perturbation of this cycle can lead to cellular dysfunction and disease. Mitochondrial fusion is associated with increased oxidative phosphorylation, mtDNA stability and sufficient distribution of mtDNA among the mitochondrial network in a cell [134]–[136]. Meanwhile, fission is associated with organelle biogenesis and clearance of damaged mitochondrial fragments by mitophagy [137][138]. Mitochondrial morphology alters with the cell cycle. Mitochondria are highly inter-connected at

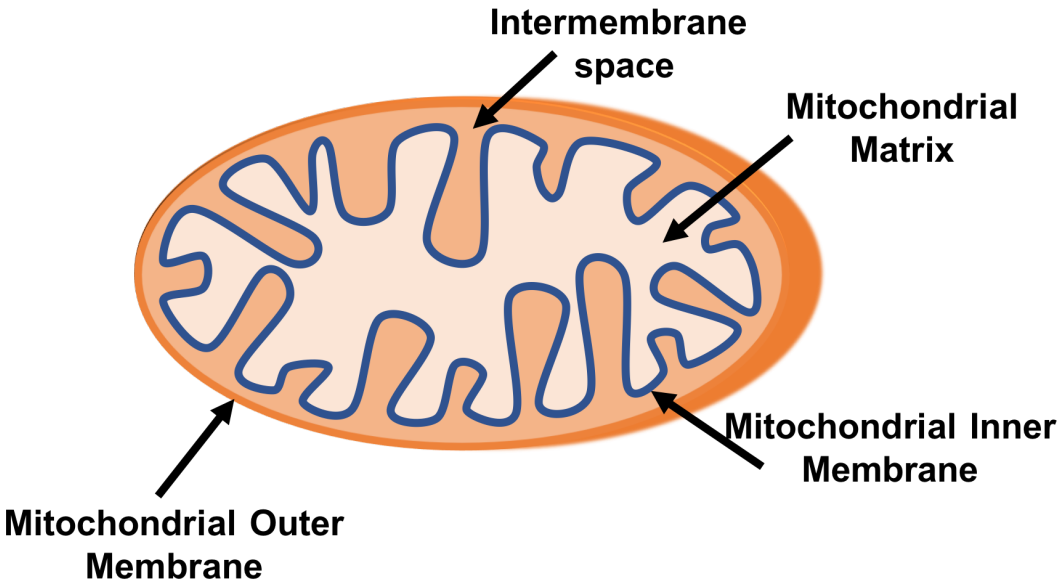

Figure 1.7: Mitochondrial Structure. Schematic cross-sectional view of the structure of mitochondria. The organelle is surrounded by the smooth mitochondrial outer membrane. The mitochondrial inner membrane forms extensive folds called cristae to increase the surface area for oxidative phosphorylation, as the electron carriers of the electron transport chain and the ATP synthase complex are embedded in this membrane. The mitochondrial matrix is the site of numerous metabolic reactions including the citric acid cycle.

early stages of the cell cycle to ensure sufficient energy production for proliferative processes, as fused mitochondria are associated with increased oxidative phosphorylation and ATP production. However, fission increases at later stages of the cell cycle to ensure equal distribution of mitochondria to daughter cells [139]–[141]. Fragmentation is also associated with apoptosis, as fission is coordinated with mitochondrial outer membrane permeabilization to release matrix components into the cytoplasm to induce the programmed cell death cascade [142]. Mitochondrial ROS, generation of which increases with fragmentation [143], further contribute to induction of apoptosis. Differentiation and functional activation of a cell can also be governed by the fusion/fission state. For instance, the activation state of T lymphocytes is determined by mitochondrial dynamics [144] and mitochondrial dynamics have been shown to be indispensable during development [145].

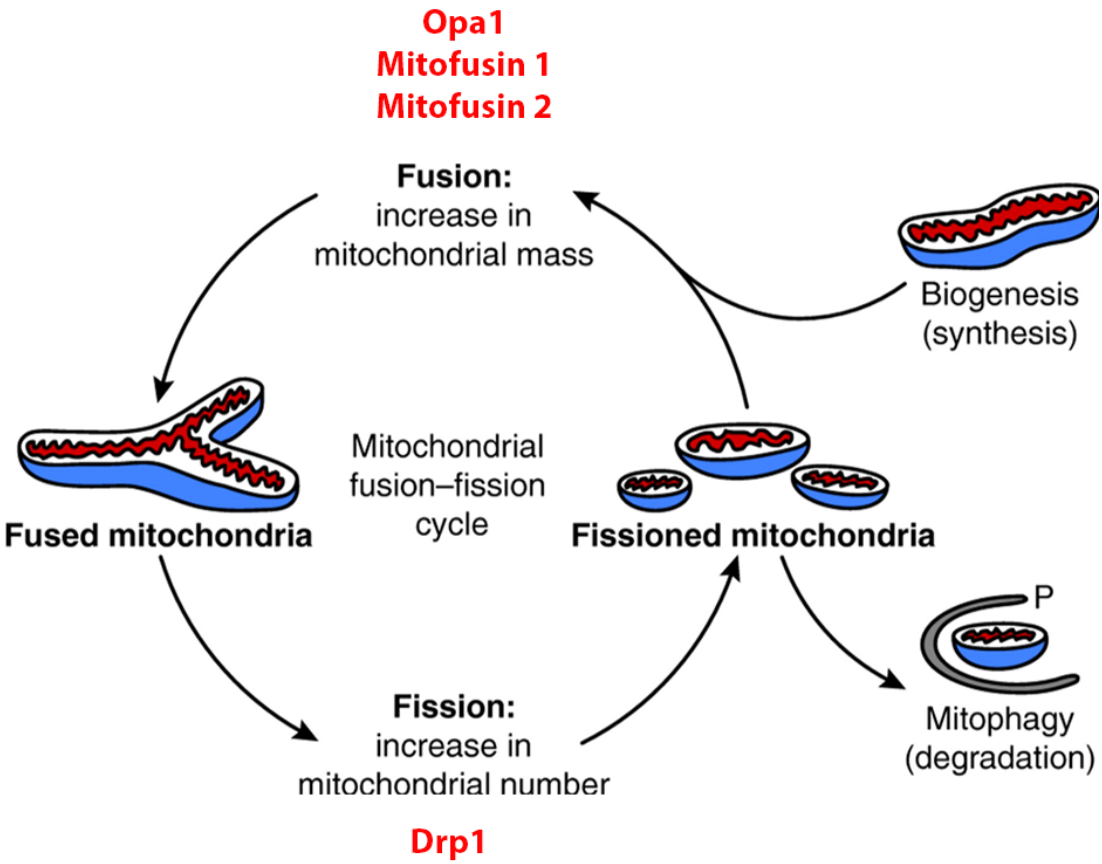

Figure 1.8: Mitochondria undergo cycles of fusion and fission. Mitochondria form dynamic networks within a cell and are in a constant cycle of fusion and fission, determined by cellular requirements. Fused mitochondria are associated with mtDNA stability and increased ATP production by oxidative phosphorylation. Fragmented mitochondria are linked with biosynthesis, mitophagy, apoptosis and ROS production. These processes are regulated by a number of highly conserved GTPases, as shown in red. Figure adapted from [133]

Given these important impacts on cellular function and fate, the cycle of mitochondrial fusion and fission is tightly regulated and is controlled by a number of GTPases highly conserved throughout evolution (**Figure 1.8**). Fusion of the outer membrane is facilitated by the action of mitofusin 1 and mitofusin 2, while Opa1 facilitates fusion of the inner membrane [146]. Fission is orchestrated by the cytosolic protein Dnm1 (also called Drp1) which translocates to the mitochondrial outer membrane on activation and constricts the organelle, leading to division [147]. The mitochondrial membrane potential also has an important impact on the fusion/fission state of the mitochondria. Intact membrane potential is essential for

mitofusin 1, mitofusin 2 and Opa1 function for fusion [148][149] and, therefore, reduction of membrane potential leads to fragmentation.

Mitochondrial alterations are seen in a variety of diseases [150]. Mitochondrial fragmentation is a well-established feature of neurodegenerative disorders, particularly Parkinson's disease where loss of PINK1 and parkin proteins leads to accumulation of Dnm1 [151]. Charcot-Marie-Tooth disease is a peripheral neuropathy caused by mitofusin 2 mutations [152], while Opa1 mutations are associated with optic atrophy [153]. Meanwhile, alterations to mitochondrial morphology are seen in cancer cells, with extensive fragmentation observed in cells from a number of cancer types [154]–[156]. This fragmentation is important for the proliferation and survival of cancer cells both *in vitro* and *in vivo*, as decreased proliferation and increased apoptosis is seen when fission is inhibited [155][156]. Fragmentation is linked to augmented metastatic potential, while decreased mitofusin 2 levels seen in some cancers promotes proliferation [156]. Recent work has shown that fragmentation in RAS driven transformed cells is dependent on post-translational modification of Dnm1 by the MAPK pathway and inhibition of Dnm1 function has a negative effect on tumour growth [157][158]. It is clear from these investigations that altered mitochondrial phenotype is an important feature of cancers, the importance of which is only just beginning to be understood.

1.7 Cancer Associated Inflammation

The links between cancer and inflammation have been recognised for many years. The association was first described in the mid 19th century when Virchow described the presence of leukocytes in tumours [159][160]. Since this initial finding, extensive investigations have uncovered a vital role in carcinogenesis for inflammatory cells, particularly in solid tumours.

Cancer and inflammation are linked by a number of mechanisms. Firstly, sites of chronic inflammation are highly predisposed to cancer development and the presence of persistent inflammation has been shown to increase the risk of cancer development in numerous organs including the lung and GI tract [161]–[163].

Secondly, analogous cellular signalling mechanisms are seen in both processes. For instance, RAS, NF-κB and STAT3 all show enhanced activity in both inflammatory and oncogenic environments [163]–[166]. Both intermediates and products of these inflammatory signalling pathways can act as growth factors and induce oncogenic transcription factor activation leading to down-stream effects that ultimately advance growth and survival of transformed cells [167]–[170]. Inflammatory mediators also propagate oncogenic signalling by activating additional pathways that control pro-tumourigenic processes including proliferation, angiogenesis and evasion of anti-tumourigenic inflammatory responses, as well as invasion and metastasis [160][163], with high concentrations of inflammatory cytokines found at the leading edge of invasive tumours [171][172].

The central role of the tumour microenvironment in disease development and progression has recently been at the forefront of research. As a result, mechanisms which promote inflammatory cell infiltrates are more clearly understood and the function of recruited leukocytes are beginning to be elucidated. It is now recognised that numerous inflammatory cell types; including neutrophils, macrophages, dendritic cells, NK cells and T and B lymphocytes [160], [173]–[177]; are present in the tumourigenic niche. Signalling factors in the tumour microenvironment can polarise these recruited inflammatory cells towards both pro- and anti-tumourigenic functions, the balance of which determines the ultimate progression or rejection of the tumour. While anti-tumourigenic inflammatory responses have the capacity to completely eradicate transformed cells before they go on to develop a tumour, these responses are often dysfunctional as a result of manipulation of the $CD8^+$ T cells and NK cells responsible for these functions by transformed cells [178]. Instead, oncogenic signalling primes the microenvironment for tumour promoting inflammatory responses, often establishing a chronic inflammatory environment [178]. For this reason, cancers are often referred to as “wounds that do not heal” [179].

Metabolic alterations in the tumour microenvironment can interact with inflammatory responses to influence tumour development and progression. As

mentioned above, oncogenic and inflammatory processes share numerous signalling processes, alterations to which can influence inflammatory responses. Metabolic end products are also known to interact with leukocytes. For instance, lactate, which is commonly found at high concentrations in tumours as a result of the Warburg Effect (See Section 1.5), can have inhibitory effects on cytotoxic T lymphocytes and dendritic cells, while localised acidosis as a result of lactate production can inhibit leukocyte migration [180]–[182]. Also, in a wounding scenario, Irg1l-dependent β-oxidation of fatty acids drives mitochondrial ROS production and leads to MMP-9 dependant macrophage recruitment [183]; a mechanism that could be similarly active in cancers. As our understanding of tumour metabolism continues to grow, the interactions between metabolic and inflammatory signalling processes and their effect on oncogenic processes will be further defined.

One of the most frequent inflammatory infiltrates in tumours are tumour associated macrophages (TAMs), which are recognised to have disease-altering effects in the tumour microenvironment [174]. TAMs are highly plastic and can be polarised towards classical pro-inflammatory M1 or alternative anti-inflammatory M2 phenotypes, although such basic classification is disputed by macrophage biologists. TAMs are generally considered M2 in nature, as they are typically polarised to produce immunosuppressive mediators such as IL-10 and TGF-β [184]. In this way, TAMs manipulate the response of other inflammatory cells and contribute to suppression of anti-cancer responses. However, TAMs also contribute to tumour progression by generating pro-inflammatory cytokines including TNF-α and IL-6 and via non-cell-autonomous mechanisms such as production of VEGF to promote angiogenesis [185]–[187].

Although less well characterised than TAMs, tumour associated neutrophils (TANs) are now appreciated to have important functions in the tumour microenvironment. Similar to other inflammatory cells in the vicinity of developing cancers, polarising factors in the tumourigenic niche, including those produced by TAMS, determine neutrophil phenotype [188]. For example, IFN-β signalling prompts an anti-tumourigenic neutrophil phenotype [189], while TGF-β promotes a pro-

tumourigenic neutrophil response [188]. The mechanisms by which TANs contribute to tumour progression are complex and multiple pro-tumourigenic mechanisms are thought to be simultaneously active. Inflammatory mediators produced by neutrophils contribute to various tumourigenic processes, including proliferation and survival [190]. Also, the granular nature of neutrophils provides ROS and nitric oxide species (NOS) [191] which drive DNA instability and activate proteolytic enzymes leading to DNA damage and breakdown of the ECM, thereby assisting tumour development and invasion.

These inflammatory infiltrates are known to have important functions in the tumour microenvironment but mechanisms of recruitment at very early stage of cellular transformation and the consequential effect on pre-neoplastic cells are as yet undetermined. Research has shown that $HRAS^{G12V}$-transformed cells recruit leukocytes at very early stages of development *in vivo* and interactions with recruited neutrophils are important for pre-neoplastic cell growth [192][193]. However, the mechanisms that regulate these processes remain elusive. Greater understanding of these mechanisms could provide targets for therapeutic intervention for cancer prevention and/or treatment.

1.8 The Zebrafish as a Model Organism for Cancer Biology

Zebrafish (*Danio rerio*) are small, freshwater teleosts that are indigenous to the rivers of India, although now found all over the world. Zebrafish were first developed as a model organism for scientific investigations by Streisinger, *et al*, who developed a method to produce homozygous diploid clones [194]. For many years, the model was used almost exclusively in the field of developmental biology. In recent times, use of the zebrafish as a model organism has grown considerably and is now generally accepted as a valid and influential vertebrate model organism. Zebrafish models are utilised in a wide variety of research areas including cancer, neuroregeneration and inflammation, with numerous human diseases having been recapitulated for *in vivo* investigations using zebrafish models.

As a model organism, the zebrafish has a number of advantages. Importantly, there are high levels of genetic conservation between human and zebrafish genomes. This permits investigation of genetic components of developmental and disease mechanisms and increases translational propensity. Zebrafish are also highly amenable to genetic alterations, which has led to the development of a number of well-characterised transgenic zebrafish lines and genetic disease models. Another key advantage is the optical translucency of embryonic and larval developmental stages [195][196]. This allows unprecedented access for manipulation and visualisation of cellular processes *in vivo* and in real time. Zebrafish females produce large numbers of externally fertilised eggs that develop *ex utero* [197]. This not only allows for ease of sample collection at required developmental stage, but also enables generation of larger data sets in a relatively short time period. Various additional advantages specific to the research question at hand also exist. For example, of interest to this project is the sequential development of the immune system. During development, innate inflammatory cells begin to appear at approximately 15 hours post fertilization (hpf). However, functional adaptive immune cells do not arise until after two weeks post fertilization [198][199]. Therefore, early larval studies provide a model to investigate innate inflammatory reactions without complications from adaptive immune signalling mechanisms.

These advantageous features give rise to three major approaches to zebrafish research. The first of these is genetic manipulation for identification and characterisation of genes and the processes they govern. Early zebrafish work involved large-scale mutagenesis screens which induced random mutations with the chemical mutagen ethylnitrosourea (ENU) [200][201]. These large-scale forward genetic screens are simply assessed in zebrafish by phenotypic screening using optical microscopy. Genetic alterations can also be generated using reverse-genetics approaches including permanent gene inactivation via TILLING [202] and transient knockdown using morpholinos [203]. Finally, transgenic approaches using transposon-mediated transgenics [204] facilitates generation of a continually expanding catalogue of transgenic zebrafish lines. Implementation of these genetic

approaches, both individually and in combination, have been used to identify a great number of genes, characterise the processes they control and monitor alterations in disease states [196]. These approaches have also been used to develop genetic disease models for broader studies. These disease models are now commonly utilised for the second major pillar of zebrafish research; drug discovery. Efficient embryo production, rapid development and optical transparency place zebrafish in an ideal position as an *in vivo* vertebrate model for large-scale pharmacological drug screens for identification of lead compounds and preliminary pharmacodynamic investigations [205]. Recent technological advances in robotics have further enhanced productivity and small-molecule screens in zebrafish have led to the discovery of various classes of small molecules for further study in numerous disease settings [206]–[209]. The final major approach to zebrafish studies is *in vivo* imaging. Optical transparency of embryonic and larval developmental stages allows monitoring of cellular interactions in real time. Incorporation of *in vivo* imaging with genetic approaches discussed above allows monitoring and manipulation of disease processes and gives unprecedented access to cellular interactions *in vivo*.

The use of the zebrafish as cancer model was proposed as early as the 1980's, when exposure to carcinogens was found to cause tumour formation [210]. Since then, a great many cancer models have been developed using various approaches and targeting numerous different tissues, reviewed in [211]. These models have contributed to enhancing our understanding of cancer mechanisms *in vivo*. One of the first transgenic zebrafish cancer models to be developed expressed the Myc oncogene under the control of the *rag2* promoter to model leukaemia and found that fluorescently labelled transformed cells could be monitored and tracked *in vivo* [212]. A number of melanoma models have been developed using the BRAF [213] and RAS oncogenes [70][214]. These models were subsequently used to identify cancer-associated genes using the miniCoopR approach [215] and to monitor melanocyte differentiation and cell fate [216] and leukocyte recruitment to transformed cells [192]. Comparative genomic studies in a zebrafish T cell acute lymphoblastic leukaemia has been used to identify functionally important cancer genes [217].

Recently, a new model which allows conditional induction of epithelial cell transformation in larval zebrafish was developed for the study of very early oncogenic processes *in vivo* [74][218]. This KalTA4-ER^{T2}/UAS based system permits temporal and spatial control of oncogene expression so oncogenic processes can be assessed from the very earliest stages of inception. These models, and others [211], highlight the significant contribution of zebrafish research to the cancer field, and demonstrates the versatility and range to the model system.

1.9 Approaches to assess cancer metabolism *in vitro* and *in vivo*

As discussed above, complex metabolic alterations occur in cancers (See Section 1.5 and 1.6). This complexity necessitates a variety of technical approaches to thoroughly elucidate these intricate metabolic mechanisms and evaluate their contribution to cancer development and progression. Both *in vitro* and *in vivo* approaches have been developed to assess metabolic processes, all of which help further our understanding of cancer metabolism, but also present challenges which must be addressed.

In vitro metabolic studies can generally be divided into three main categories; nutrient utilisation, metabolomics and functional assays, with each of these broken-down into further sub-categories. Nutrient up-take by cancer cells can be monitored directly using nutrient analogues which cannot be fully metabolised. For instance, accumulation of the fluorescently-labelled glucose analogue 2-(N-(7-nitrobenz-2-oxa-1,3-diazol-4-yl)amino)-2-deoxyglucose (2-NBDG) in cells can be measured using a simple spectrophotometer to assess glucose uptake [219]. Similar approaches are used using radio-labelled nutrient analogues. Substrate utilisation can also be assessed indirectly by measuring depletion from the cell medium using enzymatic assays which couple metabolic substrates and intermediates to probes which can be detected by fluorescence read-out [220]. Commercial kits are widely available to assess a variety of metabolic substrates using these approaches, providing useful insights into the substrates utilised by cancer cells and helping guide the focus of experimental projects towards more sophisticated mechanistic approaches.

However, considering the limited amount of information that can be gained about a single nutrient from these simple experiments, they often prove relatively expensive.

Metabolomics, on the other hand, provides a much more detailed assessment of the metabolic profile of a sample, with a number of approaches available. Nuclear magnetic resonance spectroscopy (NMR), gas chromatography-mass spectrometry (GC-MS) and liquid chromatography-mass spectrometry (LC-MS) can all be employed, the choice of which is dependent on metabolites of interest and level of detail required. NMR is highly reproducible and produces robust results but offers low sensitivity and metabolite coverage. GC-MS and LC-MC, often used in combination, are much more specific and offer a broader metabolite range but are often difficult to reproduce [220]. These approaches can be utilised to gain detailed insights into metabolic parameters, including substrate utilization and flux through the various metabolic pathways. However, the specialist nature of these techniques makes them expensive and necessitates equipment and resources not readily available to all researchers.

While these nutrient utilisation and metabolomic approaches provide detailed information on metabolite levels, functional assays allow for detailed assessment of energetic processes. So-called Seahorse assays have been developed to test glycolytic and respiratory function in real-time in response to system manipulation [221]. These assays measure oxygen consumption rate (OCR) and extracellular acidification rate (ECAR) as read-outs for mitochondrial functions and glycolysis, respectively, and are widely used with cellular systems to determine metabolic phenotype [222][223]. While these assays are highly sensitive and provide real-time information, they require specialist analysers and costly consumables.

Overall, these *in vitro* approaches provide a detailed insight into the metabolic profile of cellular systems and how they change in response to manipulation. However, it is well established that the tumour microenvironment plays a vital role in cancer development. The complex cellular inter-play between cancer cells and other cells in the surrounding microenvironment simply cannot be replicated *in vitro* and, therefore, to fully understand the role of metabolic processes in cancer, *in vivo*

approaches must be considered. The metabolomics approaches described above can also be utilised *in vivo* and have successfully been used to determine metabolic profiles in various murine [224]–[226]and zebrafish models. [227]–[229] Despite this, an additional major caveat to this approach must be considered; the amount of substrate required is often limiting, be that technically, financially or ethically. As technology advances and these techniques are fine-tuned to be able to accommodate smaller and smaller samples this limitation may be overcome to allow the metabolomics approach to become the gold standard for metabolism research, but this constraint is presently a barrier for many *in vivo* applications.

In vivo imaging techniques have been developed and utilised to monitor metabolic processes both in research and in the clinic. As mentioned previously, PET imaging uses an FdG glucose analogue tracer to quantifiably monitor glucose uptake in patients for both diagnosis and disease monitoring [94]–[99]. Amino acid and lipid metabolism can also be assessed by PET imaging using appropriate probes, including ^{18}F-fluoro- ethyl-tyrosine (FET) [230], ^{11}C-methionine [230], ^{18}F-flurothymidine (FLT) [231], ^{18}F-choline [232] and ^{11}C-acetate [233], all of which have been successfully utilised in the clinic.

Due to the sensitive, quantifiable and longitudinal *in situ* details gained from *in vivo* imaging, this approach is highly desirable for mechanistic metabolic investigations in addition to clinical monitoring. As discussed above, the zebrafish presents itself as an ideal model organism for such investigations, with the optical transparency of larval stages and genetic tractability providing clear advantages over their rodent counterparts. To date, a variety of fluorescently-labelled metabolic tracers have been used in zebrafish models to investigate glycolytic and mitochondrial processes, as well as lipid metabolism [234]. Transgenic zebrafish lines have been developed to monitor gluconeogenesis, hypoxia and ROS production [229], [235], [236]. Despite these advances, the potential of the zebrafish for *in vivo* monitoring of metabolic processes has yet to be fully realised. The number of both probes and transgenic lines available remains limited and this lack of tools hinders progress in the field. Development of new transgenic zebrafish lines for specific

metabolic processes would allow unprecedented insights into metabolic mechanisms *in vivo* and in real-time. Combining these new tools with the metabolomic approaches described above would provide a powerful and more complete picture of metabolic landscapes in numerous disease settings, including cancers, and increase our disease understanding, potentially leading to diagnostic or therapeutic targets.

1.10 Hypothesis and Aims of the Project

While it has been established that metabolic and mitochondrial alterations are important features of cancers, their role during tumour initiation and development are less well defined. The hypothesis for this project is that metabolic and mitochondrial alterations occur at the very early, pre-neoplastic cell (PNC) stage of tumour initiation *in vivo* and are important for development and survival of pre-neoplastic cells. Specifically, it is hypothesised that upregulation of the oncogene $HRAS^{G12V}$ leads to disruption of the mitochondrial network, causing a metabolic shift towards glycolysis and subsequent lactate production. This lactate may then alter inflammatory cell recruitment and behaviour and polarise the tumour microenvironment towards pro-tumourigenic functions (**Figure 1.9**).

The overall aim for the project is to begin to define a mitochondrial and metabolic phenotype for PNCs at very early stages of tumour development and determine the effect of phenotype manipulation on PNC growth and survival. Specifically, the aims of the project are to:

- characterise a recently developed model for conditional epithelial cell transformation in superficial skin cells of the larval zebrafish,
- investigate mitochondrial morphology in PNCs at very early stage of development,
- investigate functional characteristics of the mitochondrial phenotype in developing PNCs,
- investigate glycolytic metabolism in PNCs at very early stages of development,

- identify potential therapeutic targets for further study of cancer prevention mechanisms.

Characterisation of metabolic and mitochondrial alterations at very early stages of tumour initiation and development will not only enhance our understanding of mechanisms of both tumour initiation and cancer persistence but may lead to identification of potential target for cancer prevention and/or therapeutic intervention.

This thesis first addresses characterisation of a newly developed zebrafish model for cancer initiation. Following this, mitochondrial phenotype and glycolytic alterations and the consequential effects in PNCs are described. The thesis then explains new tools under development for metabolic investigations in a zebrafish model. Finally, the findings of the thesis are discussed in the context of current knowledge in the field and future directions for the project are proposed.

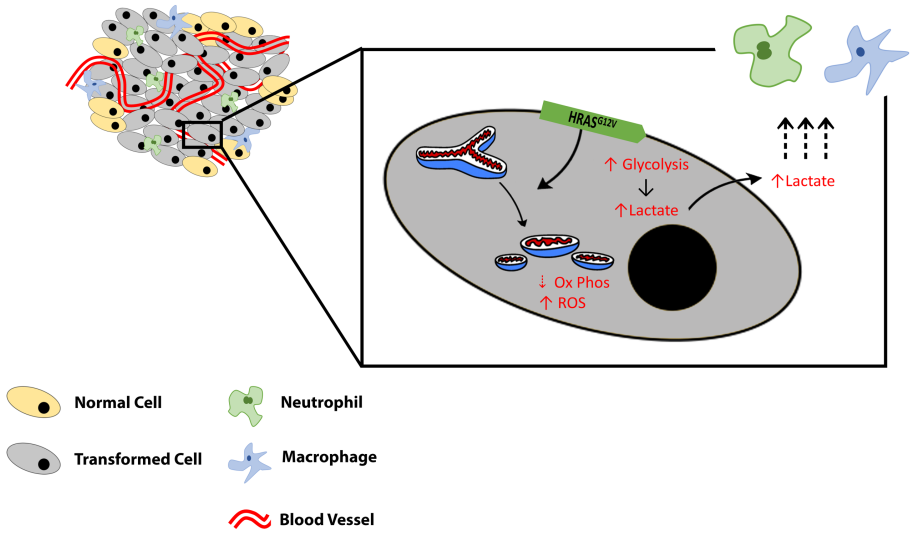

Figure 1.9 Schematic representation of the project hypothesis. The hypothesis for this project is that HRAS^{G12V} upregulation causes mitochondrial disruption leading to a metabolic shift towards glycolysis and a subsequent increase in lactate levels. This lactate alters inflammatory cell recruitment and creates a pro-tumourigenic environment.

2. Materials and Methods

2.1 Solutions

Unless specified, all reagents were sourced from Sigma-Aldrich.

30x Danieau's Solution (Diluted to appropriate concentration in H_20)

NaCl	1.7 M
KCl	21 mM
$MgSO_4.7H_20$	12 mM
$Ca(NO_3)_2$	18 mM
HEPES buffer	150 mM
H_20	

Embryo Medium

Zebrafish System Water

0.1% Methylene Blue

Induction Solution

0.3x Danieau's Solution

DMSO	5 µl/ml
4-Hydroxy Tamoxifen	5 µM

LB Broth

Tryptone	10 g
Yeast Extract	5 g
NaCl	5 g
NaOH	1 M, 1 ml
H_2O	

PBT

PBS

0.1% Triton X-100

Calcium-free Ringers Solution

HEPES	5 mM
KCl	2.9 mM
NaCl	116 mM

2.2 Construct Generation

2.2.1 Bacterial Transformation and DNA Purification

25 µl of One Shot™ TOP10 chemically competent *E. coli* (Invitrogen) were thawed on ice. 1 µl of reaction mix was added and gently mixed. Cells were incubated on ice for 30 minutes then heat-shocked at 42 °C for 30 seconds. Cells were incubated on ice for 2 minutes followed by addition of 250 µl of SOC medium (Invitrogen). Cells were incubated at 37 °C, 200 rpm for 1 hour. Cells were then plated onto appropriate antibiotic selection LB agar plates and grown at 37 °C for 18 hours.

Bacterial colonies were selected and grown in appropriate antibiotic selection LB broth at 37 °C, 200 rpm. DNA plasmids were purified using the QIAgen Spin Miniprep kit (Ref 27106), according to manufacturer's instructions and purified using Zymo Research DNA clean & concentrator kit (Cat. No. D4033) according to manufacturer's instructions.

2.2.2 Genetic Cloning

All cloning procedures were carried out using Multisite Gateway® Cloning Technology (Invitrogen). Unless otherwise stated, all reagents and plasmids were sourced from Invitrogen.

DNA of interest was PCR amplified using attB site containing primers (**Table 1**). PCR reactions were set up according to **Table 2** and run according **to Table 3**. The resulting PCR product was purified using Zymo Research DNA clean & concentrator

kit (Cat. No. D4033), according to manufacturer's instructions. 15 femtomoles of purified PCR product was combined with 100 ng of pDONR221 donor vector in TE buffer in a total volume of 8 µl, followed by addition of 2 µl of BP Clonase II enzyme mix. The reaction mix was incubated at 25 °C for a minimum of 16 hours. To isolate pME vectors, reaction mix was transformed into TOP10 competed cells, cultured (Kanamycin 50 µg/ml, Sigma-Aldrich) and purified as described above. pME entry clone generation was confirmed by sequencing with M13 Forward and T7 Reverse primers.

5 femtomoles of each required entry clone was combined with 10 femtomoles of pDest destination vector (**Table 4**) in TE buffer in a total volume of 8 µl, followed by addition of 2 µl of LR Clonase II enzyme mix. The reaction mix was incubated at 25 °C for a minimum of 16 hours. To isolate DNA plasmids, reaction mix was transformed into TOP10 competed cells, cultured (Ampicillin 50 µg/ml, Sigma-Aldrich) and purified as described above. DNA plasmid generation was confirmed by sequencing with M13 Forward and T7 Reverse primers using the Mix2Seq sequencing kit (Eurofins Genomics).

Table 1: attB site containing primer sequences for PCR amplification of DNA for Multisite Gateway cloning

Construct	Primers
Matrix-roGFP (Addgene Plasmid Number 49437)	**Fw:** GGGGACAAGTTTGTACAAAAAAGCAGGCTCCGGCGGCACCATGCTGAGCCTGCGCCA **Rev:** GGGGACCACTTTGTACAAGAAAGCTCCGTCTTACTTGTACAGCTCGTCCATGCCGAG
Cyto-roGFP (Addgene Plasmid Number 49435)	**Fw:** GGGGACAAGTTTGTACAAAAAAGCAGGCTCCGGCGGCACCATGGGCGGTAGGCGTGT **Rev:** GGGGACCACTTTGTACAAGAAAGCTCCGTCTTACTTGTACAGCTCGTCCATGCCGAG
GPD-roGFP (Addgene Plasmid Number 49436)	**Fw:** GGGGACAAGTTTGTACAAAAAAGCAGGCTCCGGCGGCACCATGGTACCGTTTAAACT

	Rev: GGGGACCACTTTGTACAAGAAAGCTCCGTCTTACTTGTACAGCTCGTCCATGCCGAG
pcDNA3.1:Peredox-mCherry (Addgene Plasmid Number 32383)	**Fw:** GGGGACAAGTTTGTACAAAAAAGCAGGCTGCCGCCACCATGgttgctagcaaagttcctgaa **Rev:** GGGGACCACTTTGTACAAGAAAGCTGGGTCtcacttgtacagttcgtccatgccgcc

Table 2: PCR reaction mix for amplification of DNA fragments for Multisite Gateway cloning

Template DNA	100 ng
Pfu Polymerase (NEB)	1 µl
10 Pfu Buffer (NEB)	5 µl
dNTP Mix (NEB)	0.5 µl
Fw Primer (10 µM stock)	1 µl
Rev Primer (10 µM stock)	1 µl
Nuclease Free H_2O	

Table 3: PCR Cycling Conditions for amplification of DNA fragments for Multisite Gateway cloning

Initial Denature	95 °C	2 minutes	
Denature	95 °C	30 seconds	32 Cycles
Anneal	Primer Optimised	30 seconds	
Extension	72 °C	3 minutes	
Final Extension	72 °C	7 minutes	

Table 4: Vectors used for construct generation with Multisite Gateway cloning.

Final Construct	p5E	pME	p3E	pDEST
UAS:eGFP-CAAX	p5E-6xUAS (A kind gift from Dr. Dirk Sieger)	pME:eGFP-CAAX (A kind gift from Dr. James Minchin)	p3E-PolyA	pDestTol2CG2
Ubi:Matrix-roGFP [237]	p5E:Ubi	pME:Matrix-roGFP	p3E-PolyA	pDestTol2CG2
Ubi:Cyto-roGFP [237]	p5E:Ubi	pME:Cyto-roGFP	p3E-PolyA	pDestTol2CG2
Ubi:GPD-roGFP [237]	p5E:Ubi	pME:GPD-roGFP	p3E-PolyA	pDestTol2CG2
Ubi:Laconic [238]	p5E:Ubi	pME:Laconic (Commercially synthesised)	p3E-PolyA	pDestTol2Cry-CFP
UAS:Laconic [238]	p5E-6xUAS (A kind gift from Dr. Dirk Sieger)	pME:Laconic (Commercially synthesised)	p3E-PolyA	pDestTol2Cry-CFP
Ubi:Pyronic [239]	p5E:Ubi	pME:Pyronic (Commercially synthesised)	p3E-PolyA	pDestTol2Cry-CFP
Ubi:Perceval-HR [240][241]	p5E:Ubi	pME:Perceval-HR (Generated by Dr. Derek Laux, Feng group)	p3E-PolyA	pDestTol2Cry-CFP
Ubi:Peredox-mCherry [242]	p5E:Ubi	pME: Peredox-mCherry	p3E-PolyA	pDestTol2Cry-CFP

2.3 Tol2 Synthesis

Tol2 RNA was generated using pT3TS/Tol2 [243], which was linearized by restriction digest using BamHI (NEB) overnight at 37 °C, then transcribed using an mMessage mMachine T3 Kit (Invitrogen AM1348), according to manufacturer's instructions.

5 µl restriction digest product was mixed with 2 µl 10x buffer, 10 µl NTP mix, 2 µl enzyme mix and 1 µl nuclease-free H_2O. The synthesis mix was incubated at 37 °C for 2 hours. Template DNA was degraded by incubating the reaction product in DNase mix for 15 min at 37 °C. RNA was extracted by standard phenol/chloroform extraction and resuspended in nuclease-free water.

2.4 Zebrafish Husbandry

Adult zebrafish (*Danio rerio*) were maintained according to standard practice [197]. Transgenic lines used during the project are shown in **Table 5** and maintained under Home Office license, held by Dr. Yi Feng. Wild-type TUE, maintained by the CBS Aquatics Facility at The University of Edinburgh, were also used during the project.

Zebrafish embryos were maintained at 28.5 °C for up to five days. For experimental purposes, embryos were anaesthetised by treatment with 0.02% buffered 3-aminobenzoic acid ethyl ester (Tricane) (Sigma Aldrich), unless otherwise stated.

Table 5: Transgenic lines used throughout the project

Transgenic Line	Phenotype	Reference
Krt4:KalTA4-ER^{T2}	Superficial skin specific inducible expression of genes under control of UAS, green heart selection marker	[74]
UAS:eGFP-HRAS^{G12V}	Expression of eGFP-HRAS^{G12V} when combined with GAL4 transcriptional activator, green heart selection marker	[74]
LysC:DsRed	Red fluorescent neutrophils	[244]
Ubi:Matrix-roGFP	Mitochondrial Matrix redox sensor, green heart selection marker	Unpublished, Generated during this project
Ubi:SecA-YFP	Fluorescently labelled Annexin V	Unpublished, Generated by Ziyuan (Elva) Chang, Feng Group

2.5 Microinjection of zebrafish eggs

Adult zebrafish were set-up in segregated pairs overnight. The subsequent morning pairs were mixed, and fertilized eggs were promptly collected following mating. Eggs were aligned on a microinjection plate and injected into the blastodisc of the one-cell stage, no more than 20 minutes post fertilisation using a borosilicate glass capillary needle (World Precision Instruments 1B100F-4) and pneumatic pico pump (Warner Instruments PLI-90A) with the aid of a micro-manipulator. Injection solution was composed of DNA construct (15 ng/µl), Tol2 RNA (20 ng/ µl, see section 2.3), 5x Danieau's Solution, Nuclease-free H_2O. DNA constructs used during the project are shown **in Table 6**.

Table 6: Constructs used for microinjection throughout the project.

DNA Construct	Phenotype	Origin
UAS:eGFP-HRAS^{G12V}	Expression of eGFP-HRAS^{G12V} when combined with GAL4 transcriptional activator, green heart selection marker	Dr. T. Ramezani (Dr. Yi Feng Group) [74]
UAS:eGFP-CAAX	Expression of eGFP-CAAX when combined with GAL4 transcriptional activator, green heart selection marker	L. Kelly, Generated during this project
UAS:mCherry-HRAS^{G12V}	Expression of mCherry-HRAS^{G12V} when combined with GAL4 transcriptional activator, green heart selection marker	I. Riberio Bravo (Dr. Yi Feng Group), Unpublished
UAS:mCherry-CAAX	Expression of mCherry-CAAX when combined with GAL4 transcriptional activator, green heart selection marker	I. Riberio Bravo (Dr. Yi Feng Group), Unpublished
Ubi: Matrix-roGFP	Mitochondrial Matrix redox sensor, green heart selection marker	L. Kelly, Generated during this project, original construct
Ubi:Laconic	Intracellular Lactate Sensor	L. Kelly, Generated during this project, original construct
UAS:Laconic	Intracellular Lactate Sensor	L. Kelly, Generated during this project, original construct

Post injection, eggs were maintained in embryo medium at 50 eggs per plate until 6 hpf, at which point non-viable embryos were removed. Embryos were maintained at 28.5 °C until experimental time-points or grown to adulthood, as previously described.

2.6 Generation of Transgenic Zebrafish Lines

Wild-type TUE fish were mated, and eggs injected with DNA constructs, as previously described. 3 dpf embryos were screened for selection marker and reporter expression. Positive embryos were grown to adulthood, according to standard practice [197]. Adult fish were crossed to TUE fish and embryos were screened for selection marker and reporter expression to identify founder fish. A minimum of two founder fish were identified for each transgenic line, and the embryos grown to adulthood. Transgenic lines were established and characterised based on screening of F2 generation.

2.7 Induction of UAS/KalTA4-ER^{T2} mediated gene expression

Krt4:KalTA4-ER^{T2} fish were mated and eggs were injected with UAS:eGFP-HRAS^{G12V}, as previously described. At 2 dpf eggs were screened to remove non-viable embryos and placed in induction solution (Section 2.1). As 4-hydroxy tamoxifen is light sensitive, embryos were maintained in the dark until specific experimental time-points. Embryos were monitored for fluorescent HRAS^{G12V} expression and screened for PNC clone coverage using a Leica M205 stereoscope fitted with GFP, DsRed, or CFP filters, as appropriate. Unless otherwise stated, this mating and injection protocol was used for all experiments.

2.8 Chemical treatment

Embryos were screened at appropriate time points and treated with 1 µM mDIVI (Sigma-Aldrich) or 100 mM 2DG (Sigma-Aldrich) by immersion at 28.5 °C for specified time-frames, determined by experimental requirements. For glucose

supplementation, 100 mM D-Glucose solution (Sigma-Aldrich) was injected into the yolk sac at specified time points.

2.9 Electron Microscopy

Embryos were anesthetised and imaged (without embedding) using a Leica M205 stereoscope fitted with a GFP filter. Embryos were fixed in primary electron microscopy fixing solution (4% glutaraldehyde, 1% paraformaldehyde, 0.05 M sodium cacodylate, 1 mM $MgSO_4$, 1% sucrose, H_20, solution sourced from the COIL facility at the Wellcome Trust Centre for Cell Biology, The University of Edinburgh) for 30 minutes at 4 °C with light shaking, before embryo decapitation and return to primary electron microscopy fixing solution overnight at 4 °C with light shaking.

Samples were then sent to the COIL facility at the Wellcome Trust Centre for Cell Biology, The University of Edinburgh for further processing. Briefly, samples were washed with 0.1 M cacodylate buffer then incubated in secondary electron microscopy fixing solution (2% OsO_4, 0.1 M cacodylate buffer, H_2O) for 2 hours at room temperature. Embryos were washed with 0.1 M cacodylate buffer then serial dehydrated with ethanol. Samples were then infiltrated with epoxy resin and hardened to produce sample blocks for sectioning. These steps, as well as sectioning and preparation for imaging were completed by Dr. Steven Mitchell at the COIL facility at the Wellcome Trust Centre for Cell Biology, The University of Edinburgh.

Samples were imaged using a Jeol JEM1400 Plus Transmission Electron Microscope at the COIL facility at the Wellcome Trust Centre for Cell Biology, The University of Edinburgh, with assistance from Dr. Steven Mitchell. Images were viewed using FIJI (Version 2.0.0-rc-65/1.52b).

2.10 Confocal Microscopy

Embryos were anesthetised, screened and transferred to a glass bottomed 35 mm imaging dish. 1% low-melting point agarose (Thermo Fisher Scientific) was heated to 80 °C (or until melted) then allowed to cool before addition to embryos. Embryos were appropriately aligned on the imaging dish using a pointed manipulator

prior to agarose setting. Once agarose was completely set, an appropriate volume of solution was added to the dish, determined by specific experimental requirements. Images and time-lapse videos were captured using a Leica TCS SP5 confocal microscope with installed Leica LAS AF software, Leica TCS SP8 confocal microscope with installed Leica LAS X software or Andor XDi Spinning disk confocal microscope with installed Andor iQ3 software, using the appropriate optical lens, as indicated.

2.10.1 Observation of PNC phenotype by long-term *in vivo* imaging

Embryos were screened at appropriate time points and embedded, as described above. Embryos were imaged using an Andor XDi Spinning disk confocal microscope fitted with a Super Apochromat 20x objective lens at 10-minute intervals for a duration of 24 hours. Videos were viewed using Imaris 8 (Version 8.3.1). Tile-scan images of whole embryos were obtained using a Leica TSM SP8 confocal microscope fitted with an HC PL APO 10x CS2 objective lens at a pixel density of 512x512. Images were viewed using FIJI (Version 2.0.0-rc-65/1.52b).

2.10.2 *In vivo* live imaging of Annexin V localisation

Ubi:SecA-YFP fish were crossed to Krt4:KalTA4-ER^{T2} fish and eggs were injected with UAS:mCherry-HRAS^{G12V} followed by induction at 2 dpf, as previously described. Embryos were screened for YFP (Annexin V) and mCherry (PNC) expression at appropriate time points and embedded as described above. Embryos were imaged using a Leica TSM SP5 confocal microscope fitted with an HCX PL APO W 40x water immersion objective lens at a pixel density of 512x512 with bidirectional scanning using the 514 nm argon and 543 nm lasers. Images were viewed using FIJI (Version 2.0.0-rc-65/1.52b).

2.10.3 Analysis of neutrophil recruitment by *in vivo* imaging

LysC:DsRed fish were crossed to Krt4:KalTA4-ER^{T2} fish and eggs were injected with UAS:eGFP-HRAS^{G12V} followed by induction at 2 dpf, as described previously. Embryos were screened for DsRed (neutrophils) and GFP (PNCs) expression at appropriate time points and embedded as described above. Embryos were imaged using an Andor XDi Spinning disk confocal microscope fitted with a Super Apochromat 20x objective lens at 10-minute intervals for a duration of 24 hours using the 488 nm and 561 nm lasers. Videos were viewed and analysed using Imaris 8 (Version 8.3.1). Neutrophil recruitment was assessed by using the Spots module to monitor the number of neutrophils at each time-frame of the movie. The number of PNCs in the first frame of the movie was manually counted for normalisation.

For drug treatment experiments, drugs were added approx.30 minutes prior to the start of time-lapse imaging. Time-lapses were imaged using a Leica TSM SP5 confocal microscope fitted with an HC PLAN APO 20x objective lens at a pixel density of 512x512 at intervals of 2 minutes for a duration of approximately 16 hours using the 488nm and 543 nm lasers. Movies were viewed and analysed using Imaris 8 (Version 8.3.1). Neutrophil recruitment was assessed by using the Spots module to monitor the number of neutrophils at each time-frame of the movie. The number of PNCs in the first frame of the movie was manually counted for normalisation.

2.10.4 *In vivo* live Imaging of Laconic

UAS:Laconic was co-injected with UAS:mCherry-HRAS^{G12V} into Krt4:KalTA4-ER^{T2} fertilised eggs and induced at 2 dpf, as described previously. Embryos were screened for reporter (and PNC, as necessary) expression at appropriate time points and embedded as described above. Embryos were imaged using a Leica TSM SP8 confocal microscope fitted with an HC PL APO 40x CS2 objective lens at a pixel density of 512x512 with bidirectional scanning using the 514 nm and 561 nm lasers.

TFP and YFP emission collection ranges were determined by lambda scanning using the 514 nm laser. Emission peaks were detected at 495 nm and 530 nm, as expected. Emission collection bands were set to a 20 nm range centred on each of

these peaks to isolate YFP and TFP fluorescent channels. Images were acquired sequentially to reduce bleed-through. An additional mCherry channel was added for PNC imaging, excited using the 561 nm laser and acquired during the same scan sequence as the TFP channel.

Images were viewed and analysed using FIJI (Version 2.0.0-rc-65/1.52b) and FIJI ratio profiler was used to generate a YFP/TFP channel.

2.11 Immunohistochemistry

Unless otherwise stated, all washes and incubation steps were carried out at room temperature with light shaking (60-65 rpm). For mDIVI and 2DG treatment experiments, embryos were treated 16 hours prior to fixation.

Embryos were screened for PNC expression at appropriate time points and fixed in 4% PFA for 2 hours at room temperature (static). Embryos were washed 3 times with PBT for 5 minutes, before incubation with blocking solution (PBT + 5% Goat serum (Sigma-Aldrich)) for 2 hours. Embryos were incubated in primary antibody according to **Table 7**. Embryos were washed 10 times in PBT for 15 minutes, followed by incubation in secondary antibody (1:200 Alexa Fluor 488 goat anti-rabbit IgG (H+L) Invitrogen A11008 or Alexa Fluor 633 goat anti-rabbit IgG (H+L) Invitrogen A21071) for 2 hours. Embryos were washed 3 times in PBT. Where appropriate, embryos were incubated with Hoechst 33342 for 30 minutes, followed by 3 washes with PBT. Embryos were embedded and imaged, as described previously.

PCNA samples were imaged using a Leica TSM SP5 confocal microscope fitted with an HCX PL APO W 40x water immersion objective lens at a pixel density of 512x512 with bidirectional scanning using the 488 nm and 633 nm. Images were viewed using FIJI (Version 2.0.0-rc-65/1.52b).

Table 7: Antibodies used for immunohistochemistry

Antibody	Concentration	Staining Conditions
GFP (D5.1)XP® Rabbit mAB (Cell Signalling Technology 2956)	1:200	4 °C, overnight
Purified Rabbit Anti-active Caspase 3 (BD 559565)	1:200	Room temperature, 2 hours
Anti-PCNA (Sigma SAB2701819-100ul)	1:200	4 °C, overnight

Caspase 3 samples were imaged using a Leica TSM SP8 confocal microscope fitted with an HC PL APO 40x CS2 objective lens at a pixel density of 1024x1024 with bidirectional scanning using the 488 nm and 633 nm lasers. Samples were quantified by manual cell count of PNCs and caspase 3 positive cells using FIJI (Version 2.0.0-rc-65/1.52b).

2.12 EdU staining

EdU staining was completed using the Click-iT™ Plus Edu Alexa Fluor™ 647 Imaging Kit (Thermo Fisher Scientific, C10640). Unless otherwise stated, all washes and incubation steps were carried out at room temperature with light shaking (60-65 rpm). For mDIVI and 2DG treatment experiments, embryos were treated 16 hours prior to fixation. For glucose supplementation experiments, D-Glucose was injected into the yolk sac 2 hours prior to fixation.

Embryos were screened at appropriate time points. 500 mM EdU was injected into the yolk sac of embryos 2 hours prior to fixing in 4% PFA for 30 minutes at room temperature. Embryos were incubated with 3% bovine serum albumin (Sigma-Aldrich) in PBT for 5 minutes, PBT for 20 minutes, then 3% bovine serum albumin in PBT for 5 minutes. Embryos were incubated in reaction mix (1x Click-iT reaction

buffer, copper protectant, Alexa Fluor™ picolyl azide, reaction buffer additive, according to manufacturer's instructions) for 30 minutes. Embryos were washed 3 times in PBT for 5 minutes and once in 3% bovine serum albumin in PBT for 5 minutes before immunohistochemistry staining for GFP, as described in section 2.11.

Embryos were imaged using a Leica TSM SP5 confocal microscope fitted with an HCX PL APO W 40x water immersion objective lens at a pixel density of 1024x1024 with bidirectional scanning. Images were viewed using Imaris 8 (Version 8.3.1) or FIJI (Version 2.0.0-rc-65/1.52b).

For quantification of PNC proliferation, PNCs were isolated using the Surfaces module based on absolute GFP intensity in individual images. The EdU channel was subsequently masked outside PNC surfaces and the Spots module was used to count EdU positive cells within the PNC surface. However, due to inaccuracies of PNC surface generation in fixed and antibody stained samples, it became clear that some EdU signal from PNC neighbouring cells was included in the masked channel. Therefore, Edu signal in the masked channel was manually assessed to verify PNC specificity. Percentage of proliferating PNCs was then calculated following manual counting of PNCs. Due to inconsistencies associated with this method of analysis, automated co-localisation of EdU signal with Hoechst staining was also attempted using Imaris and a newly developed nuclear segmentation software package called PickCells (Dr. Sally Lowell Group, The University of Edinburgh), but again 3D segregation of PNCs caused inaccuracies.

To assess Edu signal in the PNC niche, the Edu channel was masked to include all EdU signal inside the PNC surface and within 15 µm (approximately one cell diameter) of the surface. The number of EdU positive cells within this area was then counted using the Spots module. Proliferative capacity was assessed by normalising this automated Edu count to the manual count of the number of PNCs.

2.13 TUNEL staining

TUNEL staining was completed using the Click-iT™ TUNEL Alexa Fluor™ 647 Imaging Assay (Thermo Fisher Scientific, C10247). Unless otherwise, all washes and incubation steps were carried out at room temperature with light shaking (60-65 rpm).

Embryos were screened at appropriate time points and fixed in 4% PFA for 2 hours at room temperature (static). Embryos were washed 4 times with PBT for 5 minutes. Embryos were incubated with proteinase K (10 µg/ml) for 30 seconds followed by 2 rinses with PBT and re-fixation with 4% PFA for 20 minutes at room temperature. Embryos were washed 4 times for 5 minutes with PBT prior to incubation with TdT reaction buffer for 10 minutes at 37 °C with shaking, followed by incubation for 1 hour with TdT reaction mix (TdT buffer, EdUTP, TdT enzyme, according to manufacturer's instructions) at 37 °C. Embryos were washed once for 5 minutes with PBT, then 3% bovine serum albumin in PBT for 30 minutes and again twice for 5 minutes with PBT. Embryos were incubated with Click-iT TUNEL reaction cocktail (1x Click-iT TUNEL reaction buffer, copper protectant, Alexa Fluor™ picolyl azide, 10x Click-iT TUNEL reaction buffer additive, according to manufacturer's instructions) for 30 minutes at 37 °C. Embryos were washed 3 times in PBT for 5 minutes and once in 3% bovine serum albumin in PBT for 5 minutes before immunohistochemistry staining for GFP, as described in section 2.12.

Embryos were imaged using a Leica TSM SP5 confocal microscope fitted with an HCX PL APO W 40x water immersion objective lens at a pixel density of 512x512 with bidirectional scanning. Images were viewed using Imaris 8 (Version 8.3.1).

2.14 MitoTracker Staining

Embryos were screened at appropriate time points then incubated with 500 nM MitoTracker Red CMXRos (Thermo Fisher Scientific M7512) or 500 nM MitoTracker Deep Red FM (Thermos Fisher Scientific M22426) for 30 minutes at 28.5 °C in the dark followed by washing 3 times with 0.3x Danieau's solution for 30 seconds. Embryos were embedded and imaged, as described previously. During

imaging, embryos were maintained in freshly prepared induction solution and kept in the dark. For all mDIVI treatment experiments, embryos were treated two hours prior to staining.

Embryos were imaged using a Leica TSM SP5 confocal microscope fitted with an HCX PL APO 63x glycerol immersion objective lens at a pixel density of 2048x2048. Resulting images were analysed using Imaris 8 (Version 8.3.1). PNCs were isolated using the Surfaces module based on absolute GFP intensity in individual images. Each MitoTracker channel was subsequently masked outside PNC surfaces to allow for analysis of mitochondrial staining specifically within PNCs. Mitochondrial fragments were then isolated using the Surfaces module based on absolute intensity of the respective channels in individual images to generate feature statistics as reported.

Colocalization of dual MitoTracker staining was assessed using the Coloc module of Imaris (Version 8.3.1). Masked MitoTracker channels (above) were plotted on a 2D histogram, followed by automatic calculation of colocalization thresholds. This results in generation of a Coloc channel with a number of associated statistical parameters, including the Pearson's coefficient of colocalization which is independent of fluorescence intensity, as reported.

2.15 Staining for reactive oxygen species

Embryos were screened at appropriate time points then incubated with 5 µM CM-H2DCFDA (Invitrogen C6827) or 10 µM DHE (Invitrogen D11347) for 15 minutes at 28.5 °C in the dark followed by washing 3 times with 0.3x Danieau's solution for 30 seconds. Embryos were embedded and imaged, as described previously. During imaging, embryos were maintained in freshly prepared induction solution and kept in the dark.

Embryos were imaged using a Leica SP5 confocal microscope fitted with a HC PLAN APO 20x objective lens at a pixel density of 512x512 with bidirectional scanning. Images were viewed using Imaris 8 (Version 8.3.1).

2.16 Characterisation of Ubi:Matrix-roGFP

F2 generation Ubi:Matrix-roGFP embryos were screened for reporter expression at 3 dpf. Positive embryos were embedded for imaging, as described previously. Embryos were imaged using the Andor XDi Spinning disk confocal microscope fitted with a Super Apochromat 20x objective lens.

Still images were taken prior to wounding. Embryos were wounded using the 337 nm nitrogen laser as part of the MicroPoint module, immediately followed by time-lapse capture at 140 millisecond intervals for a duration of 45 minutes post wounding. Movies were viewed using Imaris 8 (Version 8.3.1).

2.17 Analysis of glucose uptake

Embryos were screened at appropriate time points. 5 mg/ml 2-NBDG (Invitrogen) or 100 mM Se-NBD-glucose (Vendrell group, The University of Edinburgh) was injected into the vasculature immediately followed by embryo embedding, as previously described. Embryos were embedded and imaged 1-hour post injection using a Leica TSM SP8 confocal microscope fitted with an HC PL APO 40x CS2 objective lens at a pixel density of 1024x1024 with bidirectional scanning. Images were viewed using Leica LASX software (Version 1.1.0.12420).

2.17.1 Characterisation of Se-NBD-glucose *in vivo*

Wild-type TUE eggs were collected from natural matings and injected (as previously described) with 4.2 ng/embryo Anti-sense *glut2* morpholino (5'-ATGACCTGCAGAC AACAAGGACACC-3') [245]. At 28 hours post fertilisation, control and *glut2* morphants were injected into the yolk sac with 100 mM SE-NBD-glucose followed by embryo embedding as described above. Embryos were imaged using a Leica TSM SP8 confocal microscope fitted with an HC PL APO 10x CS2 objective lens at a pixel density of 512x512. Images were viewed using Leica LASX software (Version 1.1.0.12420).

2.18 Analysis of neutrophil recruitment to a tailfin wound

LysC:DsRed eggs were collected from natural matings and maintained according to standard protocol. At 3 dpf, embryos were screened for fluorescent neutrophils. Tailfin transection was performed just below the tip of the notochord using a scalpel. Embryos were treated with 100 mM 2DG. At 6 hpw, embryos were fixed with 4% PFA for 2 hours at room temperature. Embryos were embedded as described above and imaged using a Leica SP5 confocal microscope fitted with a HC PLAN APO 20x objective lens at a pixel density of 512x512 with bidirectional scanning. Images were viewed and analysed using FIJI (Version 2.0.0-rc-65/1.52b). For analysis of neutrophil recruitment, all neutrophils within 200 µm of the wound site were manually counted.

2.19 Respiratory and Glycolytic Measurements

Oxygen consumption rates (OCR) and extracellular acidification rates (ECAR) were collected using the Seahorse XFe24 Extracellular Flux Analyser (Agilent Technologies). All experiments were carried out in collaboration with Dr. Roderic Carter, Morton Group, The University of Edinburgh.

Sensor cartridges were hydrated overnight in Seahorse XF Calibrant Solution (Agilent Technologies). Approximately 45 min prior to the start of the experiment, 75 µl of appropriate treatments (see **Table 8** and **Table 9**) were loaded into injection ports on the sensor cartridge plate and inserted into the XFe24 analyser for calibration.

Embryos were anaesthetised by treatment with 55 mg/L eugenol (Sigma), screened, dechorionated, and loaded into an islet capture plate (Agilent Technologies) (1 embryo/well) in a randomised order according to **Figure 2.1**. Islet capture screens were added to keep embryos in position. A final volume of 525 µl 0.3x Danieau's Solution was added to each well. Islet capture plate was incubated at 27 °C until sensor calibration was complete.

Following sensor calibration, the islet capture plate was loaded into the XFe24 analyser. The experimental protocol assigned to the plate is outlined in **Table**

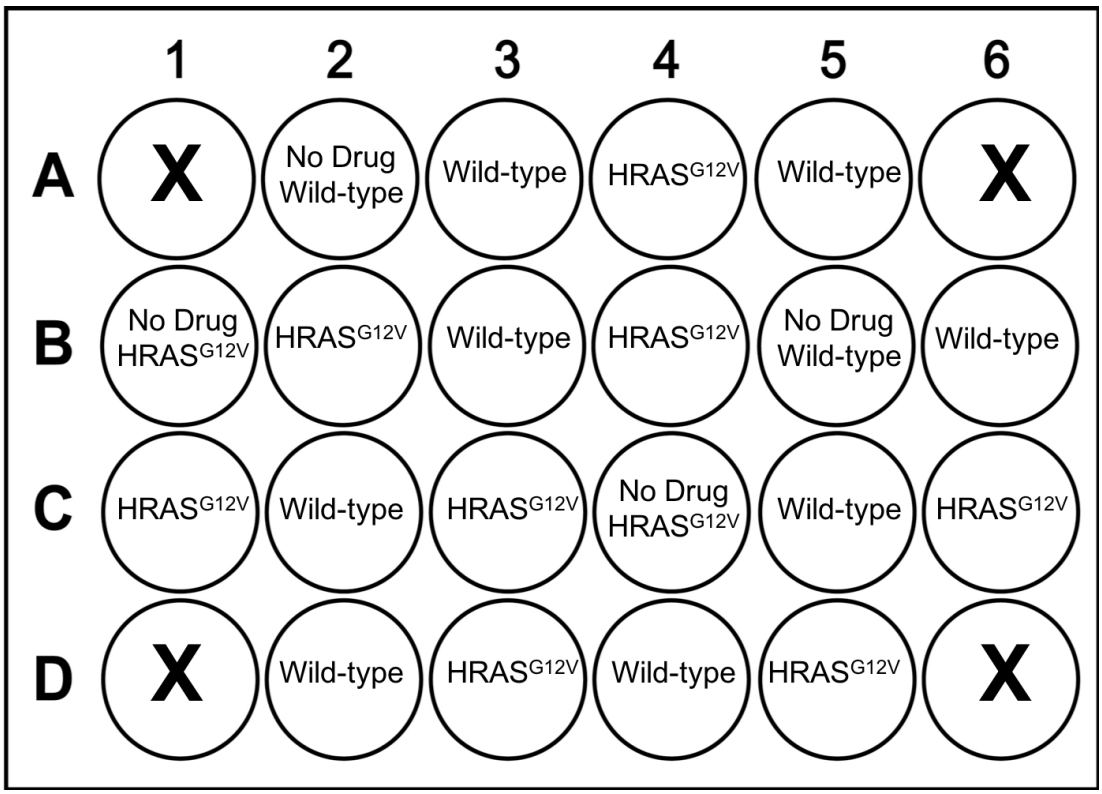

Figure 2.1: Plate layout for respiratory and glycolytic measurements. Islet capture plate was loaded (1 embryo/well) in a randomised order. Four well were left empty (marked X) to normalise for temperature fluctuations across the plate. Four well held embryos that were treated with only Danieau's solution to normalise for technical fluctuations resulting from drug injection.

8 or **Table 9,** as appropriate. Experiments were carried out at approximately 27 °C (+/- 1 °C). All treatments used were from Seahorse XF Cell Mito Stress Test Kit (Agilent technologies 103015-100) or Seahorse XF Glycolytic Rate Assay Kit (Agilent Technologies 103344-100) diluted in 0.3x Danieau's Solution. Controls were treated with 0.3x Danieau's Solution. Post run analysis was completed using Agilent Seahorse Wave software (Version2.6).

Table 8: Experimental Protocol for respiratory analysis using the Seahorse XFe24 Extracellular Flux Analyser

	No. Cycles	Mix	Wait	Measure
Basal	4	2 min	1 min	2.5 min
FCCP (5 µM)	4	2 min	1 min	2.5 min
Antimycin/Rotenone (2 µM / 2 µM)	9	2 min	1 min	2.5 min

Table 9: Experimental Protocol for glycolytic analysis using the Seahorse XFe24 Extracellular Flux Analyser

	No. Cycles	Mix	Wait	Measure
Basal	6	2 min	1 min	2.5 min
2DG (100 mM)	2	2 min	1 min	2.5 min
FCCP (5 µM)	4	2 min	1 min	2.5 min

2.20 Embryo dissociation and analysis by flow cytometry or FACS

Embryos were screened at appropriate time points (50 embryos per group) then incubated on ice in calcium free Ringer's solution for 15 minutes. Embryos were rinsed twice in calcium free Ringers' solution before addition of dissociation solution (Calcium free Ringer's solution, 2 mM $CaCl_2$, 0.25% Collagenase D (Gibco)) and incubation at 28.5 °C with vigorous shaking (200 rpm). Embryos were additionally mechanically dissociated by vigorous pipetting at 5-minute intervals. When embryos were sufficiently dissociated (approx. 20 minutes), cells were pelleted by centrifugation at 3,000 rpm for 3 minutes. Cells were washed twice with PBS by centrifugation at 3,000 rpm for 3 minutes, then resuspended in 500 µl PBS and filtered using a 40 µm cell strainer (Corning).

For analysis of cell cycle by flow cytometry, cells were incubated with 1 µg/ml Hoechst 33342 at 37 °C for 45 minutes. Cells were then analysed using a BD LSRFortessa cell analyser, with assistance from staff at the Queen's Medical Research Flow Cytometry and Cell Sorting Facility.

For FACS analysis, cells were processed by staff at the Queen's Medical Research Flow Cytometry and Cell Sorting Facility using a BD FACS Aria II cell sorter.

2.21 Analysis of gene expression by RT-PCR and qRT-PCR

Embryos were screened at appropriate time points (50 embryos per group). All solution was removed and TRIzol reagent (Invitrogen) was added to maintain RNA integrity. Embryos were frozen at -80 °C for a minimum of overnight. Samples were thawed and manually homogenised using a pestle, by passing through a 27.7G needle (BD Microlance) and vigorous vortexing. RNA was isolated from the resulting cellular suspension using the Direct-zol RNA MiniPrep Kit (Zymo Research Cat. Number R2050), according to manufacturer's instructions. RNA was eluted into a final volume of 15 µl. For cDNA synthesis, the BioRad iScript™ Advanced cDNA synthesis Kit for RT-qPCR (Cat. Number 1725037) was used. 15 µl of isolated RNA was mixed with 4 µl 5x iScript Advanced Reaction Mix and 1 µl iScript Advanced Reverse Transcriptase and incubated at 46 °C for 20 minutes then 95 °C for 1 minute. cDNA was stored at -20 °C for further analysis.

For RT-PCR, cDNA was added to PCR reaction mix, as shown in **Table 10** and run according to **Table 11**. PCR product was mixed with gel loading dye (NEB) and run on a 2.5 % agarose gel at 100 V for 1.5 hour then images using the GelDoc-Ite Imaging System.

Table 10: RT-PCR reaction mix for analysis for gene expression

cDNA	10 µl
dNTP Mix (Promega)	1 µl
Fw Primer (10 mM)	1 µl
Rev Primer (10 mM)	1 µl
Q5 Reaction Buffer (NEB)	1 µl
Q5 DNA Polymerase (NEB)	0.5 µl
H_2O	39.5 µl

Table 11: RT-PCR cycling conditions for gene expression analysis

Initial Denature	95 °C	2 minutes	
Denature	95 °C	30 seconds	35 Cycles
Anneal	Primer Optimised	30 seconds	
Extension	72 °C	2 minutes	
Final Extension	72 °C	7 minutes	

For qRT-PCR, cDNA was added to PowerUp™ SYBR™ Green Master Mix (Thermo Fisher Scientific A25742) and loaded into a 96-well PCR plate (MicroAmp® EnduraPlate™ Optical 96-well Fast Clear Reaction Plate, Applied Biosciences, 4483485) with appropriate primers at 1 mM (**Table 13**) to a final volume of 10 µl per well. qRT-PCR was performed using the StepOne™ Real-time PCR system according to the protocol shown in **Table 12** and analysed using Microsoft Excel (Version 16.16.1).

Table 12: qRT-PCR cycling conditions for analysis of gene expression

	Temperature	Duration	Cycles
UDG Activation	50 °C	2 minutes	Hold
Dual-lock DNA polymerase	95 °C	2 minutes	Hold
Denature	95 °C	15 seconds	40 cycles
Anneal/extend	60 °C	1 minute	

Table 13: Primer Sequences for RT-PCR and qRT-PCR

Gene	Primer Sequence
rps11	Fw: ACAGAAATGCCCCTTCACTG Rev: GCCTCTTCTCAAAACGGTTG
Dnm1l	Fw: AGCCAGTCAGGTGATCGCCGA Rev: CGCAGGGTTCGCGTGAAGGG
Opa1	Fw: GCCGGAAGTGTAGTTACCTG Rev: AGGTGGTCTCTGTGGGTTGT
Mitofusin 1	Fw: TCGGGTCCCGTCAACGCCAA Rev: ACTGAACCACCGCTGGGGCT
Mitofusin 2	Fw: GCTGGGACGCATCGGCCAAT Rev: GAGCGATCCACCACCCGCAG
GLUT2	Fw: GGCTATTGTCATTGGCATCCTT Rev: GACACACCAGCAGTAGCAGACTCT
MCT4	Fw: GACACGGCTTGGATCTCCTCTA Rev: TGCCAAGACCATACCCAATGA
SOD2	Fw: CTGGGGCTGGCTGGGCTTTG Rev: GCAGCTTGGAAACGCTCGCT
LDHa	Fw: TCCTTCTCAAGGATCTGACCGA Rev: TGTGCGTCTTGAGAAACAGGC
Hexokinase 1	Fw: GGTGAATTGGACGAAGGGCTTTAA Rev: CCTCTTGATCCCCTCTCTCAGAAG
dlat	Fw: GAGACCTGCTGGCTGAAATC Rev: CTGGTGCCCTCAGAAATCAT

2.22 Lactate Assay

Lactate concentrations were assessed using a commercially available lactate assay kit (Sigma-Aldrich MAK064), according to manufacturer's instructions.

Embryos were screened at appropriate time points (20 embryos/group) and mechanically homogenised in as small a volume as possible using a pestle. 200 µl assay buffer was added and samples were centrifuged for 10 minutes at 13,000 g. Samples were filtered using a 10 KDa molecular weight cut-off filter (Amicon® Ultra 2 ml Centrifugal filters Ref: UFC201024). The filtrate was mixed with enzyme mix and substrate and incubated at room temperature for 30 minutes in the dark with gentle shaking (60 rpm). Absorbance was measured at 450 nm using a Biotek Synergy HT plate reader.

2.23 Statistical analysis

All graphs were generated were using GraphPad Prism 7 (Version 7.0c). Where appropriate, statistical analysis was completed using GraphPad Prism 7 (Version 7.0c), as indicated with corresponding figures.

3. Characterisation of a zebrafish model of pre-neoplastic cell initiation in the superficial epithelial skin layer.

Our knowledge of established cancers continues to expand, and yet our understanding of the earliest stages of tumour initiation and development remains relatively under-developed. This is largely due to difficulties detecting and visualising these processes *in vivo.* To overcome this barrier, an *in vivo* larval zebrafish model for conditional epithelial cell transformation was developed [74][218]. This model makes use of a modified GAL4/UAS expression system, whereby the human estrogen receptor α (ER^{T2}) is fused to the KalTA4 transcriptional activator [246]. The system allows for spatial control by using a specific promoter for tissue of interest to restrict expression of KalTA4-ER^{T2}. Temporal control of oncogene expression under the control of the upstream activating sequence (UAS) can then be achieved by treatment with 4-hydroxytamoxifen (4-OHT) (**Figure 3.1 A**). For the purposes of this project the KalTA4-ER^{T2} element was expressed under the control of the *keratin 4* (Krt4) promoter, which is specific for the superficial epithelial skin layer of the zebrafish (**Figure 3.1 B**), while oncogene transformation was achieved exclusively using the fluorescently tagged human $HRAS^{G12V}$ oncogene.

It is well recognised that the interactions between transformed cells and their immediate microenvironment are important for cancer progression. Therefore, an ideal model for the study of the earliest stages for tumour initiation and development would permit detection and visualisation of such interactions. To achieve such, this model employs a combination of transgenic lines and transgenic construct microinjection to generate mosaic transformation of epithelial cells. This is accomplished by generating a stable transgenic zebrafish line of the Krt4:KalTA4-ER^{T2} element (**Supplemental Figure 1**) which is then microinjected at the one cell stage (**Figure 3.1 C**) with the transgenic construct for the UAS:eGFP-$HRAS^{G12V}$ element (**Supplemental Figure 2**). The addition of 4-OHT results in mosaic expression of superficial epithelial cells which express fluorescent $HRAS^{G12V}$, termed pre-neoplastic cells (PNCs). This model provides unprecedented access to and

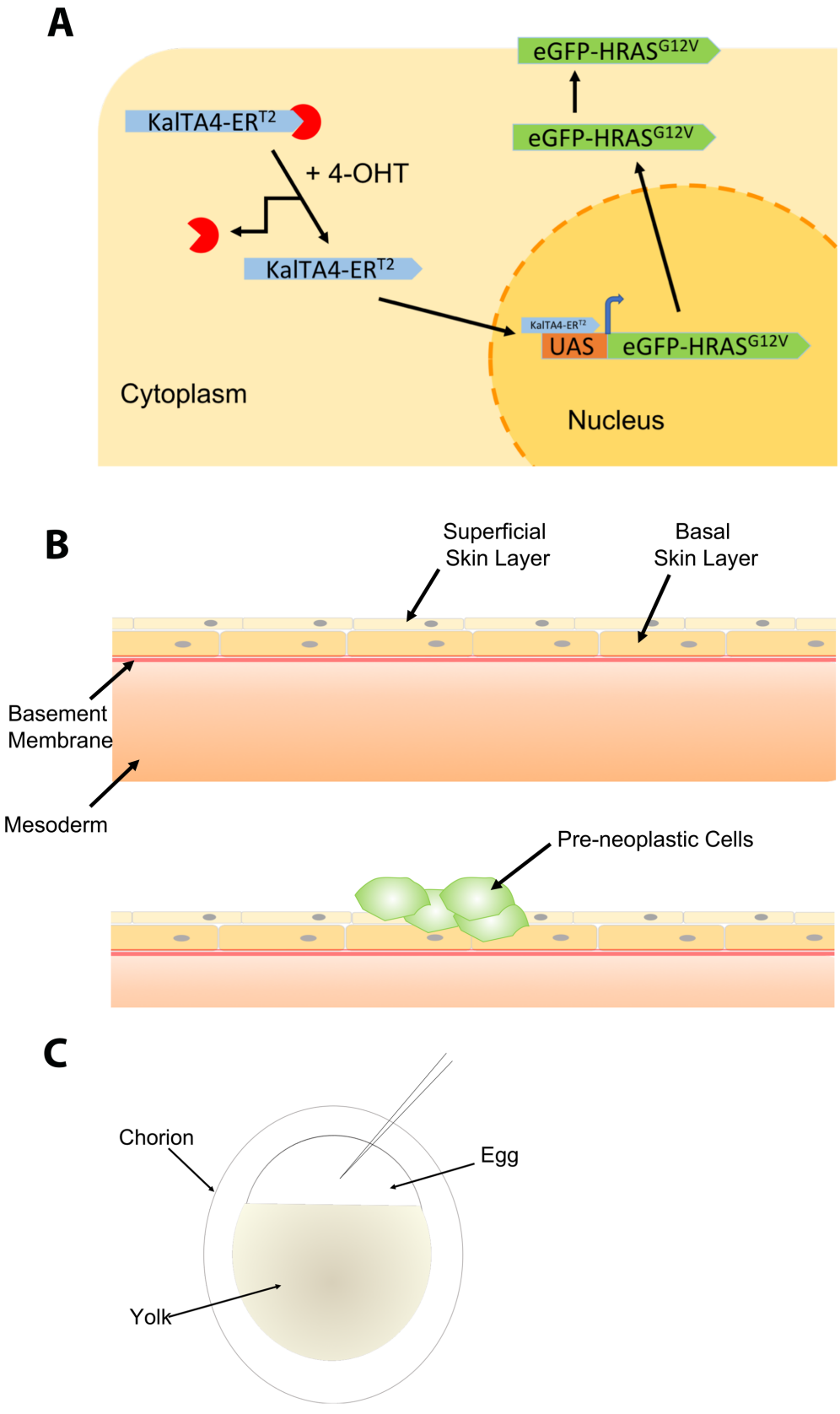
A
eGFP-HRASG12V
KalTA4-ER^{T2}
+ 4-OHT
eGFP-HRASG12V
KalTA4-ER^{T2}
KalTA4-ER^{T2}
UAS
eGFP-HRASG12V
Cytoplasm
Nucleus
B
Superficial Skin Layer
Basal Skin Layer
Basement Membrane
Mesoderm
Pre-neoplastic Cells
C
Chorion
Egg
Yolk

Figure 3.1: A Gal4/UAS based larval zebrafish model for pre-neoplastic cell initiation in the superficial epithelial skin layer. A. Schematic details for transient induction of oncogene expression. KalTA4-ER^{T2} is held in the cytoplasm by heat-shock proteins, shown in red. Addition of 4-OHT allows for dissociation of heat shock proteins and translocation to the nucleus. Binding to the UAS allows for expression of the UAS controlled oncogene of interest. Adapted from [74] **B.** Schematic cross-section of larval zebrafish skin with transformation of superficial skin cells. Larval skin is formed of two epithelial layers, and outer superficial layer atop a basal layer that is bound to the underlying basement membrane. The Krt4 promoter drives expression exclusively in superficial cells, resulting in PNC initiation specifically in this layer. Adapted from [74] **C.** Schematic of a zebrafish zygote. The fertilised egg is encapsulated in a protective chorion. Transgenic constructs are injected directly into the egg at the one-cell stage, as shown by the schematic micro-injection needle.

control of the earliest stages of tumour initiation and development *in vivo*, allowing monitoring and manipulation of developing PNCs and their dynamically forming niche.

While this model was developed primarily by Dr. Thomas Ramezani prior to commencement of this project, a complete and sufficient characterisation had yet to be carried out. Early work for this project involved characterisation of this model of HRAS^{G12V} transformation of superficial epithelial skin cells in larval zebrafish.

3.1 Morphological characterisation of the pre-neoplastic cell phenotype

PNCs were observed over-time to monitor PNC phenotype development and establish an experimental time-line. Krt4:KalTA4-ER^{T2} eggs were injected with UAS:eGFP-HRAS^{G12V} at the one cell stage and raised according to standard protocols until 2 days post fertilisation (dpf), at which point 4-OHT was added to induce oncogene expression. This was used as the standard protocol for all future experiments. Embryos were monitored at 30 min intervals for signs of fluorescent HRAS^{G12V} expression. The first signs of PNC induction were observed at approximately 6.5 hours post induction (hpi). Given realistic operating procedures, including screening large numbers of embryos and preparation for imaging, 8 hpi was determined as an appropriate time-point for experimental commencement (**Figure 3.2 A + B**).

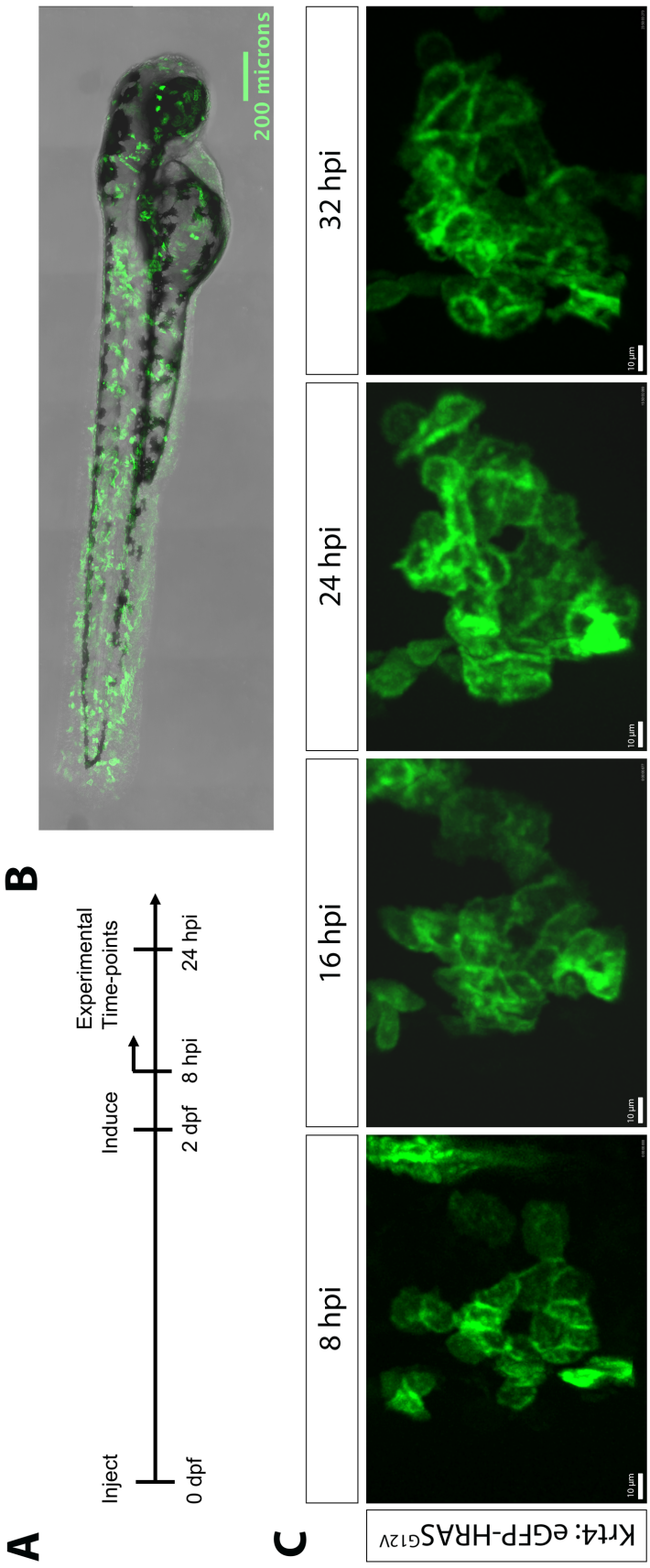

Figure 3.2: PNCs develop dynamically over time.
A. Schematic experimental time-line from egg injection at the one-cell stage through induction at 2 dpf and experimental time-points from 8 hpi **B.** Tile-scan image of a 2dpf embryo at 8hpi showing mosaic expression of PNCs in the superficial skin layer (green). **C.** Still frames from *in vivo* time-lapse microscopy (Supplemental Movie 1) monitoring PNC development over time. PNCs are seen to dynamically change morphology and become highly motile as the movie proceeds. Scale bar 10 µm

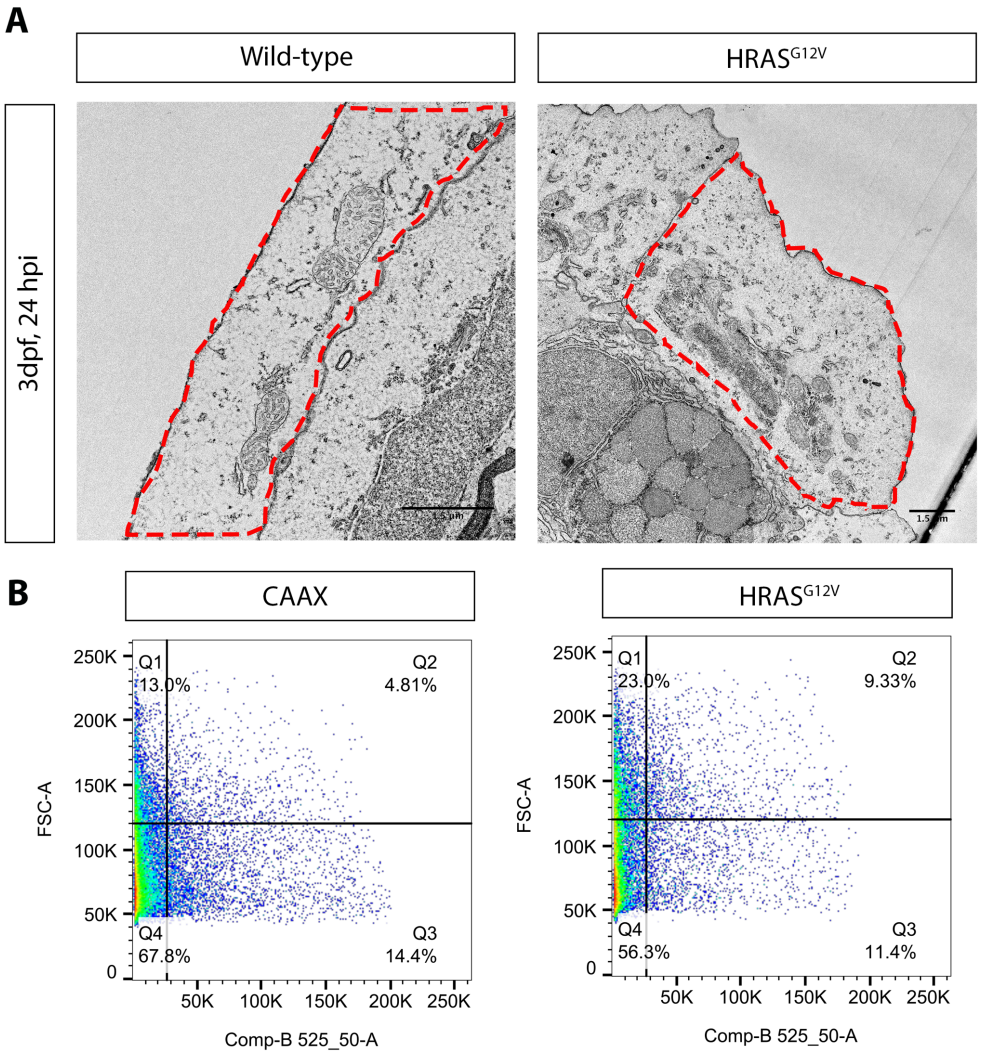
A
Wild-type
HRASG12V
3dpf, 24 hpi
B
CAAX
HRASG12V
Q1
13.0%
Q2
4.81%
Q4
67.8%
Q3
14.4%
Q1
23.0%
Q2
9.33%
Q4
56.3%
Q3
11.4%
FSC-A
Comp-B 525_50-A
250K
200K
150K
100K
50K
0
50K
100K
150K
200K
250K
C
Cell Size
FSC-Area
120000
110000
100000
90000
80000
****
p < 0.0001
CAAX
HRASG12V

Figure 3.3: PNCs show altered morphology and increased cell size at 24 hpi. A. Representative electron microscopy images of control superficial epithelial cells and PNCs showing alterations in morphology of PNCs at 24 hpi. Scale Bar 1.5 µm **B.** Representative dot plots from flow cytometry analysis of GFP expressing PNCs and control cells at 24 hpi. Flow cytometry reveals the percentage of GFP^{+}/FSC-$Area^{High}$ cells is higher in $HRAS^{G12V}$ cells than control cells, as seen in Q2, suggesting that the size of PNCs is larger than control cells. **C.** Quantification from B. The mean area of PNCs is increased relative to control cells at 24 hpi. Mean + SEM, n=10 experiments, Mann-Whitney Test, $p < 0.0001$

PNCs were monitored over time from 8 to 32 hpi at 10 min intervals (**Figure 3.2 C, Supplemental Movie 1**). It was observed that PNCs develop dynamically over time, becoming highly motile and heterogeneously expressing $HRAS^{G12V}$ as PNC initiation progresses. The phenotype appears to be quite aggressive as cellular morphology alters dramatically over time (**Figure 3.2 C)** and occasional PNC death is observed (see Section 3.3). Drastic alterations to cell morphology were confirmed with electron microscopy (**Figure 3.3 A**), while flow cytometric analysis revealed an increase PNC size (**Figure 3.3 B + C**).

3.2 Detection of proliferation in pre-neoplastic cells and the pre-neoplastic cell niche

As cancer is a disease of excessive proliferation of transformed cells, one would postulate that proliferation of PNCs is a requirement for disease development and progression. *In vivo* time-lapse imaging (discussed above) suggests that PNC proliferation increases over time, as occasional cell division can be observed. A number of approaches were attempted to define PNC proliferative capacity.

Proliferating cell nuclear antigen (PCNA) is an important component of cellular replicative machinery, acting as a cofactor for DNA polymerase δ [247][248]. Hence, expression is observed in proliferating cells. Protocol optimisation for immunofluorescence staining for PCNA commenced. Despite comprehensive attempts to optimise an immunofluorescence protocol to detect PCNA accumulation in PNCs, a baseline PCNA signal was detected in all cells, which

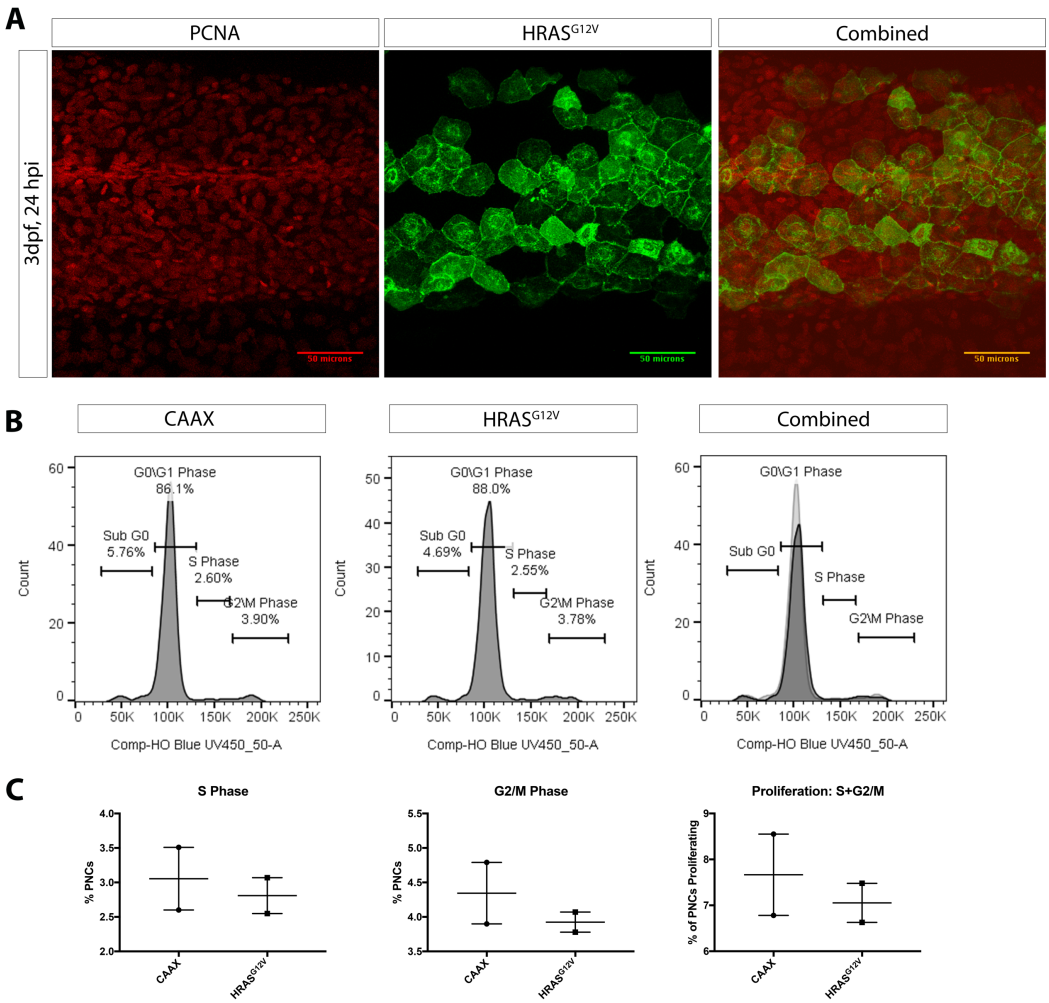

Figure 3.4: PCNA staining and Hoechst 33342 cell cycle analysis were deemed unsuitable for determination of PNC proliferation. A. Representative images from PCNA immunostaining at 24 hpi. While PCNA signal was detected, strong baseline signal made identification of proliferating cells difficult and somewhat subjective. **B + C.** Cell cycle analysis by flow cytometry following Hoechst 33342 loading of dissociated embryos at 24 hpi. Hoechst loading appears efficient, as smooth peaks are evident. However, low numbers of cells in S and G2/M phases lead to high standard deviation. No difference is seen between control and experimental groups. n = 2 experiments.

made identification of PCNA-positive proliferating cells difficult and highly subjective (**Figure 3.4 A**). Variations in fluorescence intensity within samples and slight alterations in imaging settings could skew data, therefore it was decided that PCNA detection was an unreliable method to observe PNC proliferation.

Hoechst 33342 is a widely used DNA stain that can be used to monitor cellular proliferation. As a cell transitions through the cell cycle, the quantity of DNA in the cell increases. This leads to an increase in fluorescence intensity of Hoechst staining as the cell moves into the S and G2/M proliferative stages of the cell cycle [249][250]. PNC carrying embryos were dissociated at 24 hpi, followed by Hoechst loading and analysis by flow cytometry. While Hoechst loading appeared efficient, as evidenced by smooth peaks of Hoechst intensity (**Figure 3.4 B**), the detection of proliferative cell cycle stages proved less efficient (**Figure 3.4 B + C**). Low cell numbers in S and G2/M phases coupled with high standard deviation made the data debatable. This ambiguity, in addition to large numbers of embryos required to assess sufficient numbers of PNCs for this approach and lack of *in situ* information, led to the decision not to pursue the technique further.

EdU (5-ethynyl-2'-deoxyuridine) is a thymidine analogue that is incorporated into DNA during replication for the detection of cellular proliferation [251]. Following extensive protocol optimisation, successful Edu staining was achieved (**Figure 3.5 A**). However, despite indications of enhanced proliferative capacity in PNCs during initial experiments, detailed analysis revealed remarkably low levels of PNC proliferation, with little difference detected between PNCs and control cells. A statistically significant increase in EdU incorporation is detected in PNCs at 16 hpi and 32 hpi, but given the persistently low level of proliferation, the biological relevance of this increase is debatable. Quantification of these experiments was completed by manual count of PNCs and manual count of EdU positive signal within PNCs to indicate the percentage of proliferating cells. In an effort to strengthen confidence in this result, alternative methods of quantification of EdU incorporation were attempted, but all had high margins for error and proved inaccurate. Automated cell counts using Imaris software to identify PNC surfaces and count based on Hoechst staining was attempted but was highly inaccurate. Nuclear co-localisation of EdU with Hoechst staining using a newly developed PickCells software (developed by Dr. Sally Lowell, The University of Edinburgh) was useful, but had issues isolating PNCs in 3D. Despite this, the lack of significant proliferative

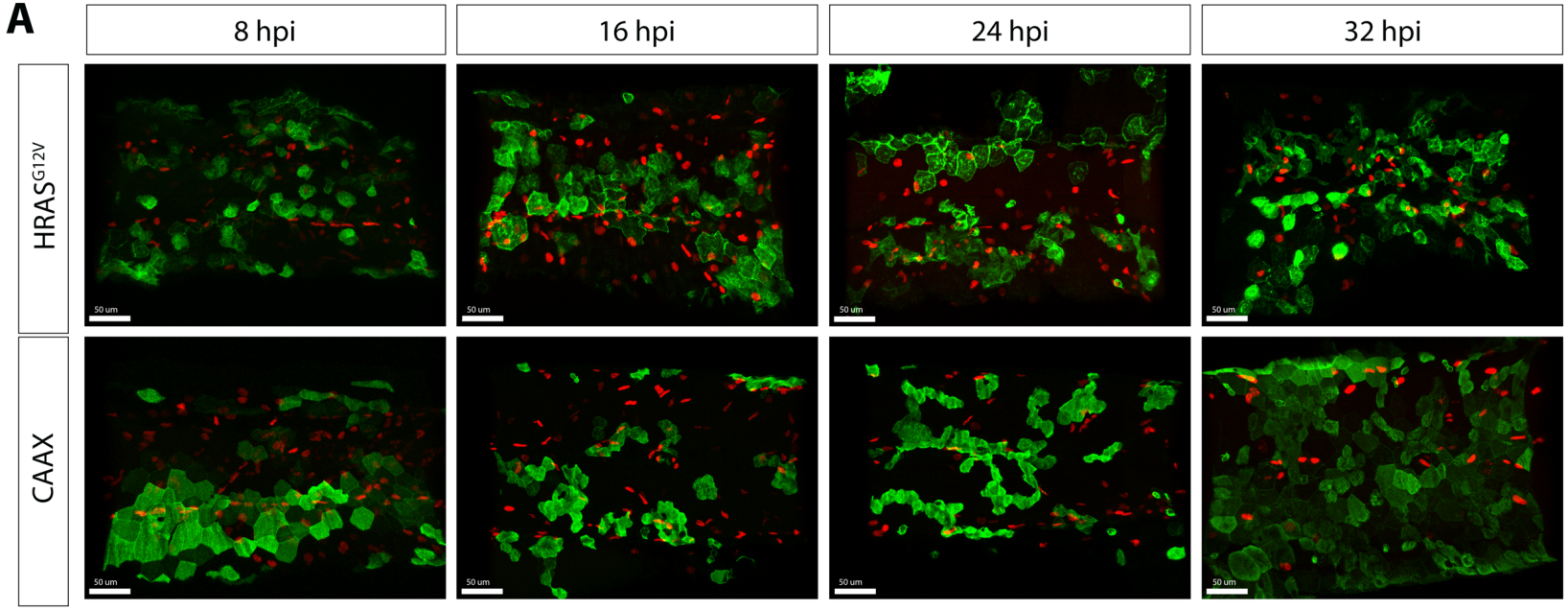
A
8 hpi
16 hpi
24 hpi
32 hpi
HRASG12V
CAAX
50 um

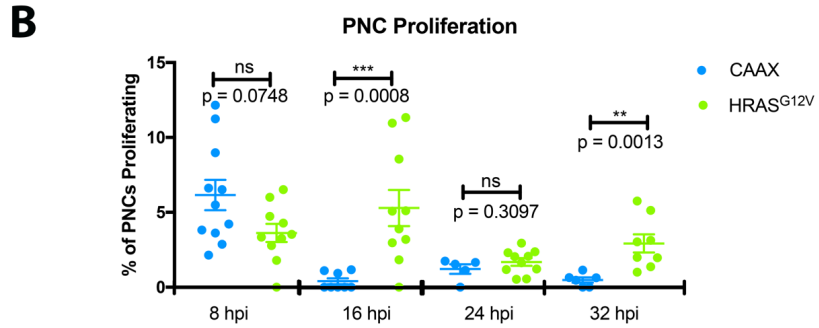
B
PNC Proliferation
% of PNCs Proliferating
15
10
5
0
ns
p = 0.0748
***
p = 0.0008
ns
p = 0.3097
**
p = 0.0013
8 hpi
16 hpi
24 hpi
32 hpi
CAAX
HRASG12V

Figure 3.5: Successful Edu staining was achieved at various time-points, but proliferation levels remain persistently low in both PNCs and control cells A. Representative images from EdU staining at 8, 16, 24 and 32 hpi in PNCs and control superficial epithelial cells. Scare bar 50 µm **B.** Quantification from A achieved by manual cell count of PNCs and EdU positive signal inside PNCs. Results show the percentage of proliferating PNCs over time is low and biologically relevant alterations are not observed. Mean + SEM, n ≥ 5 embryos from 3 independent experiments, Mann-Whitney Test between individual groups as shown.

increases detected using EdU, combined with observations from the numerous other technical approaches (described above), lead to the conclusion that superficial PNCs do not display significant proliferative capacity and show no increase relative to control superficial cells.

3.3 Detection of apoptotic cell death of pre-neoplastic cells

Based on observations of *in vivo* time-lapse imaging, discussed above, it was clear that some PNCs undergo cell death as induction continues post 24 hpi. The level of cell death was assessed to further understand mechanisms of PNC induction and as a parameter for monitoring PNC manipulation in later experiments.

Annexin V is a cellular protein that binds to phosphatidylserine (PS). Externalisation of PS is a feature of apoptotic cell death, whereby PS is flipped across the cell membrane, allowing annexin V to bind [252]. Hence, annexin V is widely used as a marker for apoptotic cells. To investigate apoptotic cell death in this model, a transgenic line with annexin V fluorescently tagged with YFP under the control of the *ubi* promoter (Ubi:SecA-YFP) generated in the lab was used. Incorporating this with the PNC initiation model using mCherry tagged $HRAS^{G12V}$, as opposed to GFP, allowed for *in vivo* imaging of annexin V activity in PNCs. Live-imaging revealed increased annexin V activity in embryos carrying PNCs relative to control cells at later stages of PNC initiation (**Figure 3.6**). However, the annexin V transgenic line was highly granular in nature, making signal quantification difficult and, therefore, while the data were encouraging and consistent with previous

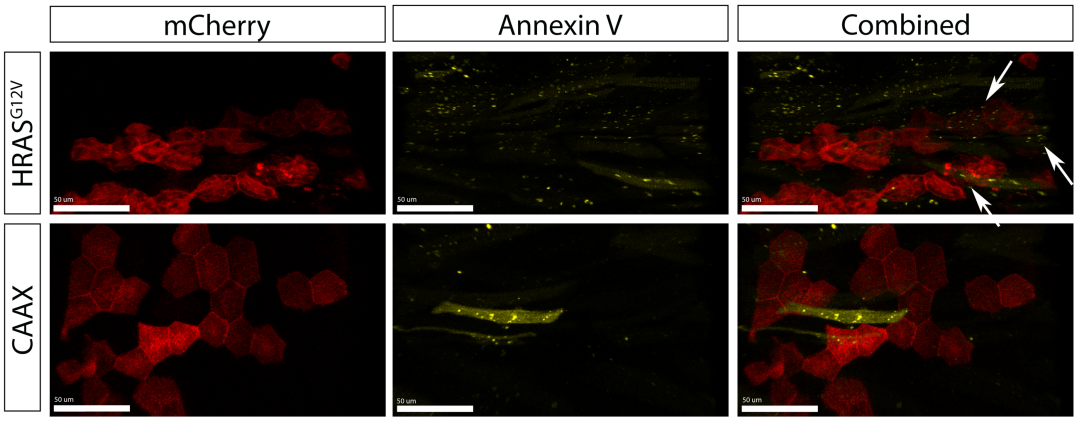

Figure 3.6: Detection of annexin V activity in PNCs. Annexin V activity was monitored in PNCs by combining the Ubi:SecA-YFP transgenic line with mCherry tagged $HRAS^{G12V}$. Live-imaging reveals that there is increased annexin V activity in PNCs relative to control superficial epithelial cells at 32 hpi, as indicated by the white arrows, consistent with observed PNC cell death at later stages of PNC induction. However, the annexin V transgenic line shows some non-specific signal and is quite granular nature, making it difficult to quantify. Scale bar 50 µm.

observations from *in vivo* imaging, alternative methods for quantification of apoptosis were pursued.

Terminal deoxynucleotidyl transferase dUTP nick end labelling (TUNEL) is an *in situ* apoptosis assay based on incorporation of modified dUTPs at the 3' end of fragmented DNA which can then be fluorescently labelled to identify apoptotic cells [253]. Protocol optimisation for TUNEL staining in the PNC initiation model was undertaken, however various issues arose. Apoptotic PNCs were successfully detected, however off-target, extra-nuclear labelling was also observed (**Supplemental Figure 3**). During staining, PNC morphology had deteriorated, which was thought to be due to the use of proteinase K during the TUNEL protocol, which can damage barrier integrity and cause shedding of superficial skin cells when used to excess. Titration of proteinase K to optimise the protocol and reduce loss of cellular integrity was unsuccessful, as sufficient concentrations to achieve TUNEL staining and maintain PNC integrity could not be achieved.

Instead, immunostaining for cleaved-caspase 3 activity was used as a marker for apoptotic cell death. Caspase 3 is a well-recognised member of the cellular apoptotic pathway. Proteolytic cleavage of caspase 3, primarily by caspase 8, 9 and

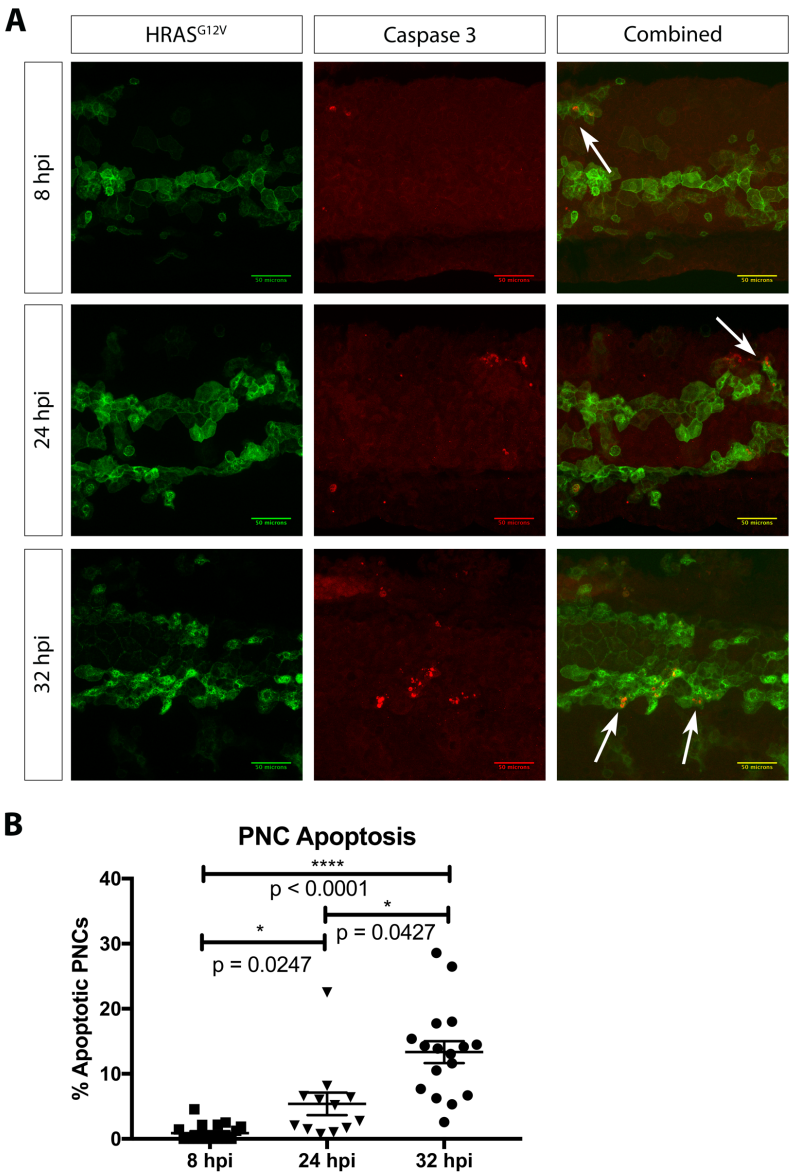

Figure 3.7: Cleaved caspase-3 activity increases over time in PNCs. A. Representative images of cleaved caspase-3 activity in PNC over time. PNC specific caspase-3 activity increases over time during PNC development, as indicated by the white arrows. Scale bar 50 µm **B.** Quantification from A. Apoptotic cell death in PNCs significantly increases over time, reaching 15% by 32 hpi. Mean + SEM, n = 12 embryos from 3 independent experiments, Kruskal-Wallis test, $p < 0.0001$.

10, results in protein activation and leads to induction of apoptotic cell death via the so-called "execution pathway" [254]–[257]. Immunostaining reveals that caspase 3 activity increases over time during PNC development (**Figure 3.7 A**). Quantification

by manual cell counting shows that, by 24 hpi approx. 5% of PNC are positive for cleaved-caspase 3 activity. This increases to approx. 15% by 32 hpi (**Figure 3.7 B**). This finding is consistent with *in vivo* observations and provides a parameter for monitoring PNC status following manipulation in later experiments. Also, it reveals that dynamic signalling during PNC development results in a complex PNC microenvironment with divergent PNC fate. While interesting and highly relevant, this feature is outside the scope of this project but is being investigated by other members of the group.

3.4 Observation of neutrophil recruitment to developing pre-neoplastic cells

Previous work by the group , and others, has shown that alternative models of developing PNCs initiate an inflammatory response, whereby innate immune leukocytes are recruited, a response which was found to be important for the proliferation on PNCs [192]. It was therefore necessary to confirm that similar recruitment of leukocytes was seen in this new model of PNC initiation. To monitor neutrophil recruitment to PNCs the neutrophil reporter line LysC:DsRed [244] was incorporated into the model. Krt4:KalTA4-ER^{T2};LysC:DsRed eggs were injected with UAS:eGFP-HRAS^{G12V}, resulting in embryos carrying PNCs as previously described with the addition of red fluorescently labelled neutrophils [244]. Time-lapse *in vivo* imaging commenced at 8 hpi and recruitment of neutrophils to developing PNCs was monitored at 10 min intervals over the course of 24 hours (**Supplemental Movie 2**). This interval allows for analysis of the number of neutrophils recruited while maximising embryo survival due to phototoxicity. However, such an interval does not allow for more detailed analysis of individual neutrophil behaviour due to the speed at which neutrophils migrate. Analysis of *in vivo* imaging shows that the recruitment of neutrophils to PNCs persists from 8 hpi (**Figure 3.8**) and the number of neutrophils remains constant. As mentioned, this imaging interval does not allow for detailed behavioural analysis. Further study is required to investigate the mechanisms of neutrophil recruitment to PNCs and analyse functional behavioural

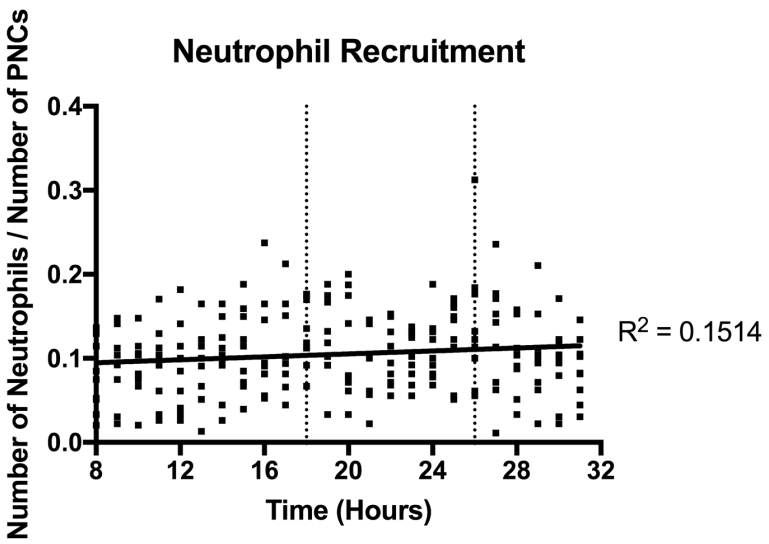

Figure 3.8: Neutrophil recruitment to PNCs increases over time. Quantification of recruited neutrophil numbers over time for *in vivo* time-lapse imaging. Number of neutrophils recruited to PNCs remains constant over time. Aligned replicates with linear regression analysis, n = 9 embryos from 3 independent experiments.

alterations in the PNC niche. While important, this is outside the scope of this project.

3.5 Discussion

Development of a new model for human $HRAS^{G12V}$-transformed PNC initiation in superficial epithelial larval zebrafish skin has provided an opportunity to investigate previously undetectable stages of cancer initiation in an *in vivo* setting. While technical development of this model was complete prior to this project beginning, a detailed characterisation of phenotype development was an initial priority. Observational studies determine that PNCs are detected at approximately 6.5 hpi and continue to develop dynamically over time. Cellular size and morphology are dramatically altered, and cells become highly motile, while apoptosis is observed at later stages of induction. Recruitment of neutrophils to developing PNCs is consistent with previously reported observations.

Morphological alterations observed by *in vivo* imaging were verified using electron microscopy. These images suggest changes in cell shape and polarity, providing more detailed indications of phenotypical characteristics of PNCs. While changes in cell size were quantified by flow cytometry, alterations in morphological

characteristics observed by electron microscopy were not quantified. Due to the mosaic nature of this model and loss of fluorescence during the fixation procedure, positional markers are used to determine the position of PNCs for electron microscopy. However, the fixation procedure causes sample shrinkage, which increases the scope for error and adding considerable time to sectioning and imaging. Completion of sufficient numbers of embryos for quantifiable analysis is highly time-consuming and, while these morphological alterations are an important feature of the model, would not provide data that contributes to the metabolic phenotypes under investigation in this project. Should time and funding become available, a more detailed and quantifiable electron microscopy analysis of morphological characteristics of PNCs could be completed in the future.

It is evident from these observations that superficial PNCs do not exhibit enhanced proliferative capacity. Quantification of EdU staining indicated low proliferation index in both PNCs and control cells and, while statistically significant differences are detected at some time-points, the biological significance of these changes are thought to be negligible. In contrast to cells of the more stem-like basal epithelial layer, superficial epithelial cells are fully differentiated. During the blastula period of zebrafish development, superficial epithelial cells become remarkably flat, become lineage-restricted and their cell cycle becomes longer and less synchronous [258]. Therefore, given the developmental stage of embryos in these experiments, it is not altogether surprising that control cells are not highly proliferative. However, the finding that oncogenic RAS transformed PNCs do not increase proliferative capacity was somewhat unexpected. Murine models have shown that transformed keratinocytes have the ability to escape differentiation-associated growth controls [259], yet overexpression of $HRAS^{G12V}$ in superficial epithelial cells in this model does not appear sufficient to induce proliferation. Perhaps additional cellular insults are required to overcome the differentiation state and induce a proliferative phenotype in superficial PNCs, similar to the BRAF/p53 cooperation required for melanoma formation in some zebrafish models [213]. This theory that the proliferative capacity of epithelial PNCs is linked to their differentiation state is strengthened by the

knowledge that similar experiments using this model in the basal epithelial layer found significantly increased proliferation in basal PNCs (Feng Lab, Unpublished data). With this in mind, it can be concluded that the basal epithelial model would be more appropriate to assess proliferative parameters moving forward, as $HRAS^{G12V}$ transformation does not appear sufficient to induce proliferation in superficial epithelial cells.

Observations also reveal that, at later stages of induction, some PNCs undergo cell death. To assess this an annexin V transgenic line, developed by fellow group member Ziyuan (Elva) Chang was used. This line revealed increased annexin V activity in PNCs at later stages of induction, consistent with previous observations. However, quantification of this line was difficult due to the granular nature of the signal. Therefore, alternative approaches were considered. Issues arose with TUNEL protocol optimisation, thought to be due to proteinase K treatment, although further consideration of optimisation approaches highlights that method of fixation may also have been an issue [260]. Instead, cleaved caspase-3 was ultimately used as a marker for apoptotic cell death, as caspase 3 cleavage initiates programmed cell death pathways. Immunostaining revealed increased caspase-3 activity at later stages of induction, reaching up to 15% by 32 hpi. This apoptotic cell death could be a response to hyper-active $HRAS^{G12V}$ expression due to differential concentrations of UAS in each cell following micro-injection or could be an inherent phenotype arising from PNC communication and required for tumour initiation. This is an interesting finding as it reveals divergent phenotypes of PNCs during tumour initiation and development. It highlights that this model represents a heterogenous population of PNCs, a phenotype also observed by morphological and behavioural divergences during *in vivo* microscopy. While the signalling and cellular interactions at these later stages of induction may be vital for ultimate tumour initiation and progression, they remain outside the scope for this project, but are under investigation by fellow group members.

Inflammatory cell recruitment has been shown to be vital for PNC progression in previously established PNC initiation models [192]. This new model allows for

temporal resolution of cellular interactions from the very earliest stages of PNC initiation. Therefore, determination of a time-line of neutrophil recruitment to developing PNCs was made possible. Neutrophil numbers are seen to increase from eight hpi and appear to remain constant over time. Inflammatory mechanisms in the PNC niche remain to be elucidated, though the contribution of secondary characteristics of the phenotype, such as cell death, cannot be overlooked. These detailed inflammatory mechanisms are an active area of research within the group, with various inflammatory pathways under investigation by fellow group members.

4. Mitochondrial and Metabolic Alterations Occur Very Early During Pre-Neoplastic Cell Development and are Potential Targets for Cancer Prevention.

Having gained sufficient understanding of the newly developed model system for inducible $HRAS^{G12V}$ transformation of superficial epithelial skin cells in larval zebrafish, the project set about investigating metabolic alterations in the developing PNC niche. There are a great many metabolic processes that have been shown to be altered in established cancer and may play a role during PNC initiation, ranging from processes involved in glycolysis and oxidative phosphorylation to lipid and amino acid metabolism. Each could be investigated in their own right, but such a body of work is vastly beyond the capacity of a single research project. It was therefore decided to take a broad approach to potential metabolic alterations by considering the location where a number of metabolic processes occur, the mitochondria, and investigating glycolytic processes that are known to be altered in established cancers to determine the role of these processes during tumour initiation and development.

4.1 Mitochondrial morphology is altered at very early stages of PNC initiation.

Mitochondrial hyper-fragmentation is a feature of established cancer cells and is required for tumour growth and survival [154]–[156]. Mitochondrial morphology in PNCs was investigated to determine if this was also a feature of early PNC initiation. Using an *in vivo* confocal microscopy approach, fragmentation of mitochondria was observed at very early stages of initiation (**Figure 4.1**). Control epithelial cells display an elongated, tubular morphology (**Figure 4.1 A** CAAX, white arrow). Meanwhile, PNCs have a highly fragmented morphology at 24 hpi (**Figure 4.1 A** $HRAS^{G12V}$ white arrows), consistent with observations in more established cancer cells. Quantification of staining reveals there is a significant increase in the number of mitochondrial fragments in PNCs relative to control cells (**Figure 4.1 B**) and a significant decrease in the size of those fragments (**Figure 4.1 C**), indicating that mitochondrial fragmentation has occurred. Due to the resolution limits of confocal microscopy, individual mitochondria could not be observed using this

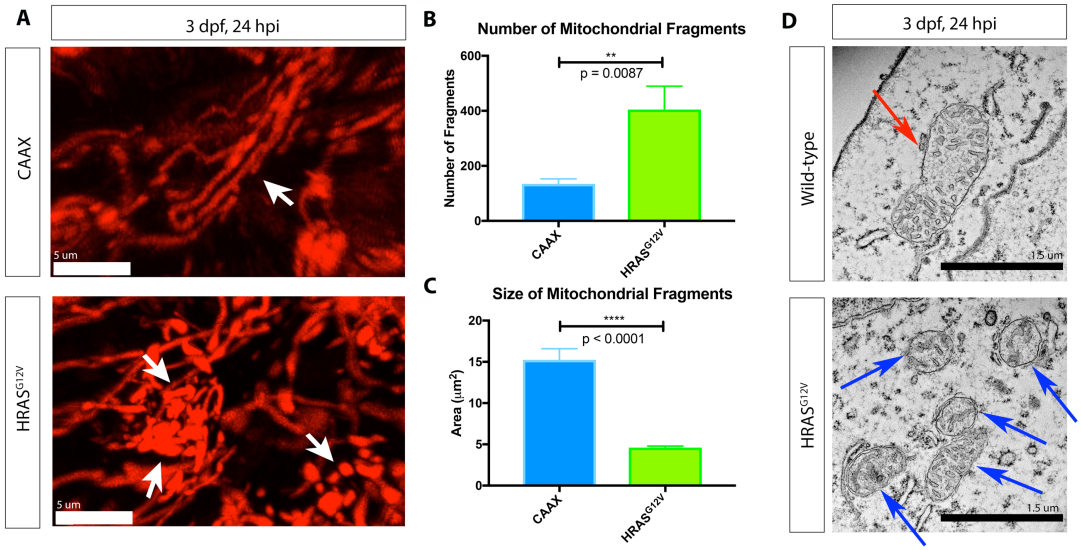

Figure 4.1: Mitochondrial Fragmentation is observed in PNCs. A. Representative images from *in vivo* MitoTracker Deep Red FM staining at 24 hpi. Control epithelial cells have an elongated, tubular structure, as indicated by the white arrow. PNCs show highly fragmented morphology, as indicated by the white arrows. Scale bar 5 µm. **B + C.** Quantification from A. Automated analysis using Imaris software to generate surfaces for mitochondrial staining specifically in PNCs to analyse numerous parameters. Analysis reveals a significant increase in the number of mitochondrial fragments (B) and a significant decrease in the size of mitochondrial fragments (C) in PNCs relative to control epithelial cells. Mean + SEM, Mann-Whitney Test, n ≥ 6 embryos from ≥ 3 experiments **D.** Representative images from electron microscopy at 24 hpi. Control epithelial cells show a stereotypical mitochondrial morphology, indicated by the red arrow. PNCs show smaller and more numerous mitochondria, indicated by the blue arrows. Scale bar 1.5 µm

technique. To verify the fragmentation phenotype and visualise individual mitochondrial fragments in PNCs electron microscopy was performed. Resulting images confirm that mitochondria in PNCs appear smaller and more numerous relative to control epithelial cells (**Figure 4.1 D**). While the double membrane structure appears potentially compromised in these smaller fragments, cristae structure appears intact, suggesting these mitochondrial fragments are still functional. This phenotype has been observed at the earliest measured time-point of 8 hpi and persists over time. In fact, while no change in the number of mitochondrial fragments is seen, the fragments appear to become significantly smaller over time (**Figure 4.2**). This suggests that despite the fragmentation events occurring early,

functional consequences may become more pronounced over time, although further experimental replicates are necessary to confirm this. Together, these data suggest that mitochondrial fragmentation is a very early alteration following HRAS^{G12V} oncogene activation and this phenotype may have a dynamic effect on PNC development over time.

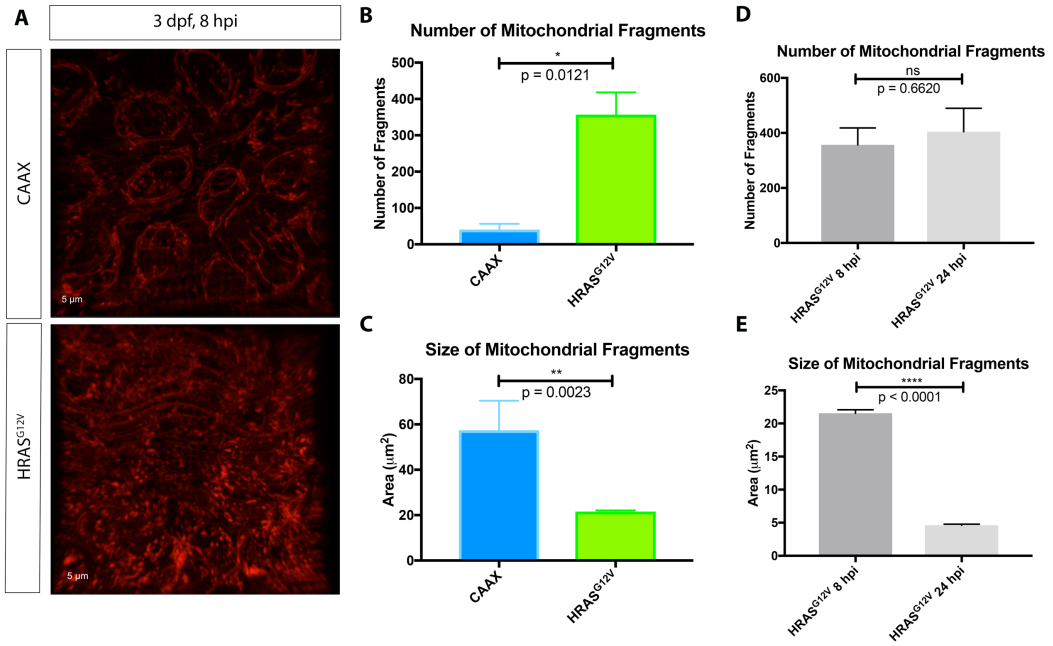

Figure 4.2: Mitochondrial fragmentation is observed at very early stages of PNC development and persists over time. A. Representative images from *in vivo* MitoTracker Deep Red staining at 8 hpi. Control epithelial cells have an elongated, tubular structure, while PNCs show highly fragmented morphology. Scale bar 5 µm. **B + C.** Quantification from A. Automated analysis using Imaris software to generate surfaces for mitochondrial staining specifically in PNCs to analyse numerous parameters. Analysis reveals a significant increase in the number of mitochondrial fragments (B) and a significant decrease in the size of mitochondrial fragments (C) in PNCs relative to control epithelial cells. Mean + SEM, Mann-Whitney Test, n ≥ 3 embryos from ≥ 2 experiments. **D + E.** Comparison of number and size of mitochondrial fragments at 8 hpi and 24 hpi. There appears to be no change in the number of mitochondrial fragments overs time, indicating that the phenotype persists over time. There is a significant decrease in the size of fragments over time, suggesting that condensation of fragments may occur over time. Mean + SEM, Mann-Whitney Test, n ≥ 3 embryos from ≥ 2 experiments.

4.2 Mitochondrial fragmentation is dependent on the mitochondrial fission regulator Dnm1l.

Following determination of a mitochondrial fragmentation phenotype in PNCs, possible mechanisms for the phenotype were investigated. The cycle of mitochondrial fragmentation that naturally occurs in cells is governed by a number of regulatory proteins, including Dnm1, Opa1, Mitofusin 1 and Mitofusin 2 (See Section 1.5). Initially, RT-PCR was performed to visualise changes in gene expression of these regulatory proteins by gel electrophoresis. Data revealed an apparent increase in expression of the fission protein Dnm1l in embryos carrying PNCs relative to wild-type embryos, while expression of the mitochondrial fusion protein Opa1 appeared to be reduced (**Figure 4.3 A**). This was encouraging but bands on the gel electrophoresis were quite weak and sometimes difficult to visualise. Following much protocol optimisation, data from qRT-PCR showed no significant difference in the expression of the fission regulatory protein Dnm1 or the fusion regulatory proteins Opa1, Mitofusin 1 or Mitofusin 2 (**Figure 4.3 B**). While expression alterations were not detected, this is not altogether surprising. cDNA

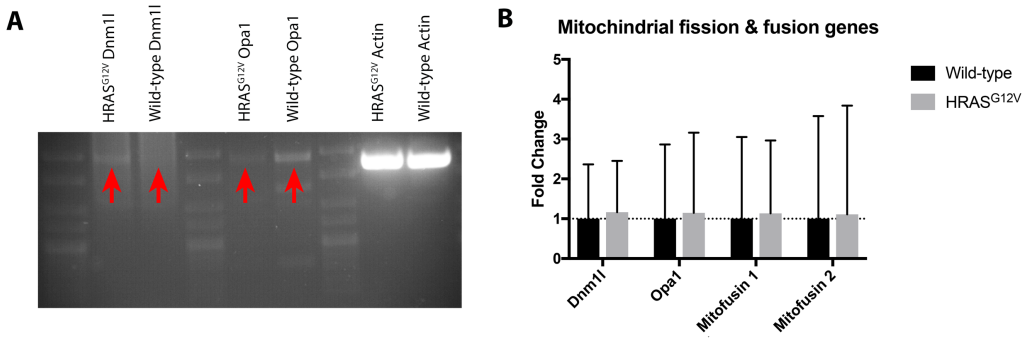

Figure 4.3: Upregulation of Dnm1l expression in PNCs was not quantifiably detected. A. Representative image of gel electrophoresis following RT-PCR. Stronger expression of the mitochondrial fission protein Dnm1l is detected in PNC carrying embryos relative to wild-type embryos. Meanwhile, reduced expression of the mitochondrial fusion protein Opa1 is detected in PNCs carrying embryos. **B.** Fold change of gene expression detected by qRT-PCR. Analysis reveals no change in the expression of Dnm1l, Opa1, Mitofusin 1 or Mitofusin 2 in the presence of PNCs. Mean + SEM, n = 7 independent experiments, Multiple t tests between groups

used for these experiments was isolated from whole embryos with mosaic expression of PNCs in superficial epithelial skin (n = 50 embryos per group). The ratio of transformed cells relative to the total number of cells in a zebrafish embryo is quite small and changes of gene expression in PNCs will be masked by that of non-transformed cells. Therefore, detected changes are expected to be subtle and one must remain conscious of potential false negatives. Isolation of cDNA from FACS isolated PNCs was attempted but achieving sufficient numbers of PNCs for RNA isolation and cDNA synthesis without the need for costly amplification was not achieved.

Previous studies indicate that mitochondrial fragmentation in oncogene transformed cells is a direct result of upregulation of the mitochondrial fission protein Dnm1 (often referred to as Drp1), which is phosphorylated by members of the MAPK signalling pathway [158][157]. The zebrafish orthologue of Dnm1, Dnm1l, a 1:1 orthologue, shares close to 90% homology with the human protein, with all functional elements conserved (**Supplemental Figure 4**). Although inconclusive, the trend towards Dnm1l upregulation in embryos carrying PNCs detected by RT-PCR, combined with reports that Dnm1l is also controlled at the post-translational level [261]–[263], was sufficient to hypothesise that mitochondrial fragmentation in PNCs is dependent on Dnm1l upregulation. To test this theory, embryos were treated with the Dnm1 specific small molecule GTPase inhibitor mDIVI-1 [264]. Treatment resulted in rapid recovery of mitochondrial phenotype to wild-type morphology (**Figure 4.4 A**, white arrows). Reduced number (**Figure 4.4 B**) and increased size of mitochondrial fragments (**Figure 4.4 C**) is observed at two hours post treatment (hpt), suggesting that fragmentation is dependent upon Dnm1l activity.

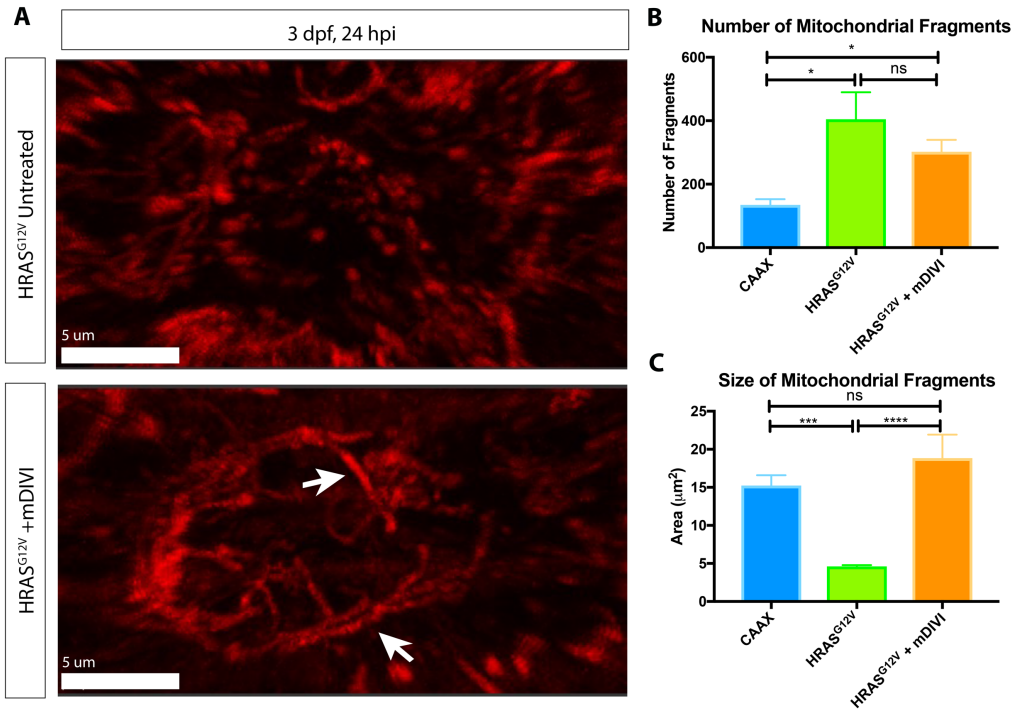

Figure 4.4: Mitochondrial fragmentation in PNCs is dependent on Dnm1l activity. A. Representative images from *in vivo* MitoTracker Deep Red staining at 24 hpi following 2 hr treatment with the Drp1 specific GTPase inhibitor mDIVI-1. Treatment restores mitochondrial morphology to wild-type (White arrows). Scale bar 5 µm **B + C.** Quantification from A. Automated analysis using Imaris software to generate surfaces for mitochondrial staining specifically in PNCs to analyse numerous parameters. Analysis reveals a significant decrease in the number of mitochondrial fragments (B) and a significant increase in the size of mitochondrial fragments (C) in PNCs following mDIVI-1 treatment. Mean + SEM, Mann-Whitney Test, n ≥ 6 embryos from ≥ 3 experiments.

4.3 Dnm1l-dependent mitochondrial fragmentation has consequences for mitochondrial function.

Although mitochondrial fragmentation appears quite extreme in PNCs, fragmentation is a normal process at certain stages of the cell cycle. It was therefore investigated if functional alterations are associated with the fragmentation phenotype.

Mitochondrial staining using dyes with differential dependence on mitochondrial membrane potential was undertaken to determine if membrane potential was altered. Co-staining with MitoTracker Red CMXRos and MitoTracker

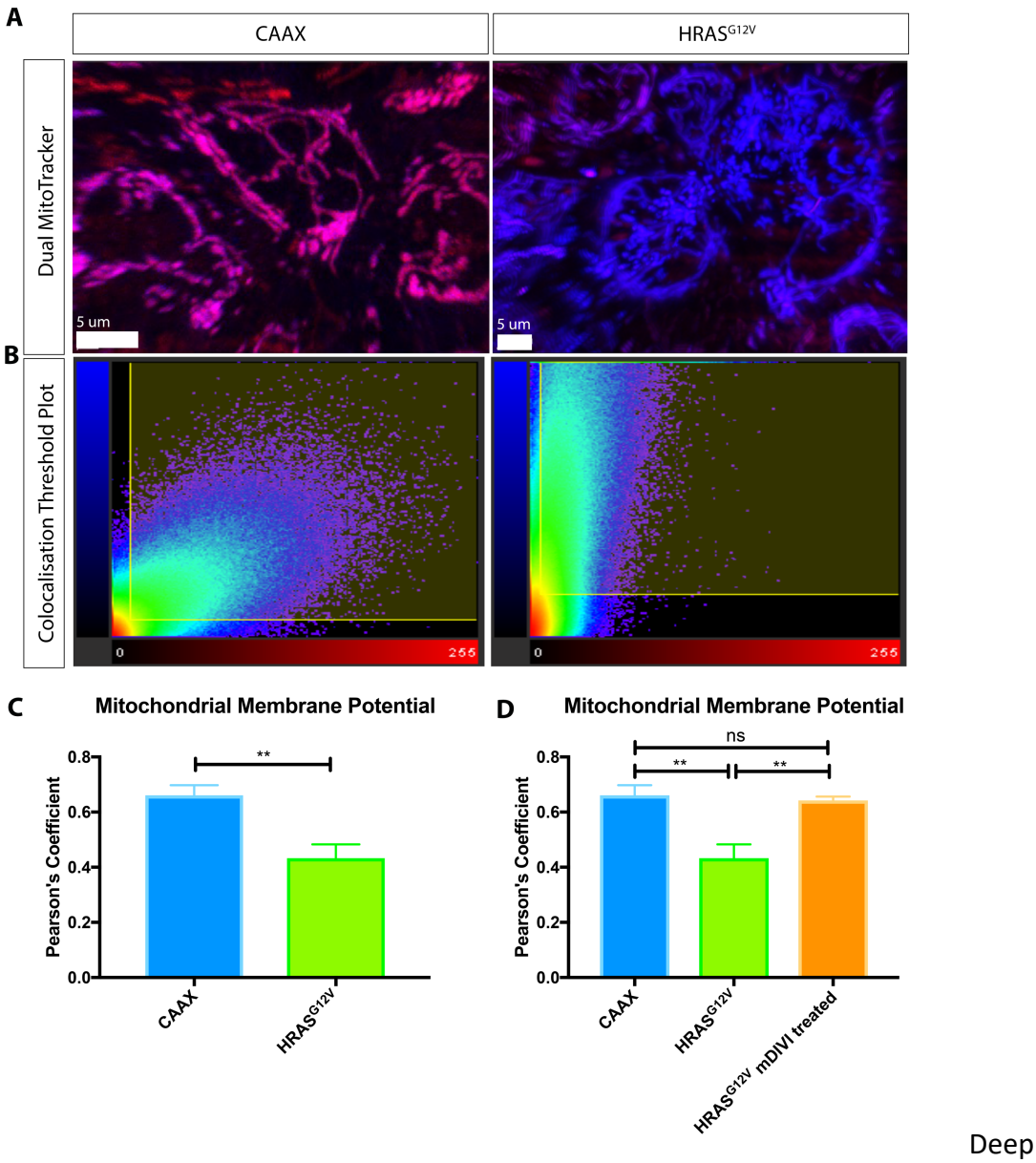

Deep

Figure 4.5: Dnm1l dependent reduced mitochondrial membrane potential is detected in PNCs. A. Representative images from co-staining with MitoTracker Red CMXRos and MitoTracker Deep Red FM at 24 hpi. There are clear differences in dye accumulation between PNCs and control epithelial cells, with PNCs showing less MitoTracker CMXRos staining and, thus reduced mitochondrial membrane potential. Scale bar 5 µm **B.** Quantification from A. Imaris software was used for automatic and unbiased quantification of dye colocalization (See Section 2.14). Colocalization threshold plots reveal vastly reduced accumulation of MitoTracker CMXRos in PNCs, suggesting reduced membrane potential. **C + D.** Quantification from A + B. Colocalization analysis reveals reduced Pearson's Coefficient of Colocalization in PNCs at 24 hpi (C), which is recovered following treatment with mDIVI-1 (D), indicating that loss of mitochondrial membrane potential is reversible. Mean + SEM, Mann-Whitney Test, n ≥ 6 embryos from ≥ 3 experiments

Red FM indicates membrane potential changes as MitoTracker Red CMXRos is more highly dependent on membrane potential, hence, perturbation of membrane potential leads to differential staining. Imaging revealed reduced mitochondrial membrane potential in PNCs relative to control epithelial cells (**Figure 4.5 A**). Colocalization analysis using Imaris software (See Section 2.14) shows drastic alteration in colocalization of dyes (**Figure 4.5 B**) and significantly reduced Pearson's coefficient of colocalization (**Figure 4.5 C**), indicating significantly reduced mitochondrial membrane potential in PNCs. Interestingly, this phenotype is rapidly recovered following treatment with mDIVI-1 (**Figure 4.5 D**). This shows that reduced mitochondrial membrane is dependent on Dnm1l activity.

Reduced mitochondrial membrane potential is indicative of reduced functional capacity but does not give indications of the type and degree of disturbance. To assess this, a protocol using the Seahorse Extracellular Flux Analyser [221] was established in collaboration with Dr. R. Carter, The University of Edinburgh. This instrument can be used to measure oxygen consumption rate (OCR) to assess respiratory function and extracellular acidification rate (ECAR) to monitor glycolytic capacity (see Section 4.5). The assay was established such that a single embryo was added to each well of a specialised 24-well islet capture plate and held in place by an overlaid securing small screen (**Figure 4.6 A**). To investigate OCR and respiratory capacity, a drug manipulation protocol was established. Following measurement of baseline OCR, treatment with the oxidative phosphorylation uncoupler FCCP permitted assessment of maximum OCR capacity. Finally, co-treatment with the complex III inhibitor antimycin and the complex I inhibitor rotenone allowed the respiratory contribution to OCR to be analysed (**Figure 4.6 B**). Implementation of this protocol in the PNC initiation model revealed no difference in baseline OCR (**Figure 4.6 C + D**), or in baseline respiratory capacity (**Figure 4.6 E + F**). However, a subtle yet significant decrease in the maximum respiratory capacity is detected in PNC carrying embryos relative to wild-type controls (**Figure 4.6 G**). This indicates that respiratory function is compromised, and cells are unable to respire to full capacity. Further experimental replicates are necessary to determine

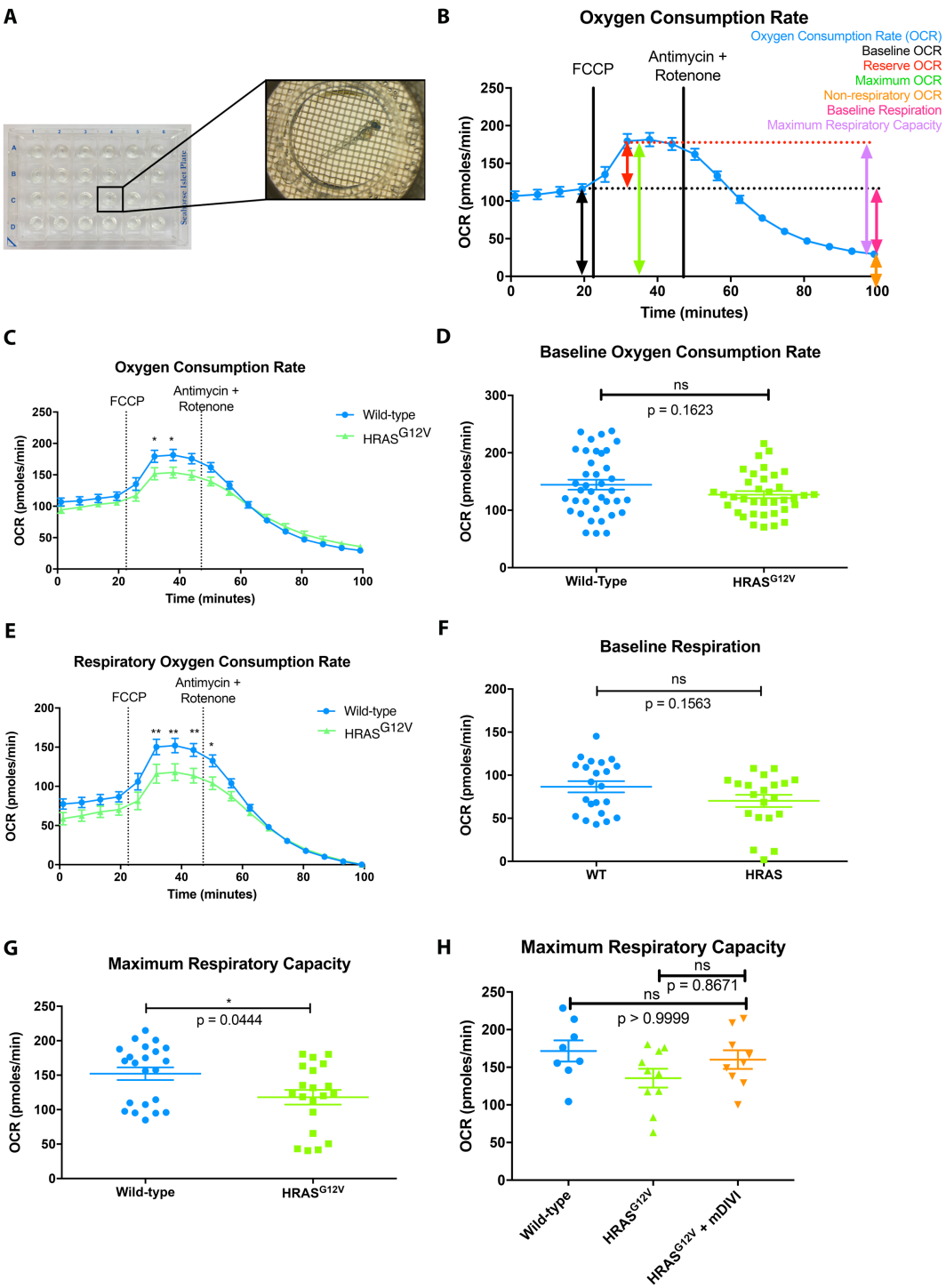

Figure 4.6: A protocol for analysis of respiratory function in zebrafish larvae reveals impaired respiratory capacity in PNC bearing embryos. A. Representative image of plate set up for extracellular flux analysis. A single embryo was added to each well of a specialised islet capture plate and secured in place by a screen. **B.** Representative schematic of drug manipulation protocol for assessment of respiratory function in larval zebrafish. The OCR readout (blue) is

Figure 4.6 (Continued) monitored over time. Following assessment of baseline OCR (black arrow) the respiration uncoupler FCCP was added (black line) to assess reserve OCR (red arrow) and maximum OCR (green arrow). Finally, co-treatment with the complex III inhibitor antimycin and the complex I inhibitor rotenone (black line) allowed the non-respiratory contribution to OCR (orange arrow) to be determined, and hence the baseline respiration (magenta arrow) and the maximum respiratory capacity (purple arrow) to be assessed. **C.** OCR readout over time according to protocol described in B. Mean + SEM, n ≥ 20 embryos from 5 experiments, Two-way ANOVA followed by Sidak's multiple comparisons test. **D.** Quantification from C. Baseline OCR, determined at cycle 4 of protocol measurement, shows no significant difference between wild-type embryos and PNC carrying embryos. Mean + SEM, n = 40 embryos from 5 experiments, Mann-Whitney test, p = 0.1623. **E.** Respiratory OCR over time, determined using data from C as described in B. Mean + SEM, n ≥ 20 embryos from 5 experiments, Two-way ANOVA followed by Sidak's multiple comparisons test. **F.** Quantification from E. Baseline respiration determined at cycle 4 of protocol measurement, shows no significant difference between wild-type embryos and PNC carrying embryos. Mean + SEM, n = 20 embryos from 5 experiments, Mann-Whitney test, p = 0.1563. **G.** Quantification from E. Maximum respiratory capacity, determined at cycle 7 of protocol measurement, shows a subtle yet significant decrease in PNC carrying embryos relative to wild-type controls. Mean + SEM, n = 20 embryos from 5 experiments, Mann-Whitney test, p = 0.0444. **H.** Maximum respiratory capacity following treatment with mDIVI. Although significance is not achieved, recovery of respiratory is seen following treatment with mDIVI-1 suggesting this phenotype is at least partly due to mitochondrial fragmentation. Mean + SEM, p ≥ 8 embryos from 2 experiments, Kruskal-Wallis test, p = 0.2198.

if this effect Is dependent on the Dnm1L-dependent phenotype as statistically significant recovery was not detected following mDIVI treatment in a small number of experiments (**Figure 4.6 H**). The small effect size is fully expected within the context of the whole-embryo approach, where the proportion of transformed cells makes up a small fraction of the total volume of the embryo. This assay, however, provides a method for *in vivo* analysis of respiratory parameters in zebrafish larvae and gives indications of the adverse functional consequences of the mitochondrial phenotype in PNCs.

4.4 Despite mitochondrial alterations, increased reactive oxygen species are not detected in the PNC niche.

Given the degree of mitochondrial change observed in PNCs, one would expect an increase in reactive oxygen species (ROS) in the PNC niche. Alternative zebrafish models of PNC initiation have also shown that hydrogen peroxide is produced in the PNC niche [192]. It was hypothesized that there may be a link between the increased H_2O_2 production and the mitochondrial fragmentation phenotype. To test this, the general oxidative stress indicator CM-H_2DCFDA was used to monitor ROS production in the PNC niche. Surprisingly, remarkably little ROS signal was detected by time-lapse microscopy from 16 – 20 hpi (**Supplemental Movie 3, Figure 4.7 A**). The dye appeared to be working as signal was detected in leukocytes in the PNC niche (**Figure 4.7 A,** turquoise arrows). Very faint signal is detected in PNCs with very strong $HRAS^{G12V}$ expression (**Figure 4.7 A**, yellow arrows), but given the intensity of mCherry-$HRAS^{G12V}$ expression and the weakness of dye it is difficult to determine if this is artefactual. In attempt to overcome this an alternative oxidative stress indicator was tested. Dihydroethidium (DHE) is a superoxide indicator that translocates to the nucleus following oxidation, resulting in red nuclear staining in cells in which superoxide has been generated. Again, remarkably little superoxide signal was detected in the PNC niche (**Supplemental Movie 4, Figure 4.7 B**). Positive DHE signal was detected in just three PNCs (**Figure 4.7 B**, magenta arrows) and three neighbouring cells at 24 hpi. Taken together, these data suggest that ROS generation is not a feature of PNC development, despite significant mitochondrial alterations.

Like all extrinsically applied compounds, these ROS indicators have technical obstacles, with a fine balance between embryo tolerance and signal detection often required. To circumvent this issue, and to robustly test that ROS generation is not a feature of PNC development, transgenic reporter zebrafish lines for localized redox stress were generated. Three individual transgenic lines were generated, with the roGFP redox stress reporter [265] localized to the cytoplasm, the mitochondrial matrix and the mitochondrial inner membrane [237] under the control of the

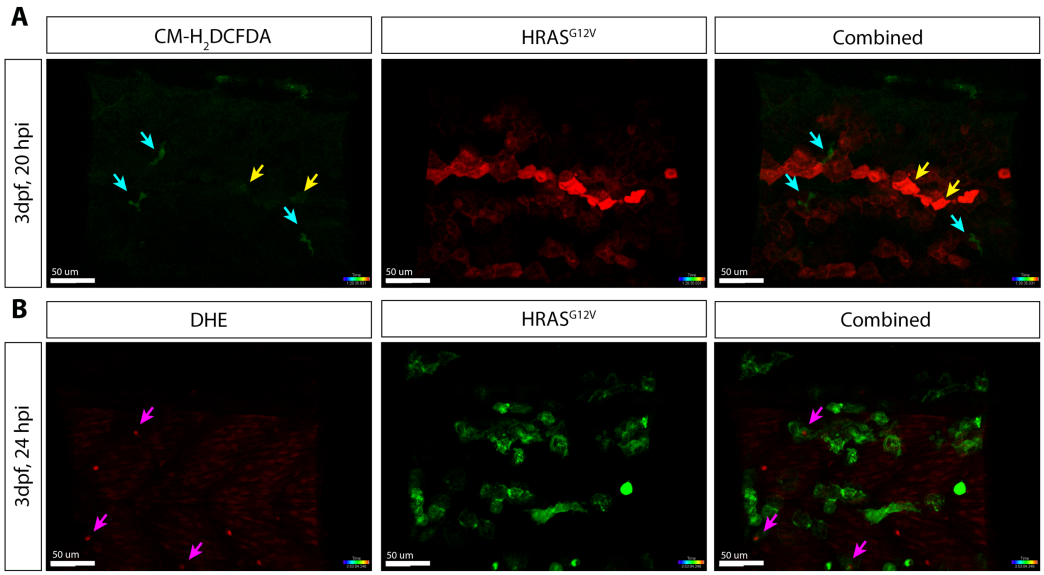

Figure 4.7: Reactive oxygen species are not detected in the PNC niche. A. Representative still images from Supplemental Movie 3 showing CM-H_2DCFDA staining in PNCs at 20 hpi. CM-H_2DCFDA signal is detected in leukocytes (turquoise arrows). However only very faint signal is detected in PNCs with very high $HRAS^{G12V}$ expression (Yellow arrows), indicating general ROS are not significantly increases in PNCS. Scale Bar 50 µm **B.** Representative still images from Supplemental Movie 4 showing DHE staining in PNCs at 24 hpi. DHE signal is detected in only three PNCs (magenta arrows), suggesting superoxide generation is not a significant feature of PNC development. Scale bar 50 µm.

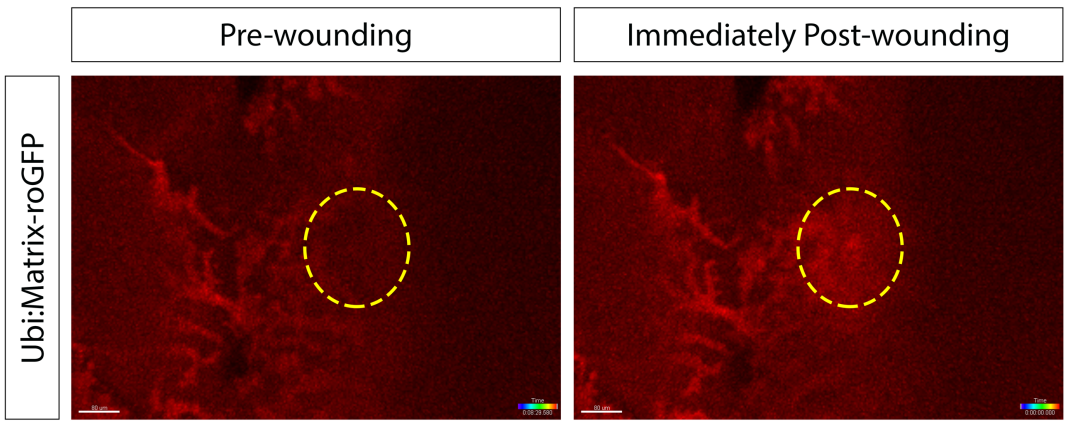

Figure 4.8: A newly generated redox sensor localised to the mitochondrial matrix shows increased oxidation following wounding. Representative images from Supplemental Movie 5 showing response to sterile laser injury (yellow circle) in Ubi:Matrix-roGFP at 3 dpf. Increased oxidative stress is seen immediately post wounding, indicating the reporter behaves as expected.

ubiquitous Ubi promoter. Owing to the time taken for generation and characterisation of transgenic zebrafish lines, only the mitochondrial matrix-localized line (**Supplemental Figure 5**) was grown to the required generation and characterised within the time-frame of this project. To verify that this reporter was behaving as expected, the response to wounding was tested. It is known that rapid ROS generation occurs post wounding in zebrafish larvae [266], therefore Ubi:Matrix-roGFP larvae were subjected to sterile laser injury at 3 dpf. Immediately post wounding an increase in oxidation was detected (**Supplemental Movie 5, Figure 4.8**), suggesting that the reporter was behaving as expected. Following this, the mitochondrial matrix redox reporter was incorporated into the PNC initiation model. Again however, little oxidative signal was detected at 24 hpi (**Supplementary Movie 6, Figure 4.9**). As further confirmation that the reporter behaves as expected, increased oxidative stress is detected in a PNC that undergoes cell death (**Figure 4.9**, white arrow). Enhanced signal is not detected in other PNCs, suggesting the ROS generation in the mitochondrial matrix is not a feature of PNC development. However, completion of the cytoplasmic redox sensor will give indications of more general oxidative stress during PNC development.

The finding that PNCs do not generate ROS during development was highly surprising. Given the drastic mitochondrial phenotype and previous published work, ROS generation was unquestionably expected, and its absence was puzzling. One possible explanation for undetectable ROS in the PNC niche is rapid detoxification to prevent cell death. To test this, expression of the mitochondrial detoxification enzyme superoxide dismutase 2 (SOD2) was assessed by qRT-PCR at 24 hpi. Increased SOD2 expression was not detected (**Figure 4.10**). As mentioned, the whole embryo approach to qRT-PCR used in this project is open to false negatives, so increased SOD2 activity cannot be ruled out using this technique, but an increase of sufficient magnitude to completely detoxify mitochondrial ROS in the PNC niche would be unlikely.

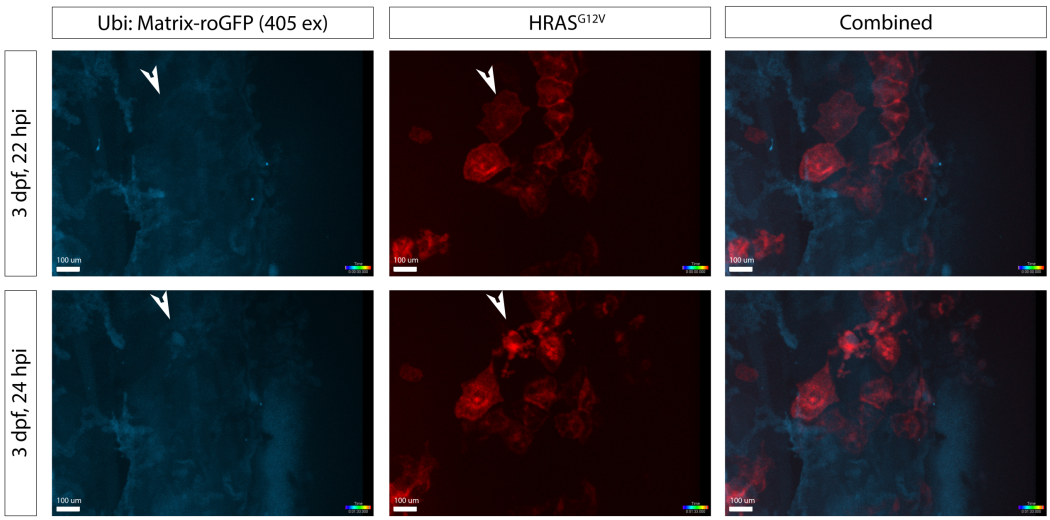

Figure 4.9: Increased oxidative stress is only detected in PNCs undergoing cell death. Representative still images from Supplemental Movie 6 showing oxidative stress in the PNC niche using Ubi:Matrix-roGFP. Oxidative stress in not detected in PNCs during development. However, when a PNC undergoes apoptosis (white arrow) oxidative stress is detected. This both verifies that the reporter behaves as expected and indicates that mitochondrial matrix ROS are not generated in the PNC niche. Scale bar 100 µm.

Figure 4.10: Increased SOD2 expression is not detected in embryos carrying PNCs. qRT-PCR expression analysis of the mitochondrial detoxification enzyme SOD2 in embryos carrying PNCs relative to wild-type controls. There is no detectable difference in SOD2 expression in PNC bearing embryos, suggesting enhanced detoxification of ROS by SOD2 is not occurring in the PNC niche. Mean + SEM, n=7 experiments, t test.

4.5 Glycolytic flux is increased following HRAS^{G12V} induction.

In addition to mitochondrial fragmentation, it is well established that mature cancer cells exhibit a metabolic switch from oxidative phosphorylation to glycolytic metabolism, termed the Warburg effect. Following the success in developing an assay of respiratory analysis using the Seahorse extracellular flux analyser, a similar assay development strategy was undertaken to assess glycolytic function in this PNC initiation model in collaboration with Dr. R. Carter, The University of Edinburgh. Again, the assay was established such that a single embryo was added to each well of a 24-well islet capture plate and secured using a screen (**Figure 4.11 A**). Baseline extracellular acidification rate (ECAR) was measured over time. Then, to assess glycolytic flux, which represents the flow of molecules through the glycolytic pathway, the competitive glucose inhibitor 2-deoxyglucose (2-DG) was added, followed by addition of the respiration uncoupler FCCP to assess the contribution of glycolysis to respiratory function (**Figure 4.11 B**). The addition of 2-DG inhibits glycolysis as glucose cannot enter the pathway, therefore the drop in ECAR is indicative of the contribution of glycolytic flux to the ECAR. Significantly increased glycolytic flux was detected in embryos bearing PNCs relative to wild-type controls at 20 hpi (**Figure 4.11 C + D**). Using the complimentary oxygen consumption rate (OCR data not shown), the contribution of glycolysis to respiratory function can be assessed by following 2-DG treatment with FCCP treatment using a similar strategy to that described in **Figure 4.6**. It was found that maximum OCR was only marginally decreased following 2-DG and FCCP treatment (**Figure 4.11 E**). This suggests that embryos can cope with respiration when glucose cannot be utilised, so clearly other inputs to the oxidative phosphorylation pathway can maintain sufficient respiratory function, indicating that, while glycolytic flux is enhanced, it is not utilised for energy production.

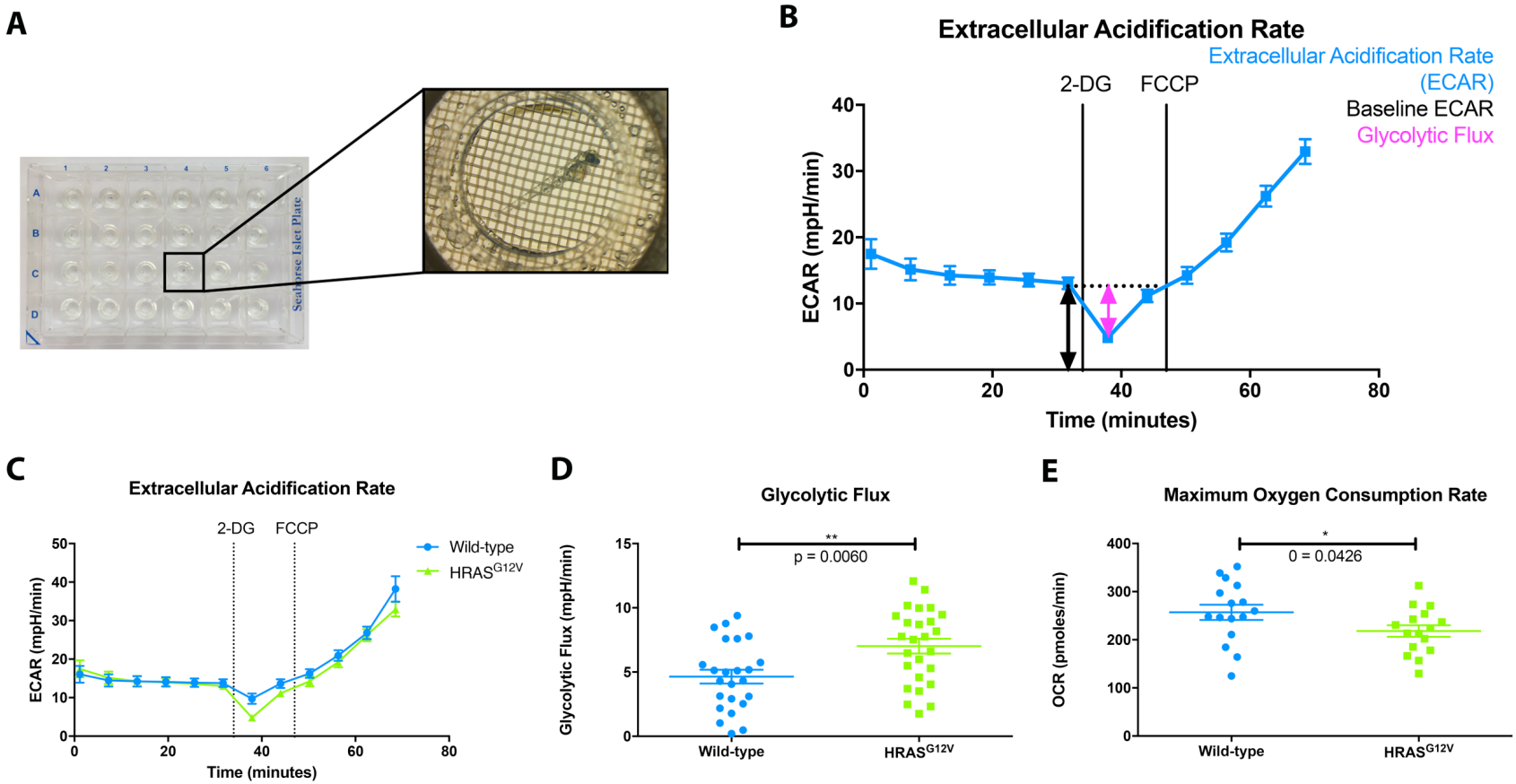
A
Seahorse Islet Plate
B
Extracellular Acidification Rate
Extracellular Acidification Rate (ECAR)
Baseline ECAR
Glycolytic Flux
2-DG
FCCP
ECAR (mpH/min)
Time (minutes)
C
Extracellular Acidification Rate
2-DG
FCCP
Wild-type
HRASG12V
ECAR (mpH/min)
Time (minutes)
D
Glycolytic Flux
p = 0.0060
Glycolytic Flux (mpH/min)
Wild-type
HRASG12V
E
Maximum Oxygen Consumption Rate
0 = 0.0426
OCR (pmoles/min)
Wild-type
HRASG12V

Figure 4.11: Glycolytic flux is enhanced in the presence of PNCs. A. Representative image of plate set up for extracellular flux analysis. A single embryo was added to each well of a 24-well islet capture plate and held in place using a screen. **B.** Representative schematic of drug manipulation protocol for analysis of glycolytic function in zebrafish larvae. The ECAR readout (blue) monitored over time. Following assessment of baseline ECAR (Black arrow), the glycolytic flux (magenta arrow) can be assessed by the addition of the glycolysis inhibitor 2-DG (black line). The respiration uncoupler FCCP was then added (black line) to assess the contribution of glycolysis to respiratory function using the complimentary OCR data (not shown). **C.** ECAR readout over time according to the protocol described in B. Mean + SEM, n = 16 embryos from 3 experiments. **D.** Quantification from C. Glycolytic flux, determined at cycle 7 of measurement, shows enhanced glycolytic flux in the presence of PNCs relative to wild-type controls. Mean + SEM, n = 16 embryos from 3 experiments, Mann-Whitney test, p = 0.0060. **E.** Maximum oxygen consumption rate determined from OCR date complimentary to that shown in C. Maximum OCR is marginally reduced in the presence of PNCs relative to wild-type controls, suggesting that enhanced respiratory function is not utilised for respiratory function. Mean + SEM, n = 16 embryos from 3 experiments, Mann-Whitney test, p = 0.0426

4.6 Glucose uptake is not increased in PNCs.

As glycolytic flux is enhanced following PNC induction, it was expected that glucose uptake would be increased in PNCs, in accordance with The Warburg Effect [92]. To test this, the fluorescent 2-NBDG compound was used to monitor glucose uptake. Surprisingly, enhanced 2-NBDG signal was not detected in PNCs relative to non-transformed cells (**Figure 4.12 A**), suggesting that glucose uptake was not enhanced in PNCs during development.

This was further verified using a red fluorescent glucose compound recently developed by Sam Benson and Dr. Marc Vendrell, The University of Edinburgh. To verify this compound, SeNBD-Glucose (Unpublished), behaved as expected in zebrafish larvae, accumulation was monitored following morpholino knock-down of the GLUT2 glucose transporter. Decreased accumulation of SeNBD-glucose was detected in the head region of GLUT2-morpholino embryos (**Figure 4.13**), consistent

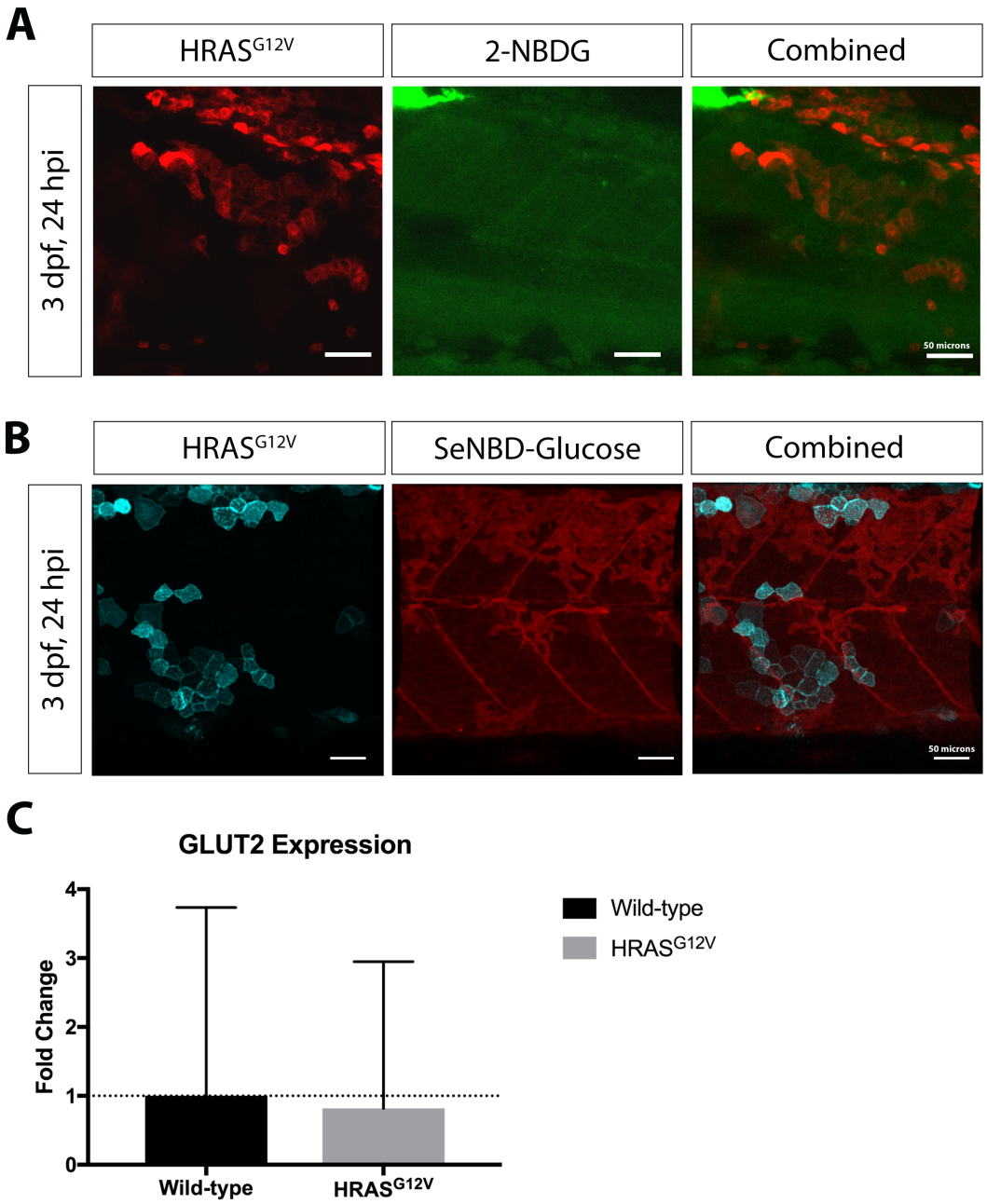

Figure 4.12: Glucose uptake is not increased in PNCs. A. Representative images from glucose tracing using 2-NBDG in PNCs at 24 hpi. Glucose uptake is not enhanced in PNCs relative to non-transformed cells. Scale bar 50 µm. **B.** Representative images from glucose tracing using the newly developed SeNBD-Glucose in PNCs at 24 hpi. Again, glucose uptake in PNCs is not increased. Scale bar 50 µm. **C.** Fold change of gene expression detected by qRT-PCR at 24 hpi. No change in GLUT2 expression is detected in the presence on PNCs relative to wild-type controls. Mean + SEM, n = 5 experiments, t test

Figure 4.13: *In vivo* characterisation of Se-NBD-glucose. Representative images following yolk injection of 100 mM Se-NBD-glucose at 28 hpf. Morpholino knock-down of the GLUT2 glucose transporter results in decreased accumulation of Se-NBD-glucose in the head region of embryos (white arrows), consistent with published work using the 2-NBDG glucose analogue [245].

with previous findings as the GLUT2 transporter is primarily neuronally expressed in zebrafish larvae [245]. Use of SeNBD-glucose similarly did not show enhanced accumulation in PNCs at 24 hpi (**Figure 4.12 B**). Given the increase in glycolytic flux detected, this was highly unexpected considering glucose is required to fuel glycolysis.

Further to this, expression of the glucose transporter GLUT2 was assessed by qRT-PCR. Despite the issues associated with the qRT-PCR approach in this project, expression of GLUT2 was assessed in the presence of PNCs relative to wild-type embryos, with no significant difference detected between the groups (**Figure 4.12 C**). However, as GLUT2 is primarily a neuronal glucose transporter in larval zebrafish [245], the contribution of this to PNC development is questionable and assessment of other glucose transporters, such as GLUT1 and GLUT5 may be more appropriate moving forward.

4.7 Alterations in lactate levels were not detected in PNCs.

At the culmination of the glycolytic pathway pyruvate has one of two fates; conversion to acetyl-coA by PDH or conversion to lactate by lactate dehydrogenase (LDH) [76]. Increased lactate levels following enhanced glycolysis are characteristic of The Warburg Effect and are associated with poor prognosis in cancer patients [267].

It was therefore of interest to determine if lactate levels are increased in PNCs at early stages of development.

To assess if lactate levels were altered in the presence of PNCs a commercially available lactate assay, similar to those described in Section 1.9, was used. This assay revealed no change in lactate concentration in PNC bearing embryos relative to wild-type controls (**Figure 4.14 A**), although subtle alterations could be masked using this whole embryo approach. Despite attempts, sufficient numbers of PNCs could not be isolated to attempt the assay in a PNC-specific manner, as the small sample size was not within the detection range of the assay. qRT-PCR analysis of LDH-A and the lactate transporter MCT4, which is commonly altered in established cancer, revealed unchanged expression in the presence of PNCs (**Figure 4.14 B**). These findings suggest that lactate concentrations in the PNC niche are not increased, although it is difficult to conclude with certainty due to the errors associated with these techniques. Moving forward, more specific approaches

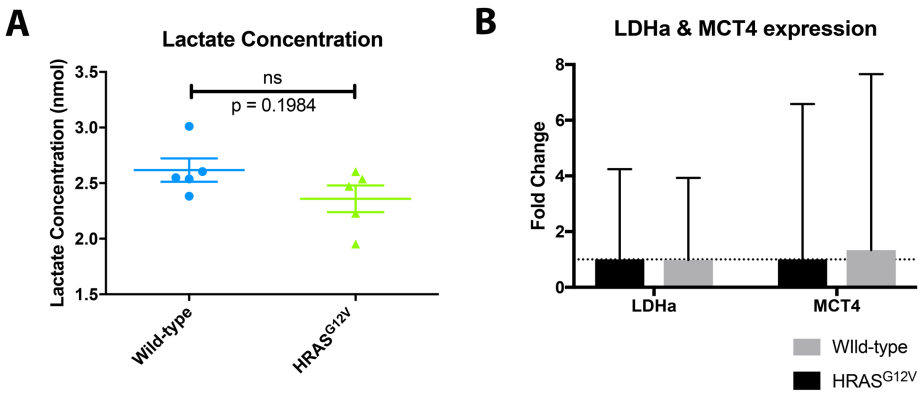

Figure 4.14: Increased lactate concentration is not detected in the presence of PNCs. A. Lactate concentration determined using commercially available lactate assay kit. A marginal decrease in lactate concentration is detected in the presence of PNCs relative to wild-type controls. Mean + SEM, n = 5 experiments, Mann-Whitney test, p = 0.1984. **C.** Fold change of gene expression determined by qRT-PCR at 24 hpi. Expression of LDH-a and the lactate transporter MCT4 remains unchanged in the presence of PNCs relative to wild-type controls. Mean + SEM, n = 5, Mann-Whitney test.

are required to assess lactate levels *in vivo*. Generation of a transgenic reporter zebrafish lines is underway to facilitate this, as further discussed in section 5.1.

4.8 PNC survival is linked to glycolytic metabolism, but not to mitochondrial fragmentation.

Having earlier demonstrated the effect of mitochondrial fragmentation on mitochondrial function, the effect of this phenotype on PNC development was investigated. To assess if Dnm1l-dependent mitochondrial fragmentation is required for PNCs survival, cleaved caspase-3 activity in PNCs was assessed as a marker of apoptosis. At 24 hpi, no change in caspase-3 activity in PNCs was detected following treatment with mDIVI-1 (**Figure 4.15**), suggesting that mitochondrial fragmentation is not responsible for induction of apoptosis and is not a requirement for PNC persistence. To assess if glycolytic signalling is important for PNC survival cleaved caspase-3 levels were assessed as a measure of apoptotic cell death. Following 2-DG inhibition, increased caspase-3 activation was detected

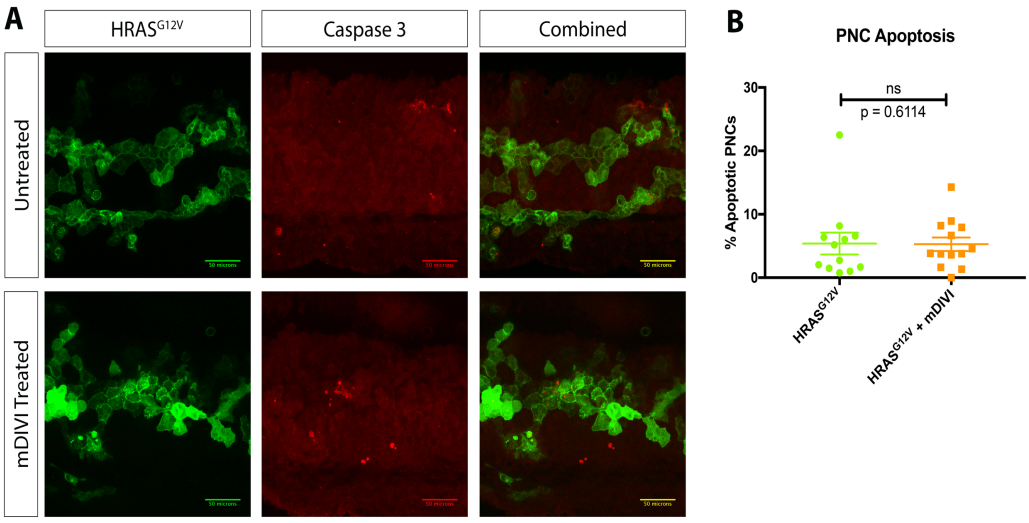

Figure 4.15: mDIVI-1 treatment does not induce apoptosis in PNCs. A. Representative images of cleaved caspase-3 activity in PNCs at 24 hpi, untreated or 16 hpt mDIVI-1. Scale Bar 50 µm **B.** Quantification from A. No difference in PNC apoptosis is detected following treatment with mDIVI-1, indicating that mitochondrial fragmentation does not induce apoptosis and is not a requirement for PNC survival. Mean + SEM, n ≥ 12 embryos from 3 experiments, Mann-Whitney test, p = 0.6114

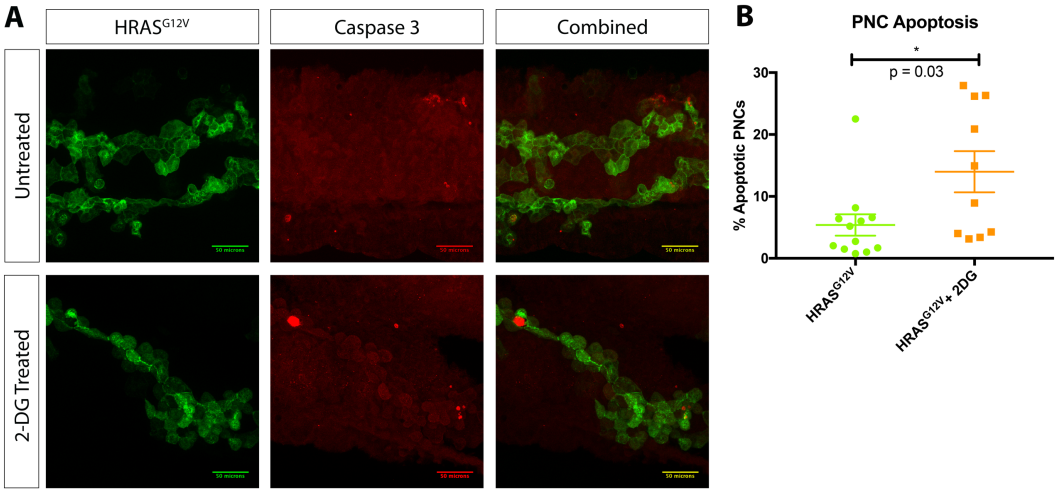

Figure 4.16: PNC apoptosis is increased following glycolysis inhibition. A. Representative images of cleaved caspase-3 activity in PNCs at 24 hpi, untreated or 16 hpt 2-DG. Scale bar 50 µm. **B.** Quantification from A. Increased apoptotic cell death is detected in PNCs following inhibition of glycolysis by 2-DG treatment, indicating glycolysis is important for PNC survival. Mean + SEM, n ≥ 10 embryos from 3 experiments, Mann-Whitney test, p = 0.03

specifically in PNCs relative to untreated controls (**Figure 4.16**). This suggests that glycolysis is important for PNC survival and elevated glycolytic flux could be vital for PNC persistence.

4.9 Neutrophil recruitment to developing PNCs is altered by glycolytic signalling, but not by mitochondrial fragmentation.

As shown in Section 3.4 (**Figure 3.8**), this model of PNC initiation is consistent with others, in that recruitment of neutrophils to developing PNCs is observed. This is a major research interest for the group and one of the hypotheses of this project is that metabolic alterations are involved in the signalling that induces this response.

To determine if Dnm1l-dependent mitochondrial fragmentation is involved in neutrophil recruitment to developing PNCs, time-lapse microscopy following mDIVI-treatment was undertaken. Analysis reveals that neutrophil recruitment is not altered by mDIVI-1 treatment (**Figure 4.17**), suggesting that mitochondrial

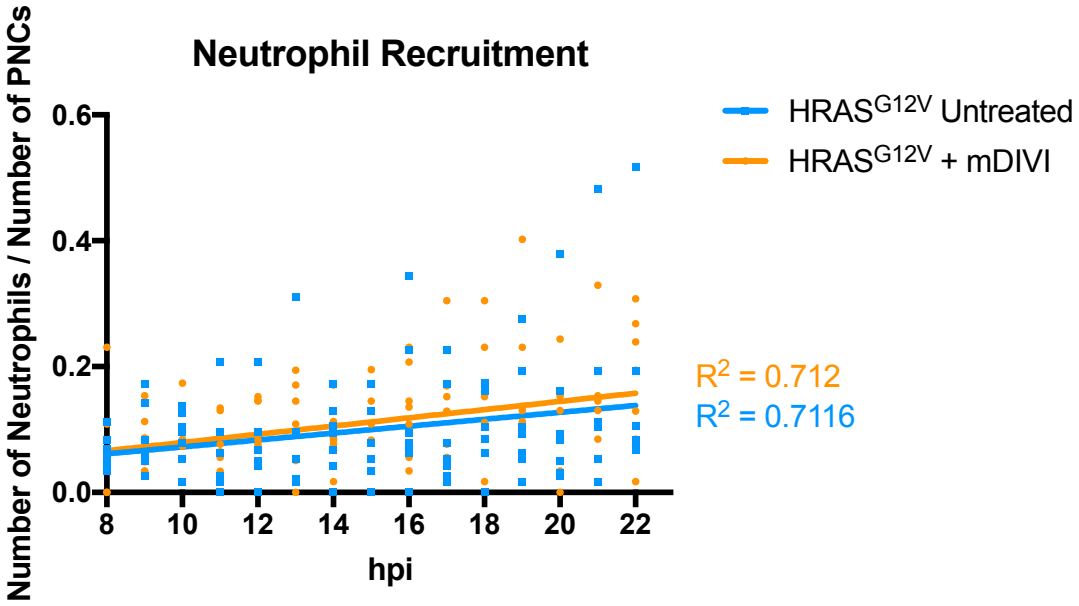

Figure 4.17: Neutrophil recruitment to developing PNCs is not altered by mDIVI-1 treatment. Quantification of recruited neutrophil numbers to PNCs following mDIVI-1 treatment. Treatment with mDIVI-1 does not alter the number of neutrophils recruited to developing PNCs, suggesting that mitochondrial fragmentation is not involved in establishing an inflammatory response in the PNC niche. Aligned replicates with linear regression analysis, n = 7 embryos from 3 independent experiments.

fragmentation does not induce the inflammatory response observed in the PNC niche.

To investigate the role of glycolytic signalling in establishing a pro-inflammatory niche, embryos were treated with 2-DG and recruitment of neutrophils to the PNC niche was monitored by time-lapse microscopy. Analysis reveals that recruitment of neutrophils is significantly reduced following treatment with 2-DG (**Figure 4.18**). However, as neutrophils are inherently highly glycolytic cells it is possible that 2-DG could be acting directly on neutrophils. To test this, recruitment of neutrophils to a wound following 2-DG treatment was assessed. Surprisingly, no change in number of neutrophils recruited to the wound at 6 hpw was detected following treatment with 2-DG (**Figure 4.19**). This suggests that glycolytic signalling in the PNC niche plays an important role in the recruitment of neutrophils at early stages of PNC initiation.

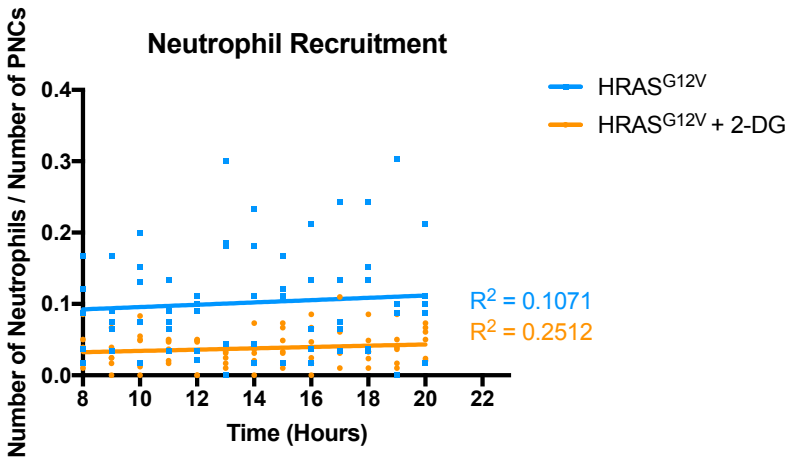

Figure 4.18: Recruitment of neutrophils to the PNC nice is impaired following 2-DG treatment. Quantification of recruited neutrophil numbers to PNCs following 2-DG treatment. Glycolysis inhibition with 2-DG appears to impair neutrophil recruitment, suggesting that glycolytic signalling is important for establishing an inflammatory response in the PNC niche. Aligned replicates with linear regression analysis, n = 6 embryos from 3 independent experiments.

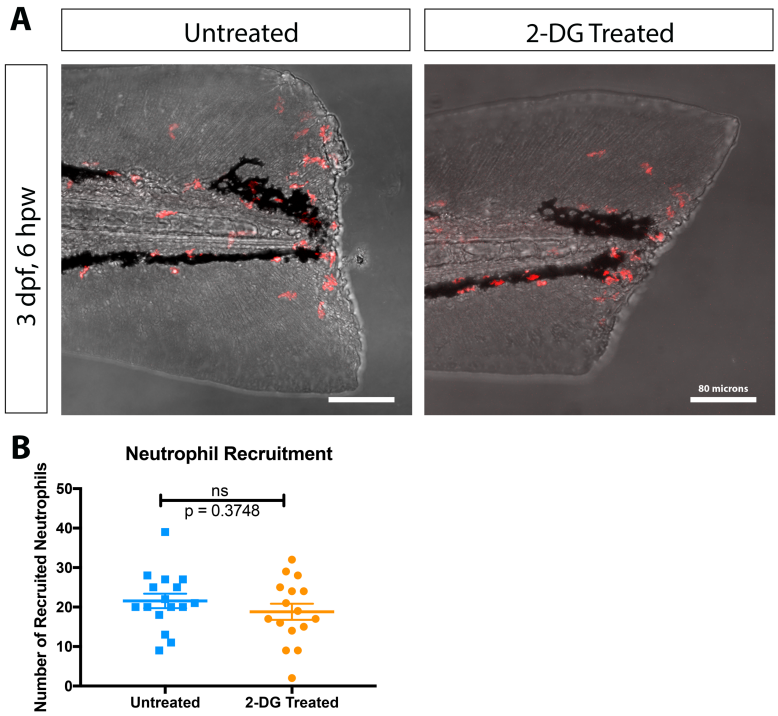

Figure 4.19: Neutrophil recruitment to a wound is not impaired following 2-DG treatment. A. Representative images from LysC:DSRed embryos at 6 hpw, untreated or 6 hpt 2-DG. Scale bar 80 µm. **B.** Quantification from A. Number of neutrophils recruited to wound at 6 hpw following treatment with 2-DG. Inhibition of glycolysis does not appear to alter recruitment of neutrophils to a wound. Mean + SEM, n = 16 embryos from 2 experiments, Mann-Whitney test, p = 0.3748

4.10 Metformin treatment induces PNC specific apoptotic cell death.

From the findings presented above, it is clear that mitochondrial fragmentation is an early alteration in PNCs and this phenotype has functional consequences, most notably impaired respiratory capacity. As this is a distinguishing feature of PNCs, it was of interest to determine if this phenotype could be targeted for therapeutic or preventative interventions.

Metformin is a mitochondrial complex I inhibitor commonly used for the treatment of type 2 diabetes. Many studies and trials are currently underway to investigate metformin in a cancer paradigm, both as a cancer treatment and for its potential in cancer prevention (reviewed in [268]). Metformin has two mechanisms of action; it acts on complex I of the electron transport chain and can activate the MAPK-dependent AMPK signalling pathway, with both processes altering a cells capacity to generate energy [268][269]. Hence, metformin alters cellular function and fate by manipulating cellular energy consumption. As PNCs in this model have altered MAPK activity as a result of $HRAS^{G12V}$-transformation and appear to have a respiratory impairment, it was of interest to probe their response to metformin. Detection of cleaved caspase-3 activity as a measure of apoptotic cell death was used to consider the effect of metformin treatment on PNCs. It was found that treatment with metformin induced rapid and PNC-specific apoptotic cell death (**Figure 4.20**). Despite a wide spread in the data, at 4 hpt caspase-3 activity in PNCs had significantly increased from 5% in untreated controls to an average of 26% in metformin treated embryos, reaching a high of 50% in some samples (**Figure 4.20 B**). In fact, by 16 hpt there appeared to be fewer PNCs for analysis in metformin treated embryos (observational detail, data not shown), suggesting that a considerable number of PNCs had died by apoptosis by this time-point. This increase in apoptotic cell death is PNC specific as caspase-3 activity was not seen in other cells in the PNC niche (**Figure 4.20 A**). This indicates that altered MAPK activity and the mitochondrial fragmentation-induced respiratory impairment seen in PNCs makes them susceptible to apoptotic cell death following metformin

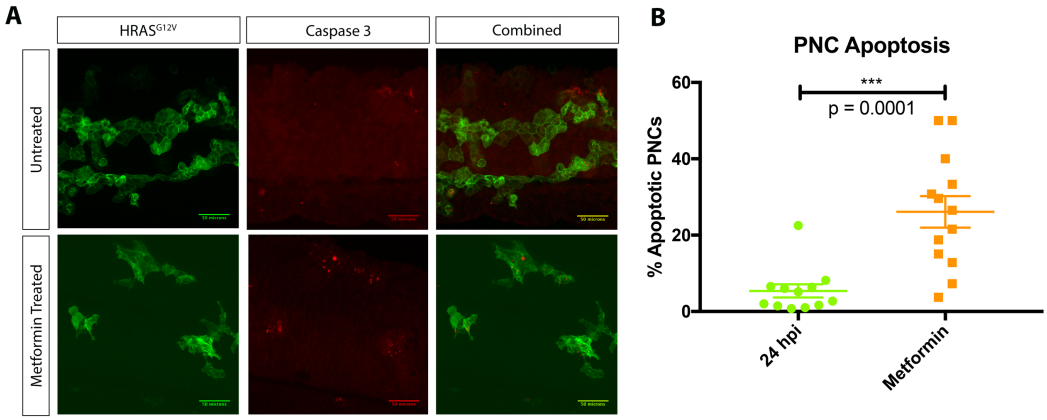

Figure 4.20: Metformin treatment induces apoptotic cell death in PNCs. A. Representative images of cleaved caspase-3 activity at 24 hpi, untreated or 4 hpt metformin. Increased caspase-3 activity is seen following metformin treatment. Scale bar 50 µm **B.** Quantification from A. Percentage of PNCs undergoing apoptosis is significantly increased following metformin treatment. Mean + SEM, n ≥ 12 embryos from 3 experiments, Mann-Whitney test, p = 0.0001.

treatment and places metformin as an ideal candidate for further investigations of cancer prevention.

4.11 Discussion

The role of mitochondrial phenotype, and downstream processes dependent upon such, during PNC initiation and development have not previously been determined. While it is known that these features play important roles in the progression of established cancers, the timing of these alterations and their role in initiation remains elusive. Using a newly established *in vivo* larval zebrafish model for tumour initiation, the mitochondrial phenotype and the possible effect of mitochondrial alterations during PNC initiation and development was investigated.

Mitochondria undergo significant Dnm1l-dependent fragmentation at very early stages of PNC development. This has functional consequences as reduced mitochondrial membrane potential and impaired respiratory capacity are observed. The phenotype does not appear to induce mitochondrial ROS and does not appear to be important for PNC survival. Treatment with the complex I inhibitor metformin

induces PNC specific apoptosis, placing mitochondrial and respiratory alterations as potential targets for preventative and therapeutic interventions.

It was determined that mitochondrial fragmentation, similar to that seen in established cancers [154]–[156], occurs at very early stage of PNC development. In fact, fragmentation is apparent from the earliest stages of PNC detection and persists over time as significant fragmentation is still detectable at 24 hpi. This would indicate that the phenotype has important roles during the initiation stages of cancer, as well as later stages of progression.

To understand how mitochondrial fragmentation might affect tumour initiation, it is important to determine mechanistic insights of how this phenotype arises. Previous work suggests that upregulation of the mitochondrial fission protein Dnm1 *in vitro* is responsible for mitochondrial fragmentation following phosphorylation by members of the MAPK pathway [157][158]. Isolation of PNCs by FACS for analysis of expression levels of mitochondrial fusion and fission proteins was attempted. PNCs were successfully isolated, but extraction of a sufficient quantity of RNA for cDNA synthesis was not achieved without the need for amplification. As amplification adds significant cost, it was instead decided, for the purposes of this project, to analysis cDNA synthesised from RNA extracted from whole embryos carrying PNCs. This approach means that expression levels in all cells in the embryo, not just PNCs, will be analysed and any changes occurring in PNCs could be masked by the basal expression level in other cells. Only highly significant alterations will be detected, and the likelihood of false negatives is high. To overcome this, recent funding has been secured to carry out RNA sequencing analysis in this model, which will test this result specifically in PNCs. In the interim, attempts were made to visualise this Dnm1l upregulation by immunostaining. Antibodies for mammalian orthologues of Drp1 with predicted reactivity for the zebrafish orthologue were trialled but proved unsuccessful.

Despite these results, previously published work [157][158], suggested that upregulation of Dnm1l was responsible for the extensive mitochondrial fragmentation seen in PNCs. A pharmacological approach to test this using the Drp1-

specific GTPase inhibitor mDIVI-1 [264] resulted in rapid recovery of conventional mitochondrial phenotype, indicating that the fragmentation phenotype is a result of Dnm1l activity. This also reveals that fragmentation is reversible, so mitochondria are not damaged beyond recovery. Excessive fragmentation induces apoptosis and therefore a delicate balance must exist in PNCs so as not to cause cell death while still enabling the downstream alterations to occur. Mitochondrial fragmentation as a result of Drp1 upregulation in cancer is not novel, but the occurrence of the phenotype so early in development suggests vital importance for oncogenic processes. Fragmentation and its downstream effects must clearly be involved in tumour establishment and progression. Given the clear importance of Dnm1l expression, this conclusion would be better supported with a non-pharmacological approach as mDIVI-1 is administered via immersion and acts globally on the embryos. Also, issues of tissue penetration and toxicity are always to be considered with pharmacological approaches. Therefore, a genetic approach to knock-down Dnm1l expression specifically in PNCs is currently under development. Using a dominant negative form of the protein [147], Dnm1l expression will be reduced specifically in PNCs to assess the effect on PNC development and reinforce these findings.

As mitochondrial fragmentation occurs naturally as part of the cell cycle, mitochondrial membrane potential was assessed to determine if the fragmentation observed in PNCs was destructive. A number of different MitoTracker stains are available to analyse mitochondria, with distinct properties and colours associated with each. When used in combination a variety of mitochondrial parameters can be assessed. To investigate membrane potential MitoTracker Red CMX-Ros combined with MitoTracker Green FM is the ideal combination. Accumulation of MitoTracker Red CMX-ROS is highly dependent on membrane potential, while MitoTracker Green FM accumulates in mitochondrial independent of membrane potential [270]. In this approach, colocalization of the two stains should occur in intact mitochondria, while loss of membrane potential can be assessed based on loss of red signal. However, due to the colour profile of this combination it could not be used in the PNC model. Instead, the far red MitoTracker Deep Red FM was used in combination with

MitoTracker Red CMXRos. MitoTracker Deep red FM is not independent of membrane potential. Accumulation occurs in mitochondria with lost membrane potential but staining intensity is altered [271]. Therefore, this approach can be used to assess reduced membrane potential, but not complete loss, provided fluorescence intensity is closely monitored. To overcome this intensity dependence on membrane potential, automated Imaris software analysis was used to calculate the colocalization independent of fluorescence intensity. This approach revealed reduced mitochondrial membrane potential in PNCs and indicated that fragmentation has functional consequences for mitochondria. As membrane potential was rapidly recovered following treatment with mDIVI-1, this further shows that the mitochondrial fragmentation phenotype is dependent on Dnm1l activity.

To further probe the consequential effect of mitochondrial fragmentation a protocol for assessment of respiratory function was developed. The Seahorse extracellular flux analyser can be used to measure oxygen consumption rate (OCR) to assess respiratory function. Originally developed for used with cell culture, there are few publications using the instrument for *in vivo* analysis. At the time of assay development just two papers had been published using the instrument for *in vivo* zebrafish analysis [272][273] and crucial details were missing from both. While Stackley, *et al,* [272] gave in-depth protocol details, information on run temperature was missing, which preliminary work revealed to be highly relevant, as data varied greatly with just minor changes in temperature. Meanwhile, Gilbert, *et al*, [273] missed vital run protocol information, temperature information and embryo staging data. Using these publications as a basis, a protocol for *in vivo* detection of respiratory function in embryos up to 60 hpf was developed. During the course of protocol optimisation treatment with the ATP-synthase inhibitor oligomycin was included to assess ATP production, as is standard with *in vitro* respiratory assays using this instrument [222]. However, tissue penetration issues arose at later developmental stages, and the compound was dropped from the final protocol. As previously mentioned, it became apparent during optimisation that temperature fluctuations can skew the data considerably. Therefore, temperature was carefully monitored

over the course of each run and only technical repeats with the same temperature range were included for final analysis. The final protocol allows assessment of baseline respiration, maximum OCR, reserve OCR, baseline respiration, maximum respiratory capacity, reserve respiratory capacity and non-respiratory OCR based on treatment with the respiration uncoupler FCCP and co-treatment with the complex III inhibitor antimycin and the complex I inhibitor rotenone (**Figure 4.6 B**). This protocol allows for *in vivo* assessment of these respiratory parameters, providing detailed information on metabolic alterations in larval zebrafish up to 60 hpf. In this PNC initiation model, impaired respiratory capacity was detected in PNC bearing embryos, which was rescued following mDIVI-1 treatment suggesting that mitochondrial fragmentation alters respiratory function in PNCs. Detecting this using a whole embryo approach, where the basal metabolism of the vastly out-numbering non-transformed cells of the embryo masks PNC alterations, suggests considerable impairment; much greater than that suggested by the data. Overall these findings indicate that respiratory impairment in induced during PNC development as a result of Dnm1l-dependent mitochondrial fragmentation.

The finding that ROS are not elevated in the PNC niche was initially surprising. Previous work in other PNC initiation models suggest important roles for hydrogen peroxide in the PNC niche [192] and there is a large and continually growing body of work to suggest that mitochondrial fragmentation is associated with elevated ROS generation in cancer (reviewed in [143]). However, further literature investigations lead to the finding that ROS generation is linked to mitochondrial membrane potential. It was previously found that a threshold mitochondrial membrane potential is required for generation of hydrogen peroxide [274]. Considering reduced membrane potential was found in PNCs, it is plausible that mitochondrial fragmentation-induced reduction of mitochondrial membrane potential is a protective mechanism against excessive ROS production in PNCs. Excessive ROS is known to lead to apoptosis. Therefore, it is possible that while sufficient levels of ROS are maintained in PNCs to allow for intracellular signalling processes, these are below detectable levels for *in vivo* imaging. Reduced mitochondrial membrane potential

prevents excessive ROS production, thereby preventing cell death by apoptosis. Considering the large body of evidence linking mitochondrial fragmentation with ROS production and the detection of excessive ROS production in a variety of cancers, this would be an unexpected mechanism. However, studies to date have involved *in vitro* work or work in established cancers. There is, therefore, potential for this mechanism to act during PNC development, before a cell is fully transformed and protected from apoptosis by resistance to oxidative stress but no longer be active in fully transformed cells. Also, previous work has shown a NOX-mediated mechanism of ROS production, as opposed to mitochondrial ROS. Based on the findings presented here, mitochondria in PNCs are not damaged, merely altered. Therefore, while mitochondrial ROS may be elevated within standard cellular range, this could be outside the detection range of the approaches used here. This would explain the lack of ROS detected using the mitochondrial matrix redox sensor, but not using the more general ROS dyes. Clearly further, more focused studies will be required to probe the link between ROS and mitochondrial fragmentation during these early stages of cancer development. The development of new transgenic lines during this project for localised redox stress will help with these investigations, aiding future work to determine the role of redox signalling in the PNC niche.

Having confidently established that mitochondrial fragmentation occurs in PNCs and has consequential effects on mitochondrial function, determination of the effect of this phenotype on PNC development followed. Inhibition of mitochondrial fragmentation does not appear necessary for PNC survival, as no increase in cleaved-caspase 3 activity is detected following mDIVI-1 treatment. This is not altogether surprising, as mDIVI-1 returns mitochondria to a more fused phenotype, generally not associated with programmed cell death. However, given the necessity of cancer cells to proliferate to establish a tumour, the identification of such a phenotype so early during PNC development is encouraging as it proves mitochondrial fragmentation is important for oncogenic processes and places the phenotype as a potential target for cancer prevention.

One of the driving forces behind this program of work is the hypothesis that metabolic alterations in PNCs are involved in signalling that initiates trophic inflammatory responses in the developing PNC niche. To test this possibility, recruitment of neutrophils in the PNC niche was monitored following mDIVI-1 treatment. Pharmacological approaches are less than ideal for this type of analysis as global compound action on both PNCs and neutrophils makes it difficult to accurately interpret the results. However, inhibition of Dnm1l expression specifically in neutrophils does not appear to alter their migration (Unpublished, correspondence with Dr. Qing Deng, Perdue University). Regardless, no change was observed in number of recruited neutrophils to the PNC niche following Dnm1l inhibition, indicating that mitochondrial fragmentation or its downstream consequences do not play a role in neutrophil recruitment. This will be verified using the dominant negative form of Dnm1l discussed above when generation and characterisation has been completed.

Alterations to glycolytic metabolism are well characterised features of established cancers but their role during early cancer development is less well established. This project set out to investigate the glycolytic phenotype at early stages of PNC development and how alterations to glycolytic signalling may be involved in PNC development. Enhanced glycolytic flux was detected and this appears to be important for PNC survival. However, how this flux is fuelled and the effect of increased glycolysis on lactate levels remains ambiguous.

Initial experiments involved optimisation of a new protocol for *in vivo* glycolytic analysis using the Seahorse Extracellular Flux analyser. To date, the limited number of publications using this instrument for *in vivo* zebrafish analysis have primarily investigated oxygen consumption rate (OCR) for respiratory manipulations [272][273][275]. While mentions of ECAR have been made [272], little conclusive findings on glycolytic capacity have been published. Standard *in vitro* protocols for glycolytic functional analysis using the Seahorse extracellular flux analyser use oligomycin treatment to determine glycolytic capacity [223]. Oligomycin treatment was included in early experimental optimisations but, as has previously been

published [273], there appeared to be tissue penetration issues at later developmental stages. For this reason, oligomycin treatment was not included in the final protocol. This penetration issue could be partially responsible for the lack of published ECAR data using this instrument for zebrafish analysis to date, as it limits the information determinable from relatively costly experiments. However, while glycolytic capacity could not be determined using this technique, glycolytic flux was successfully determined by inhibiting glycolysis using the competitive inhibitor 2-DG. The glycolytic flux represents the rate at which molecules move through the glycolytic pathway and is used as a measure of glycolytic function. The rapid decrease in ECAR function following 2-DG addition allows the contribution of glycolytic function to the ECAR to be assessed (**Figure 4.11**) [223], giving indications of the intracellular flow through the glycolytic pathway. Finally, it was of interest to determine the effect of glycolytic inhibition on respiratory function. The Seahorse extracellular flux analyser measures ECAR and OCR simultaneously. By following glycolytic inhibition with addition of the mitochondrial uncoupler FCCP, the complimentary OCR read-out could be used to monitor the ability of embryos to respire when glycose cannot be utilised as a fuel source. The rise in OCR following FCCP treatment is indicative of respiratory function, therefore the contribution of glycolysis to oxidative phosphorylation could be analysed. This protocol allows previously unattainable *in vivo* analysis of glycolytic function and its effect on respiratory capacity. However, caution is required. As previously mentioned, temperature fluctuations appear to impact on consistency, as does developmental stage of embryos. Careful embryo staging and temperature monitoring is required to ensure reproducible results. Also, high variation of baseline ECAR was observed between technical repeats. The reason for this remains unknown but could be due to inherent differences associated with using an *in vivo* system. Care must be taken when comparing technical repeats to ensure experimental conditions and baseline ECAR levels are consistent.

Implementation of this protocol in the PNC initiation model revealed significantly enhanced glycolytic flux in PNC bearing embryos. Similar to the respiratory alterations determined using this technique, detection of glycolytic

adaptations using a whole-embryo approach is indicative of substantial upregulation of glycolytic function. To identify such change at very early stages of PNC development suggest importance for oncogenic processes. However, impairment to respiratory function following glycolytic inhibition appears to be minimal as maximum OCR remains relatively unchanged following 2-DG treatment. This suggests that enhanced glycolytic function is not utilised for energy generation. Of course, the possibility remains that impairment of respiratory function following glycolytic inhibition is below detectable levels using this approach, but it seems likely that the enhanced glycolytic flux observed is at least not entirely used for energy production. Given the number of intermediates in the glycolytic pathway which can feed into other mechanistic avenues, it seems likely that enhanced flux is at least partly required for cellular functions beyond that of ATP generation.

Given these findings, it was highly surprising that glucose uptake was not enhanced in PNCs or the PNC niche. Glucose is the primary input for glycolysis and increased activity of the pathway suggests a need for more substrate. 2-NBDG is the only commercially available fluorescently labelled glucose compound for glucose tracing. This compound has been used *in vivo* in zebrafish in the past and is well tolerated. However, delicate imaging protocols are required due to the colour profile of 2-NBDG in combination with mCherry PNCs. Therefore, verification of this result was sought.

The Vendrell group based at the Centre of Inflammation Research at The University of Edinburgh is involved in generation of fluorescent compounds for dynamic imaging. Sam Benson, a PhD candidate in the Vendrell group, has recently generated a red fluorescent glucose compound, named Se-NBD-glucose. Before this compound was used for experimental purposes, characterisation of Se-NBD-glucose *in vivo* in zebrafish was undertaken, in collaboration with the Vendrell group. Se-NBD-glucose showed similar distribution to that of 2-NBDG following vascular injection (data not shown). Also, knock-down of the glucose transporter GLUT2 using a GLUT2 anti-sense morpholino revealed reduced accumulation of Se-NBD-glucose in the head of 28 hpf embryos (**Figure 4.13**), recapitulating published work using 2-NBDG

[245]. These data were sufficient for confirmation that Se-NBD-glucose behaves as a fluorescent glucose analogue *in vivo*. Following this, use of Se-NBD-glucose in the PNC initiation model replicated 2-NBDG findings, in that enhanced uptake was not observed in PNCs or the PNC niche. Unchanged expression of the glucose transporter GLUT2 further indicates that glucose uptake does not appear to be a phenotype of PNCs. However, upon reflection, it was noted that GLUT2 is primarily a neuronal transporter in larval zebrafish and expression of GLUT1 and GLUT5 may prove more informative. Nonetheless, unaltered glucose uptake in PNCs was a puzzling finding as it is at odds with the detection of enhanced glycolytic flux. It is possible that enhanced flux could be fuelled by glucose-6-phosphate generated from glycogen stores, or alternative sugar derivatives [76][276], although this seems unlikely given that the yolk composition is primarily lipids and amino acids [277][278] and independent feeding has not commenced at this developmental stage. As D-glucose inhibits 2-NBDG uptake [279], it is theoretically possible that PNCs are saturated with endogenous glucose that is transported into the cell using a glucose transporter other than GLUT2, but this too seems unlikely. This leaves the outstanding question of how enhanced glycolytic function is sustained in PNCs.

Indications that glycolytic products are not fully utilised for respiratory energy generation suggest alterations to intracellular lactate. Lactate metabolism is an active area of cancer research and has been shown to play important roles in oncogenic processes [267]. Therefore, it was of interest to investigate lactate metabolism during PNC development. A commercially available lactate assay carried out on dissociated whole embryos carrying PNCs suggests lactate concentration is not altered. This assay was attempted using FACS isolated cells, but sufficient cell numbers for lactate detection were not achieved. It is possible that PNC specific alterations in lactate levels could be masked using this method or that expression is altered below detectable levels for this kit. However unchanged expression of LDH-A also strongly suggests that intracellular lactate concentration is not increased in PNCs. Unaltered MCT4 expression indicates it is also unlikely that export of lactate from PNCs is enhanced, although this result required clarification in a PNC specific manner. While

these techniques have high margins for error, they consistently imply that lactate levels are not altered in PNCs during development. Like glucose uptake findings, this conclusion too leads to further outstanding questions. If glycolytic end-products are not necessary for respiratory function and do not lead to increased lactate, what processes are they necessary for and how does this impact PNC development?

Despite not fully elucidating mechanistic alterations to glycolytic signalling in PNCs, the pathway appears to be important for PNC survival. Increased PNC-specific apoptosis was detected following glycolytic inhibition using 2-DG, indicating that intact glycolysis is a requirement for PNC endurance. This would suggest that alterations to glycolytic metabolism in PNCs is a potential target for cancer prevention, although mechanistic determinations are required before this avenue could be pursued.

One of the ongoing interests of the Feng lab is how PNCs induce a trophic inflammatory response during initiation. While indications point towards a role for glycolytic signalling in this process, data must be interpreted with care. It seems important to address that the treated and untreated groups appear to show different neutrophil numbers from the very beginning of the time-lapse experiment. For these experiments 2-DG was added to treated embryos approximately 30 min prior to imaging commencement due to technical constraints. It is therefore plausible that 2-DG action is already in effect when imaging starts, however further experimental analysis will determine this for certain. Neutrophils are highly glycolytic cells by nature, and this is increased upon activation. Therefore, global manipulation of the environment has a high likelihood of acting directly on neutrophils. While wounding experiments do not show an effect of 2-DG treatment on peak neutrophil recruitment at 6 hpw, pharmacological approaches remain inadequate for this type of analysis. In order to appropriately determine the role of glycolytic signalling in neutrophil recruitment to PNCs, first mechanisms of glycolytic adaptations must be identified. This will allow targets to be recognised for manipulation in a PNC specific manner and allow the consequential effect on neutrophil recruitment to be assessed.

The finding that metformin treatment induces PNC specific apoptosis is highly encouraging. It reinforces the idea that mitochondrial fragmentation and the resultant respiratory impairment in PNCs have potential as therapeutic targets for cancer prevention and agrees with the growing body of evidence that places metformin as a potential cancer preventative intervention. Despite this, further work is necessary before this compound can be suggested for use in such a capacity. For instance, one issue surrounding studies of metformin is concentration. Many *in vitro* studies use concentrations that are not physiologically relevant and therefore must be interpreted with caution. Typical human plasma concentrations are in the range of 4 µM to 15 µM following a single dose of metformin [269]. While 10 mM treatment was used in this project, the plasma concentration of compound is unknown. Metformin requires active transport into cells by a number of mammalian transporter families [268]. The ability of transporters to internalise metformin in zebrafish is not well defined, therefore compound concentrations at the site of action are not known. Determination of compound uptake and plasma concentrations will allow clarification of whether induction of PNC apoptosis can be achieved with physiologically relevant concentrations of metformin. In order to fully elucidate the mechanisms of cancer prevention by metformin in this model detailed pharmacodynamic studies are necessary to first fully understand how metformin behaves in zebrafish. Then, further mechanistic studies can commence. As metformin can act through both complex I and MAPK-dependent AMPK activation [268][269], determination of mechanisms of action will be necessary. Treatment with alternative complex I inhibitors, such as rotenone, should give indications as to whether this mechanism is responsible for PNC susceptibility to metformin. Following this, studies of the effect of metformin on PNC development including analysis of the cell cycle, proliferation and inflammatory responses will further contribute to elucidation of suitability of metformin for cancer prevention *in vivo*.

The findings presented here reveal that mitochondrial and metabolic alterations occur at vary early stages of tumour initiation and are important for tumourigenic processes. While these findings are encouraging, it is clear that the

whole-embryo approach taken with many methods for these analyses is not the best means, as likelihood for false negatives introduces hesitation in drawing conclusions. Moving forward, PNC-specific techniques are required for metabolic analysis to determine mechanisms of alteration and the importance for PNC development. This will be aided by the generation of new transgenic zebrafish lines for *in vivo* imaging of metabolic processes as further discussed in Section 5.

5. Generation of new transgenic reporter zebrafish lines for *in vivo* imaging of metabolic processes.

Section 1.9 discussed the various *in vitro* and *in vivo* techniques available for metabolic investigations and highlighted the need for more sensitive and specific tools for assessment of metabolic processes *in vivo*. Throughout this project isolation of PNCs in the required numbers for the available techniques proved challenging and hindered confidence in findings. The whole-embryo approach proved insufficient for detection of metabolic alterations in such a small subset of cells and, currently, there are limited tools available to assess metabolic changes in defined cellular populations *in vivo*. As previously discussed, the zebrafish presents an exciting opportunity for development of new transgenic reporter lines. Such tools would allow sensitive and specific monitoring of metabolic changes *in vivo* and in real time, presenting a promising method for metabolic investigations moving forward.

To this end, development of a number of transgenic zebrafish reporter lines commenced during this project with the ultimate aim to generate a library of new tools to allow *in vivo* monitoring of metabolic processes which can be utilised across the spectrum of zebrafish development and disease research. Owing to the time and resources necessary for such an ambitious aim, completion of these new transgenic lines was not achieved during the time frame of this project. The below sections give details of the reporter lines currently under development and summarize the progress made to date.

5.1 Laconic: a reporter for intracellular lactate

The overarching hypothesis for this project is that metabolic alterations bring about changes in lactate levels during PNC initiation and development, altering inflammatory responses and polarising the developing microenvironment towards pro-tumourigenic roles. Given the difficulties assessing lactate levels encountered during this project, the generation of a new transgenic zebrafish reporter line for *in vivo* imaging of intracellular lactate levels would allow unprecedented analysis of lactate metabolism. The Laconic lactate sensor is a FRET-based sensor that has

proven successful for monitoring intracellular lactate concentration *in vitro* [238] and appeared a good candidate for translation *in vivo*. These FRET sensors are fusion proteins flanked by a pair of fluorescent proteins with overlapping excitation/emission spectra attached. Binding of a ligand to the sensor protein causes a conformational change leading to a change in energy transfer between the two fluorescent proteins and consequential alteration of fluorescent signal, referred to as FRET efficiency. Laconic is based on the bacterial transcriptional regulator Lldr with a TFP/Venus FRET pair which shows a decrease in FRET-efficiency when lactate binds [238]. By monitoring FRET efficiency intracellular lactate concentrations can be determined.

Initial cloning issues led to commercial synthesis of the Gateway middle entry vector construct (**Figure 5.1 A**) and, while this resulted in a time delay for transgenic line generation, it allowed the construct to be codon optimised for zebrafish, therefore expression of the final sensor should be enhanced. The reporter was then cloned under the expression of the Ubi promoter (**Figure 5.1 B**) and injected into the one cell stage of wild-type zebrafish eggs. However, initial screening of F0 generation proved problematic. Expression of a blue eye (cry:eCFP) transgenic marker included in the genetic construct was detected, but Laconic expression was remarkably weak in all F1 offspring. This could be due to poor quality tol2 RNA at the time of injection, although selection marker expression suggests otherwise. Random incorporation into the genome, as is the case with tol2 transgenics, is susceptible to variation based on the locus on integration, and therefore genomic integration at an undesirable locus can result in poor expression [280]. As this is likely the case, the Ubi:Laconic construct has been re-injected and these F0 fish will be screened to identify a founder fish upon reaching adulthood, although unfortunately this stage had not been reached at the culmination of this project.

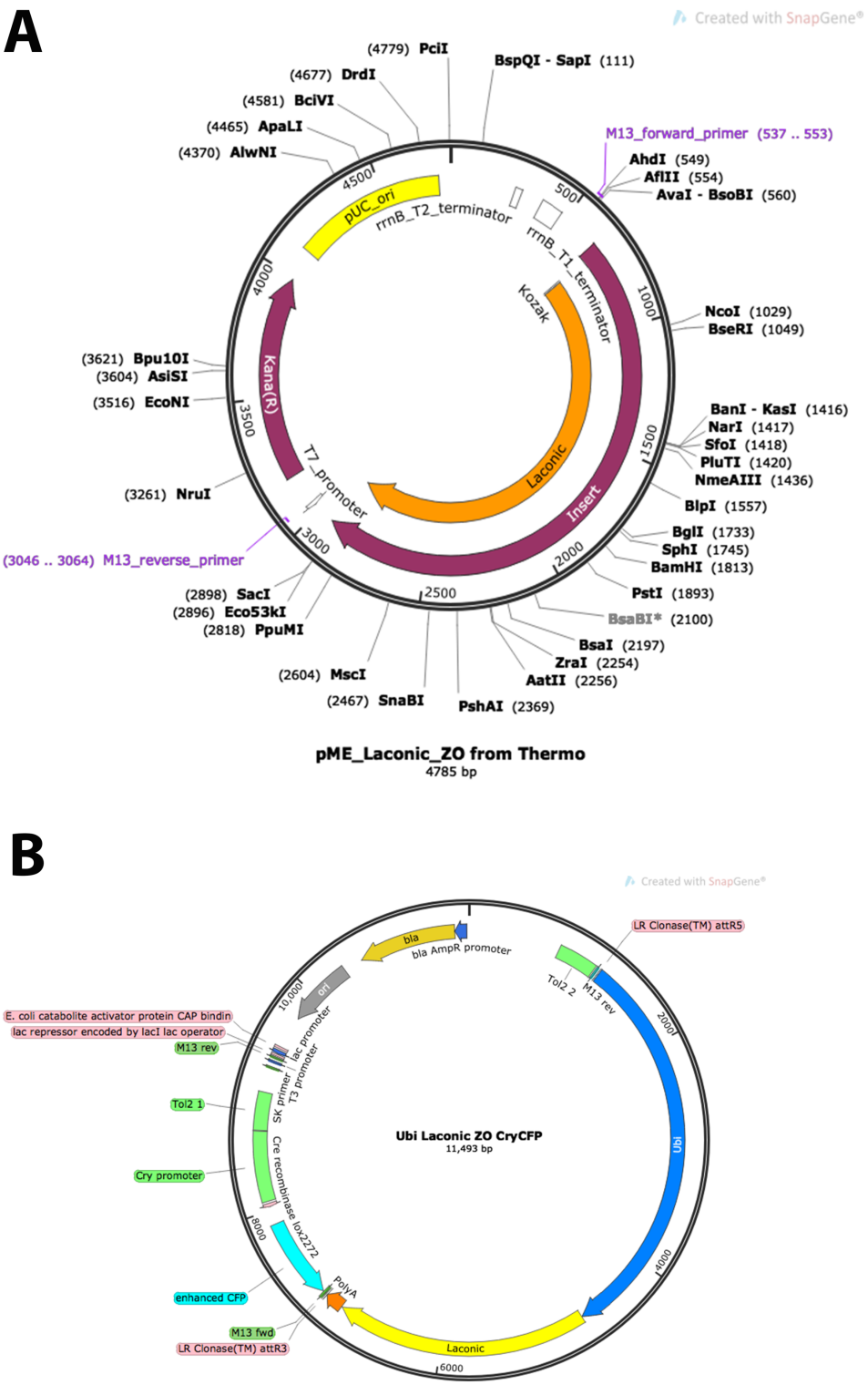

Figure 5.1: Construct maps for Laconic. A. Synthesised Gateway middle entry vector for Laconic. **B.** Final Ubi construct used for generation of Laconic transgenic zebrafish line.

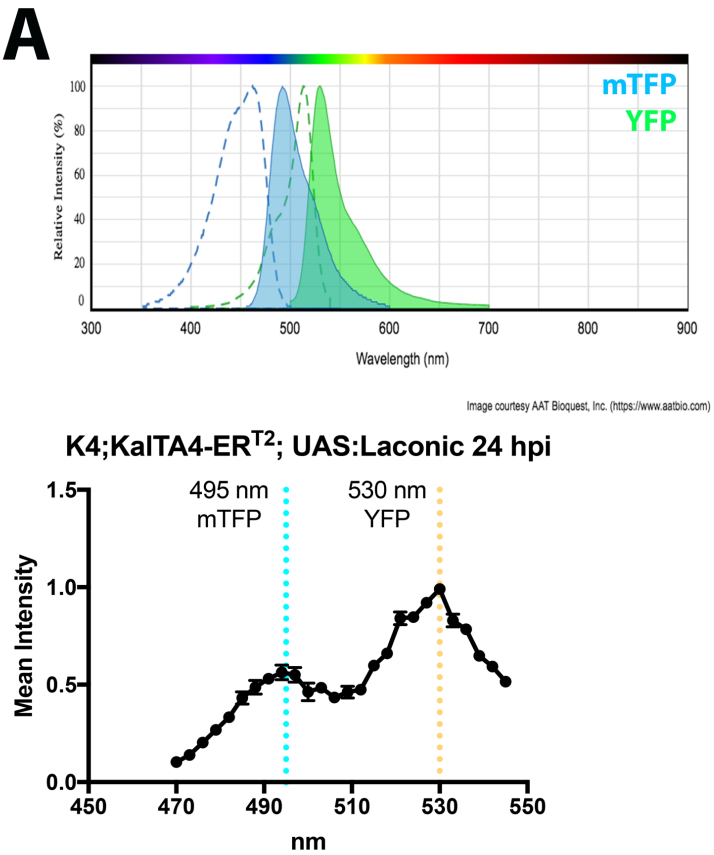

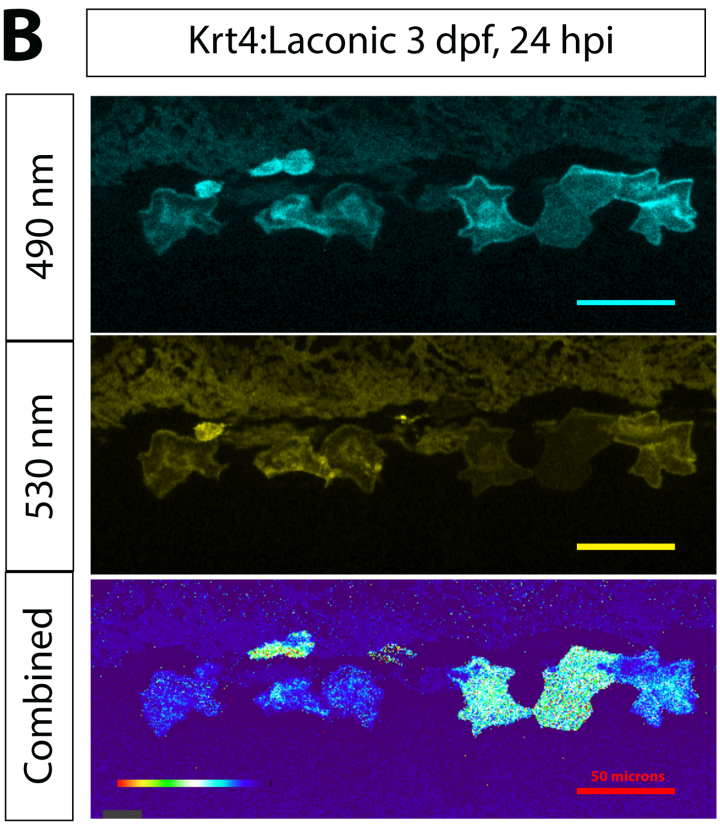

Figure 5.2: Transient expression of Laconic for visualisation of intracellular lactate. A. Excitation/Emission spectra for mTFP and YFP and Mean fluorescent intensity from lambda scan of K4:KalTA4-ER^{T2};UAS:Laconic at 24 hpi shows two peaks of fluorescence intensity, consistent with the TFP/YFP FRET pair. **B.** Representative images of transiently injected UAS:Laconic at 24 hpi in superficial skin cells. Combined image represents ratio TFP/YFP. Scale bar 50 µm.

Provisionally, Laconic was expressed under the control of the UAS promoter and used in combination with the Krt4:KalTA4-ER^{T2} line, leading to expression specifically in superficial skin cells. Although this transient approach is not ideal, it can be used to confirm reporter expression and give preliminary insights of lactate levels. Using this approach, embryos were imaged at 24 hpi to confirm reporter expression. A lambda scan shows two peaks of fluorescence, consistent with those expected for the TFP/YFP FRET pair (**Figure 5.2 A**), indicating the reporter is expressing as expected. This represents the native state of the sensor with full FRET efficiency. The low TFP peak shows energy is being quenched and released from the neighbouring YFP fluorophore. Ratiometric image analysis can then be used to monitor relative expression of TFP and YFP to assess lactate levels in superficial skin cells (**Figure 5.2 B**). Using the transient approach prohibits quantification of FRET efficiency changes, as GAL 4 overexpression leads to signal amplification and inherent differences in fluorescence intensity may be present as a result of transient injection. Despite this, these early indications of reporter signal are encouraging and affirm confidence in the final reporter line.

5.2 Pyronic: a reporter for intracellular pyruvate

Pyruvate sits at an important metabolic junction in the cell. As the product of the glycolytic reactions, pyruvate has the potential to be converted to acetyl-CoA to feed the citric acid cycle and oxidative phosphorylation or be converted to lactate under conditions of hypoxia or during aerobic glycolysis. Therefore, assessment of cellular pyruvate can be highly informative; giving information about glycolytic rate, pyruvate transport and metabolite consumption. Pyronic is an intracellular pyruvate FRET sensor, which works by a similar principle to the Laconic sensor described above. Pyronic is based on the bacterial transcriptional regulator PdhR, which is flanked by a TFP/Venus FRET pair and shows a decrease in FRET-efficiency when pyruvate binds [239]. By monitoring FRET efficiency, intracellular pyruvate levels can be assessed.

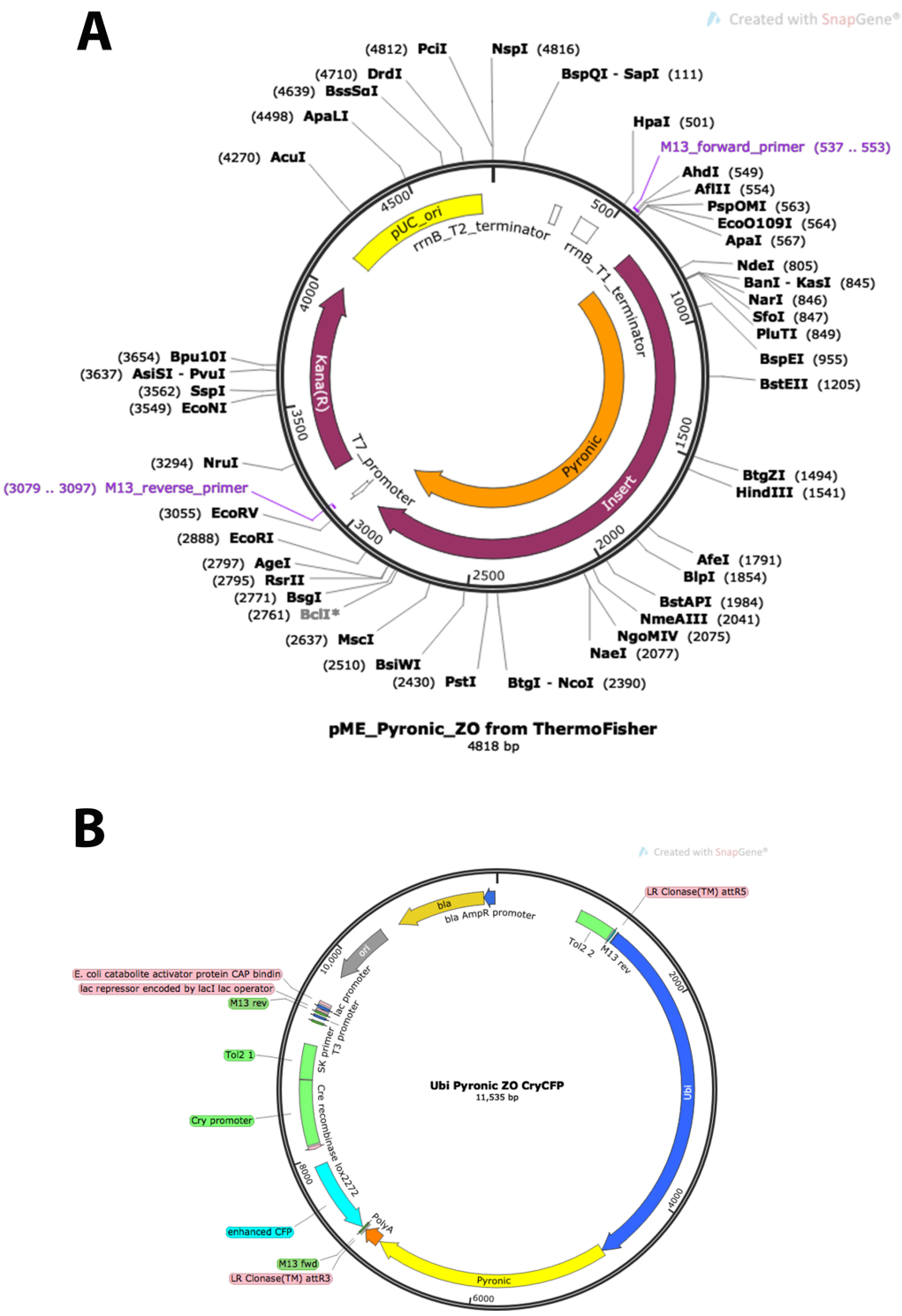

Figure 5.3: Construct maps for Pyronic. A. Synthesised Gateway middle entry vector for Pyronic. **B.** Final Ubi construct used for generation of Pyronic transgenic zebrafish line.

Similar to the circumstances with the Laconic reporter, issues encountered during initial cloning lead to the commercial synthesis of the Gateway middle entry vector (**Figure 5.3 A**), which again allowed for zebrafish codon optimisation. The reporter was then cloned under the expression of the Ubi promoter (**Figure 5.3 B**) and, following validation by sequencing, injected into the one cell stage of wild-type zebrafish eggs. F0 embryos were screened for cry:CFP (blue eye) selection marker and pyronic reporter expression at 3 dpf using a fluorescent stereomicroscope fitted with a CFP/DsRed dual filter. Strong fluorescence of both the selection marker and pyronic reporter were observed, with expression particularly strong in muscle tissues. Embryos with strong positive signal were selected and raised to adulthood. These F0 fish will be screened to identify founder fish to establish a transgenic line, but unfortunately, sexual maturity had not been reached by the end of this project.

5.3 Perceval-HR: an ATP:ADP ratio reporter

ATP is a highly important signalling molecule and energy source within cells, with regulatory functions associated with numerous metabolic functions. The ATP:ADP ratio can be used as an indicator for energy consumption and changes in cellular energy status. Traditionally, luciferase-based assays were utilised to assess ATP levels in cells, but were often hindered by low-signal levels [281]. Perceval-HR is a mammalian optimised circularly permuted fluorescent protein (cpFP) based sensor for ATP:ADP ratio [241]. cpFPs are fusion proteins generated by connecting the original fluorescent proteins N and C termini via a peptide linker which acts as a detector and creating new N and C termini in close proximity to the chromophore. Conformational changes to this new fusion protein, cause by binding of a ligand to the peptide linker, cause a change in fluorescence signal [240]. The Perceval-HR sensor has two distinct excitation peaks, corresponding to differential protein conformations when the different nucleotides are bound. ATP binding is associated with fluorescent signal at 500 nm excitation, while ADP binding increases

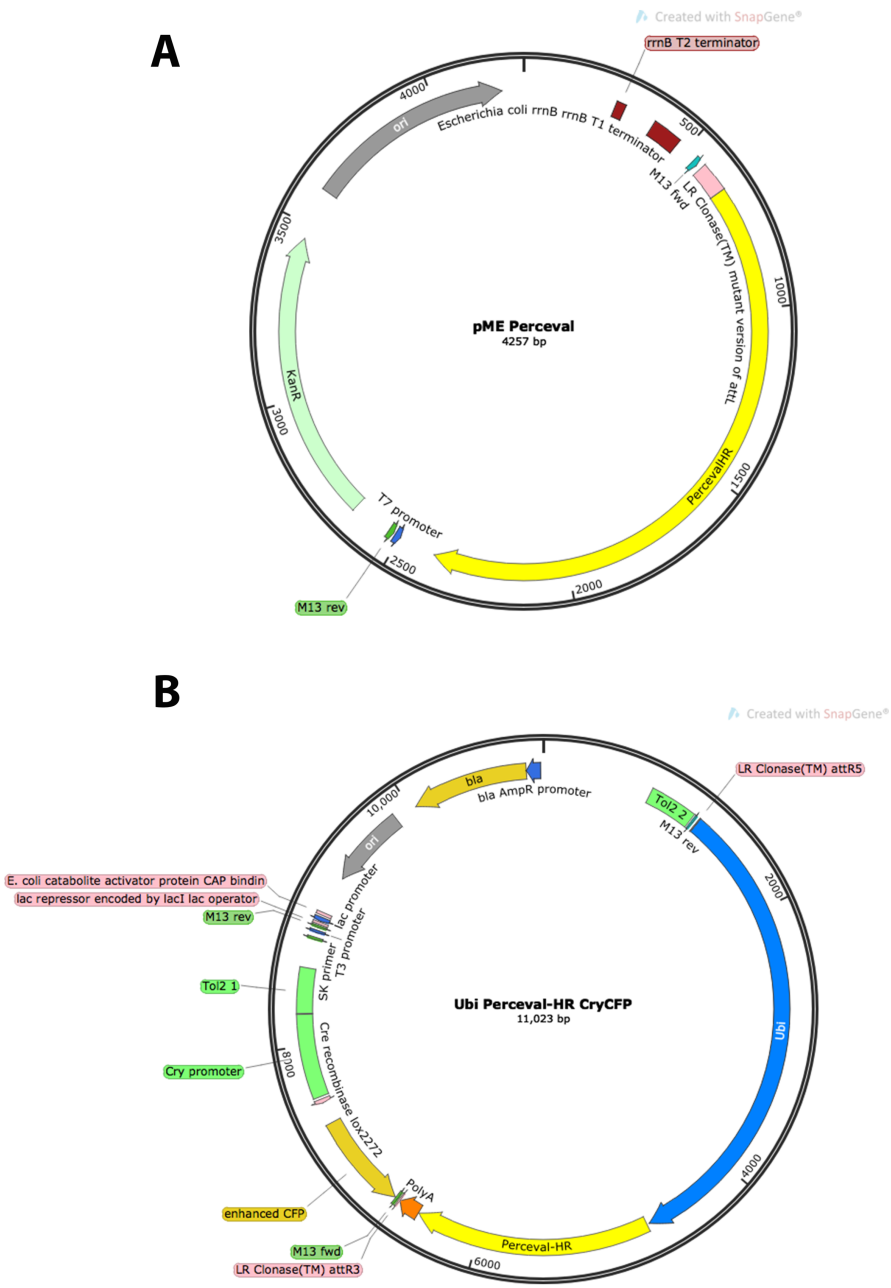

Figure 5.4: Construct maps for Perceval-HR. A. Gateway middle entry vector for Perceval-HR. **B.** Final Ubi construct used for generation of Perceval-HR transgenic zebrafish line.

fluorescence at 420 nm. By monitoring fluorescence at two excitation points, the ratiometric readout allows monitoring of ATP:ADP ratio within the cell [241].

Using a commercially available GW1-Perceval-HR (Addgene plasmid number: 49082) vector as a template, Perceval-HR was cloned into the Gateway middle entry vector pDONR221 (**Figure 5.4 A**), with successful construct generation verified by sequencing (completed in collaboration with Dr. Derek Laux, Feng Lab). The reporter was then cloned into the final destination vector for expression under the control of the ubiquitous Ubi promoter (**Figure 5.4 B**) and, following validation by sequencing, injected into the one cell stage of wild-type zebrafish eggs. F0 embryos were screened for cry:CFP (blue eye) selection marker and Perceval-HR reporter expression at 3 dpf using a fluorescent stereomicroscope fitted with an eGFP filter. Strong fluorescence of both the selection marker and Perceval-HR reporter were observed. Embryos with strong positive signal were selected and raised. Future screening of this F0 generation will allow identification of founder fish and establishment of a transgenic line.

5.4 Peredox: an NADH-NAD^+ redox sensor

NADH is a vital electron transfer cofactor with roles in various metabolic processes. Imaging approaches which monitor inherent autofluorescence of NADH have been used for many years to monitor cellular NADH-NAD^+ redox state. However, as related cofactors such as NADPH also fluoresce at the same emission, there is ambiguity as to the accuracy of this approach [242]. Peredox is a GFP based cpFP (see Section 5.3) which works through a competitive binding scheme to report the NADH-NAD^+ ratio in a cell. Binding of NADH to the sensor increases fluorescence signal, while NAD^+ binding does not alter signal intensity. By monitoring the fluorescent readout, the cellular NADH-NAD^+ ratio can be determined. As this approach is dependent on signal intensity, the sensor is tandemly linked to another fluorescent protein to normalise for protein expression [242], in this case the mCherry fluorescent protein.

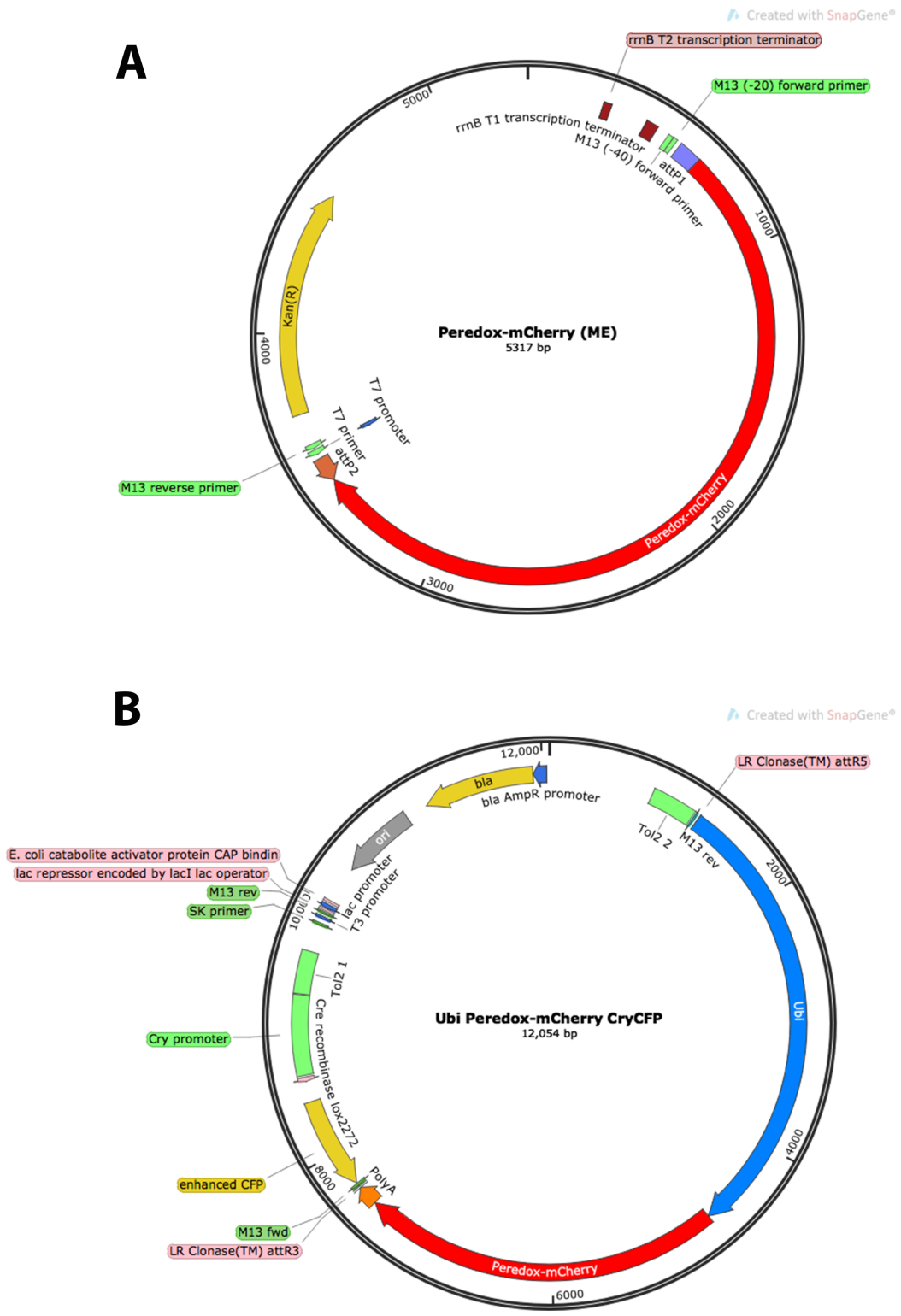

Figure 5.5: Construct maps for Peredox-mCherry. A. Gateway middle entry vector for Peredox-mCherry. **B.** Final Ubi construct used for generation of Peredox-mCherry transgenic zebrafish line.

Using a commercially available pcDNA3.1:Peredox-mCherry (Addgene Plasmid Number 32383) vector as a template, Peredox-mCherry was cloned into the Gateway middle entry vector pDONR221 (**Figure 5.5 A**), with successful construct generation verified by sequencing. The reporter was then cloned into the final destination vector for expression under the control of the ubiquitous Ubi promoter (**Figure 5.5 B**) and, following validation by sequencing, injected into the one cell stage of wild-type zebrafish eggs. F0 embryos were screened for cry:CFP (blue eye) selection marker and Peredox-mCherry reporter expression at 3 dpf using a fluorescent stereomicroscope fitted with an eGFP/DsRed dual filter. While signal could be detected, it was deemed that this injection was unsuitable for transgenic line generation due to very low fluorescence levels. This is believed to have resulted from poor quality tol2 RNA as both selection marker and reporter signal were consistently low in all embryos screened. Unfortunately, re-injection of the construct could not be completed within the time-frame of this project but is planned for the near future with the hope to successfully establish a transgenic line moving forward.

5.5 Cellular localised reporters for redox stress

As described in Section 4.4, a new transgenic line encoding a mitochondrial matrix-localised redox reporter was generated, verified and utilised during this project. roGFP is a reversible ratiometric reporter that exhibits alterations in fluorescence signal in response to redox stress [265] and can be used to assess the redox state of the cell. By tagging the reporter to specific parts of the cell, more detailed information can be gained regarding redox processes.

In addition to the mitochondrial matrix-localised roGFP, constructs for expression of roGFP specifically in the cytosol and mitochondrial inner membrane [237] were generated. Using the commercially available Cyto-roGFP (Addgene Plasmid Number 49435) and GPD-roGFP (Addgene Plasmid Number 49436) plasmids as templates, the reporters were cloned into the Gateway middle entry vector pDONR221, with successful construct generation verified by sequencing. The

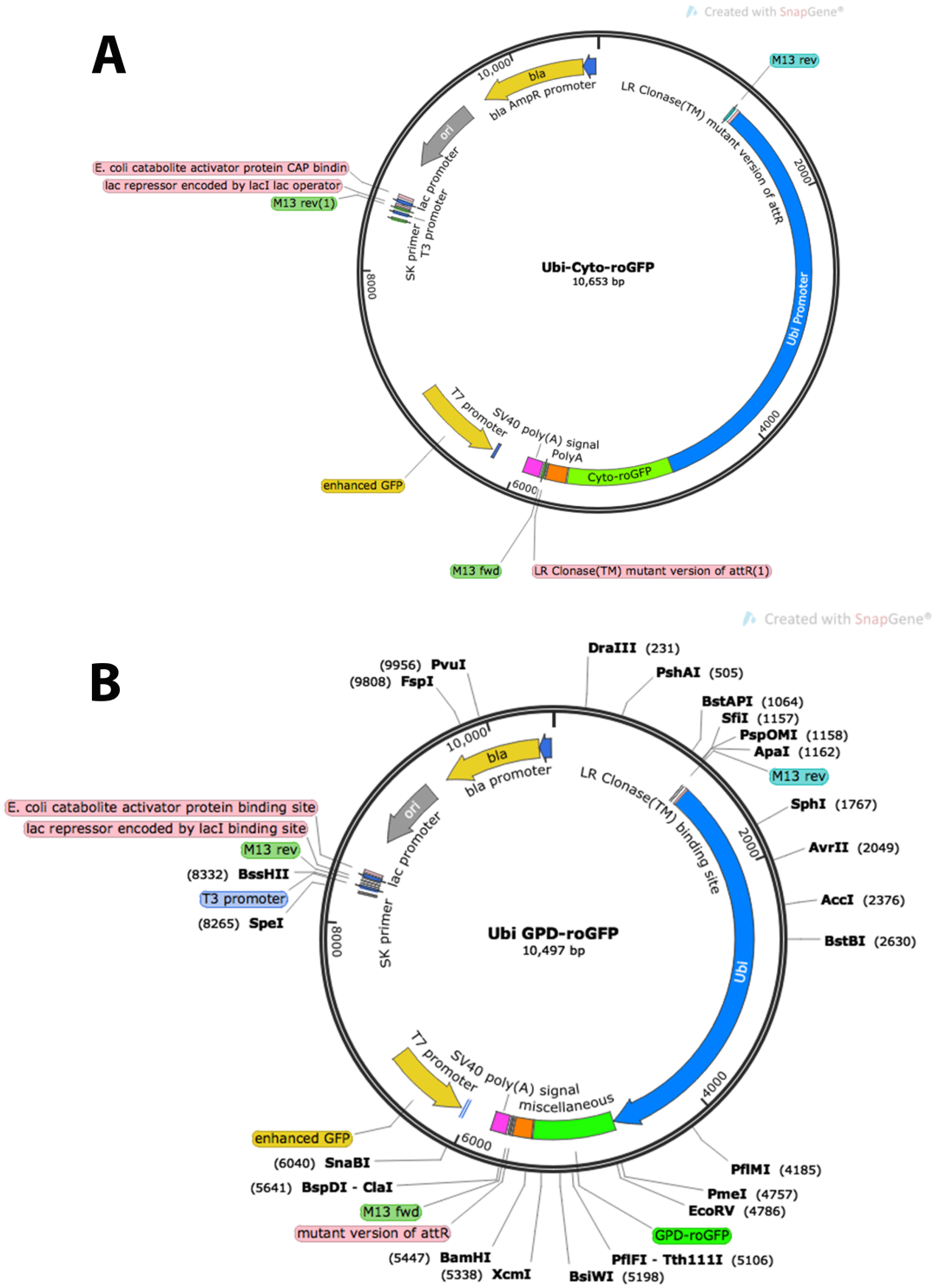

Figure 5.6: Construct maps for roGFP reporters. A. Final Ubi construct used for generation of Cyto-roGFP transgenic zebrafish line. **B.** Final Ubi construct used for generation of GPD-roGFP transgenic zebrafish line.

reporters were then cloned into the final destination vector for expression under the control of the ubiquitous Ubi promoter (**Figure 5.6**) and, following validation by sequencing, injected into the one cell stage of wild-type zebrafish eggs. F0 embryos were screened for roGFP reporter expression at 3 dpf using a fluorescent stereomicroscope fitted with an eGFP filter. Strong signal was detected for both reporter lines and positive embryos were raised to adulthood. F0 fish were screened and founders were successfully identified for both the cyto-roGFP and GPD-roGFP lines. Verification and characterisation of these lines could not be completed within the time-frame of this project, hence they were not utilised for experimental purposes. With F1 fish now growing, a full characterisation of these lines using a similar wounding approach to that used in Section 4.4 for Matrix-roGFP verification will contribute two new tools to the field and allow detailed analysis of cellular redox state to be completed.

5.6 Conclusions

The work discussed here represents the preliminary stages of a large body of longitudinal work which aims to develop a library of new tools and establish the zebrafish as an attractive model organism for *in vivo* metabolic studies. Whilst incomplete, the work done to date has made significant progress towards achieving this aim, with all the necessary construct components successfully assembled and progression to *in vivo* stages achieved for the majority of tools. Moving forward, this work will pave the way for successful generation of a number of transgenic zebrafish lines that will allow exceptional insights into metabolic processes *in vivo* and in real time.

6. Discussion

The aim of this project was to investigate alterations to cellular metabolism in PNCs and the effect these changes may have on cancer initiation *in vivo*. The project initially characterised a newly established zebrafish model for human $HRAS^{G12V}$ mediated PNC initiation in the larval superficial skin layer. Following this, the metabolic phenotype in human $HRAS^{G12V}$ driven PNCs was investigated. Assays of PNC mitochondrial phenotype, and respiratory and glycolytic functions revealed complex metabolic alterations at very early stages of PNC initiation. These were shown to be important for PNC proliferation and survival, placing these phenotypes as potential targets for cancer preventative interventions.

6.1 A new zebrafish model for PNC initiation provides improved temporal resolution.

The zebrafish has been used as a model organism for cancer research for many years now. A number of models have been developed based on xenograft and transgenic approaches using a variety of oncogenes and tumour suppressor genes in various tissues, reviewed in [211][282][283], among others. These models have been used to study different stages of cancer, from early developmental stages [192][193][284][70][72] through to later metastatic processes [285][213][286][212]. The most closely related model to that described here is the oncogenic HRAS melanoma model developed by Santoriello, *et al*, which uses the *kita* promoter to drive oncogene expression in melanocytes [70]. This model uses the GAL4/UAS system to express the $HRAS^{G12V}$ oncogene and alterations in melanocytes can be observed from 2 dpf, allowing early oncogenic processes to be monitored. However the newly established modified GAL4/UAS [246] mediated, inducible model for PNC initiation in the larval superficial skin layer [218][74] described here is the first to allow both spatial and temporal control of oncogene expression, providing access to the very earliest stages of cellular transformation. The model permits monitoring and manipulation of PNC development and interactions with the microenvironment so that very early oncogenic processes can be determined.

While the model was developed prior to this project, a thorough characterisation had yet to be completed. Early work for the project involved detailed observational studies to define the phenotype of PNC development. These observational studies revealed dynamic development of PNCs over time, with cell shape, size and behaviour vastly altered, consistent with previous models. Heterogeneous populations of PNCs appear to be present, with some cells showing dramatic alteration while others display a less drastic observed phenotype. It is possible that the transient approach taken with this model is partly responsible for this heterogeneity, as varying oncogene expression levels and insertion sites are a consequence of this method. Future single-cell PNC analysis is planned to decipher the potential differential contributions of these differing phenotypes to oncogenic processes.

While this model provides improved temporal resolution, there are a number of limitations. The transient nature of the model makes it experimentally expensive, as large numbers of fish are required and injecting large numbers of eggs is time-consuming. Despite this input, the model is low throughput. Embryos with varying numbers of PNCs are generated following injection. Therefore, careful screening and selection of embryos with consistent PNC burden is important for experimental reproducibility and often few usable embryos are generated. While these issues may delay experimental progress, careful selection of embryos with consistent PNC phenotype allows the study of processes that are prohibited in other models.

6.2 Model characteristics allow for expansive oncogenic studies in addition to those discussed here.

RAS signalling typically induces pro-survival mechanisms to inhibit programmed cell death, and yet PNC apoptosis is observed in a subset of cells. While it is possible that a percentage of this cell death could be due to excessive $HRAS^{G12V}$ oncogene expression following transient injection, this is unlikely to account for the phenotype as a whole. Persistent RAS signalling can induce replicative stress in a cell [32]. When DNA damage check-points remain intact, this stress leads to an oncogene-

induced senescence (OIS) phenotype [287], features of which are also observed in this model. However, DNA damage check-point deficiency allows proliferation to continue with accumulation of additional genetic lesions [32]. Excessive DNA damage as a result would be sufficient to induce apoptotic cell death and could account for increases seen at later stages of PNC development. Fellow lab members are investigating PNC phenotype at these later stages, including induction of PNC senescence phenotype, to determine how these divergent PNC populations contribute to tumour development. For the purposes of this project, PNC apoptosis was uses as a parameter to monitor PNC survival following mechanistic intervention, as assessed by cleaved caspase-3 activity.

Previous zebrafish models of cancer development have shown trophic innate inflammatory responses are vital for growth of transformed cells [192][193]. Although not discussed here, macrophage recruitment has also been monitored in this model and appears to show early and persistent responses to developing PNCs (data not shown). The observation that neutrophils and macrophages are similarly recruited at very early stages of development in this model reinforces previous studies and provides a platform for elucidation of temporal responses. Detailed inflammatory mechanisms are currently under investigation by the Feng group and others and future work will involve further analysis of how metabolic signalling in the PNC niche contributes to these processes.

6.3 Mitochondria retain their functional capabilities following fragmentation and alterations can be targeted for therapeutic intervention.

It is now well accepted that metabolic disruption is a feature of established cancers. A large number of metabolic changes have been well described and have been shown to play important roles in cancer progression and prognosis. Its role, however, at early stages of disease initiation and development is less well characterised, largely due to issues monitoring these early stages *in vivo.* Having established a new *in vivo* larval zebrafish model for tumour initiation which allows both spatial and temporal control of PNC induction, the metabolic changes at the

inception of PNC initiation could be monitored. In established cancers, while mitochondrial phenotype appears heterogenous among cancer types [154], fragmentation has been shown to be functionally important. The emergence of a fragmentation phenotype at such early stages of development verifies this functional importance and suggests vital contributions to oncogenic processes. *In vitro* work has shown that MAPK signalling is responsible for fragmentation downstream of RAS via a mechanism of ERK-mediated phosphorylation of Dnm1. It would appear that a similar mechanism is at play *in vivo* as pharmacological inhibition of Dnm1l recovered mitochondrial morphology in PNCs. Ongoing work for this project involves genetic manipulation of Dnm1l via expression of a dominant negative form of the protein [147] specifically in PNCs. Such an approach should verify pharmacological findings and instil further confidence in these mechanistic conclusions. While minimal alteration of expression of mitochondrial fusion and fission proteins was detected using a whole-embryo approach, planned RNA-Seq analysis in isolated PNCs will shed further light on true expression levels. It should also be pointed out that post-translation modifications of these enzymes can greatly alter their activity, as shown in *in vitro* studies [261][262][263]. Therefore, it cannot be ruled out that upregulated activity in addition to expression contributes to the overall phenotype. While phosphorylation changes are difficult to assess in zebrafish due to lack of suitably reactive antibodies, this is an important consideration when postulating mechanisms of fragmentation.

Observed Dnm1l-dependent decrease in mitochondrial membrane potential is consistent with expectations. Intact membrane potential is required for mitochondrial fusion and a decrease is associated with fragmentation [148]. While loss of membrane potential could not be measured due to the colour profiles involved, accumulation of the applied dyes is suggestive that complete loss of potential has not occurred. This indicates that, while functional alterations may arise, the mitochondria in PNCs remain active and functional, a theory that is further strengthened by the recovery of membrane potential following pharmacological inhibition of Dnm1l. Such recovery indicates that the mitochondria have retained

their functional capabilities and alterations are due to morphological changes as opposed to mitochondrial damage. Intact functional capabilities were further proven as alterations in baseline respiratory function were not detected in the presence of PNCs. Given the extensive fragmentation phenotype, maximum respiratory impairment is likely reactionary rather than an indication of mitochondrial damage, as reduced oxidative phosphorylation is a feature of mitochondrial fission.

The finding that PNCs have a hyper-fragmented mitochondrial phenotype and consequential functional alterations that appear to be necessary for PNC proliferation was exciting. Although verification of proliferation dependence is necessary, as previously discussed, indications of reduced proliferative capacity in PNCs following inhibition of the mitochondrial fragmentation phenotype is consistent with previous reports and highlights the importance of mitochondrial alterations for oncogenic processes. This importance places mitochondrial characteristics as a targetable intervention for cancer prevention. There are a number of approaches that could be taken to determine possible interventions, including large-scale drug screens or the repurposing of pre-established drugs. The former approach takes considerable time and effort, but a small-molecule drug screen is currently underway by fellow group members to identify possible compounds for further investigation. The latter is a much more biased approach but can save time as pharmacokinetic studies are often already completed and drugs can be approved for trial more readily. This approach led us to metformin. Metformin is a complex I inhibitor that has been used for the treatment of type II diabetes for many years. A number of studies are currently underway to investigate use of metformin in a cancer setting, both as a treatment and for cancer prevention [269][268]. Given the mitochondrial phenotype observed in PNCs, particularly the reserve respiratory impairment, metformin presented as a potential compound to target this phenotype for prevention of PNC development. Induction of PNC-specific apoptosis following metformin treatment is highly encouraging. Future plans for this project involve further metformin studies to greater understand the mechanisms and effects of metformin on PNC development

and add *in vivo* data to the ever-growing movement for use of metformin for cancer prevention.

6.4 Observed phenotypes do not suggest generation of mitochondrial ROS.

Lack of detectable ROS generation in PNCs is surprising. It is widely reported that generation of ROS is increased in cancer cells and ROS have been shown to have important tumour promoting functions. Previous studies in zebrafish cancer development models report NOX-mediated hydrogen peroxide generation and its role in trophic inflammatory responses [192]. This mechanism of ROS generation would appear consistent with observed phenotypes in this model. While mitochondrial alterations are clear, mitochondrial damage is not evident, and, in fact, it is possible that reduced mitochondrial membrane potential is a protective mechanism against excessive ROS production [274]. At these early stages of PNC development mitochondrially-produced ROS could be locally elevated as a result of fragmentation, but not to levels above those which are tolerable. This mechanism would maintain sufficient ROS for signalling functions but not risk induction of apoptosis and/or cellular damage. As ROS levels are within normal cellular concentration ranges, this theory would explain lack of detectable mitochondrially-produced ROS, as such concentrations are outside the detection range of most commercially available dyes. However, as the dyes used in this project are not mitochondria-specific, this theory does not explain why general ROS levels were not elevated in PNCs. It is possible that general cellular ROS are elevated in PNCs but not to concentrations within the detection range of the dyes used, but this seems unlikely as such issues have not been previously reported for these commonly used dyes. The generation of new transgenic reporter lines for redox stress should help with clarification of this issue. As mentioned above, the finding that ROS levels in the mitochondrial matrix are unchanged in PNCs is not surprising, as the mitochondrial phenotype does not suggest excessive ROS production within the organelle. However, future work involving characterisation and utilisation of the cytosolic roGFP redox reporter will further inform on more general cellular ROS alterations.

6.5 Development of a new assay for *in vivo* metabolic studies

The development of a new assay for *in vivo* respiratory and glycolytic assessment using the Seahorse extracellular flux analyser is exciting. These new protocols permit unprecedented *in vivo* analysis of metabolic functions in real time in a whole organism. While issues of phenotype magnitude may be problematic for some applications, these assays have potential to be implemented in a wide variety of disease models to assess metabolic contributions to disease phenotypes. It is believed, however, that data collection from these protocols would be improved by utilisation of the 96-well analyser, instead of the 24-well instrument used in this project. This change would remove the need to secure embryos with screens, significantly improving experimental set-up time. Additionally, increased replicates in each experiment would improve standard deviation and increase the volume of data collected from relatively expensive experiments. Local instrument availability prevented testing of this idea but use of the 96-well instrument is advised for implementation of these protocols moving forward.

6.6 More specific techniques are required to assess complex metabolic alterations in developing PNCs.

Investigations of glycolytic alterations during PNC development in this model have led to somewhat ambiguous conclusions. It appears that glycolytic flux is enhanced in the presence of PNCs and this seems important for PNC survival, consistent with the Warburg effect. However, technical issues incite doubt in numerous experiments, making it difficult to reach confident conclusions. The whole-embryo approach used in many of these experiments appears insufficient for these types of analysis and, moving forward, PNC-specific approaches will be necessary to confidently determine mechanisms and outcomes of metabolic alterations during PNC initiation.

With this in mind, a number of new transgenic zebrafish reporter lines are currently under development, as discussed in Section 5. Future characterisation and

utilisation of these new lines will provide unparalleled *in vivo* observational access to metabolic alterations at the very earliest stages of cancer development.

It is clear from the studies in this project that complex metabolic changes are taking place in PNCs during development, although precise mechanisms remain unclear. To address this complexity in an unbiased manner, future work for this project involves broad spectrum mass spectroscopy approaches to identify metabolic changes in PNCs. Targeted metabolomics and imaging mass spectroscopy (IMS) experiments are planned to identify PNC specific alterations across the entire metabolome, to establish molecules and pathways for further investigation. These experiments will be carried out with the help of a number of collaborators and optimisations of these techniques for use with this zebrafish model are already underway. These studies will be conducted alongside PNC specific RNA-Seq experiments, which will identify alterations in gene expression across the entire genome. This two-pronged approach will provide powerful data to help decipher the complex metabolic changes in PNCs at early stages of cancer development. Targets identified from these approaches will then be further investigated, with the hope to identify targets for cancer prevention interventions.

6.7 Ongoing and Future Work.

The finding that mitochondrial fragmentation occurs at early stages of PNC development via a Dnm1l-dependent mechanism is encouraging as it correlates with previous *in vitro* findings. Future analysis of the phenotype following MAPK inhibition and completion of a genetic model to express a dominant negative form of Dnm1l specifically in PNCs will allow confirmation of this mechanism and permit further, more detailed studies of the downstream effects of mitochondrial fragmentation in developing PNCs. Additionally, the suitability of metformin to target this phenotype will be investigated by further defining the effect of metformin on PNCs and determining metformin mechanism of action.

The role of ROS signalling during PNC development was not the primary focus of this project. However, work completed suggests that generation of mitochondrial

matrix ROS is not a feature of this model. Characterisation and implementation of new transgenic lines for cytoplasmic and mitochondrial inner membrane redox stress generated during this project will provide detailed insights into ROS levels in PNCs and allow more detailed studies of ROS signalling and its potential contribution to PNC development to be completed.

It is clear from these investigations that complex metabolic alterations are occurring in PNCs. Therefore, broad, unbiased approaches are necessary to fully comprehend these changes and identify pathways for further study. As discussed above, metabolomic and imaging mass spectroscopy studies are planned to give detailed insights into metabolic alterations during PNC development. These studies will give a complete and in-dept report of all metabolic changes and identify pathways and intermediates for further follow-up investigations beyond solely glycolytic parameters. It is known that lipid and amino acid metabolism are also altered in cancers. In fact, preliminary data using a BODIPY compound in this model suggests that PNCs show increased lipid uptake at early stages of induction (data not shown), further confirming the need for broader metabolic analysis. These detailed spectroscopy experiments represent a large and comprehensive body of work. Protocol optimisation has begun in conjunction with numerous collaborators and moving forward, it is hoped that this project will lead to identification of numerous metabolic parameters for further investigation.

Analysis of gene expression levels in isolated PNCs was not completed during this project. While PNCs were successfully isolated, sufficient concentration of cDNA for analysis could not be synthesised without the need for costly amplification. Recent funding has been secured for RNASeq experiments to be carried out specifically in PNCs, allowing analysis of altered gene expression across the entire genome. These experiments will allow true expression levels of the genes looked at during this project to be determined and allow assessment of expression levels of additional metabolism associated genes. Combining these data with the metabolomics studies discussed above will provide a powerful and comprehensive report of metabolic alterations developing PNCs.

While these approaches can provide comprehensive details of metabolic alterations, the capacity of this model for *in vivo* studies cannot be overlooked. A number of new transgenic lines, discussed above, will provide detailed observational studies of numerous metabolic processes to be carried out and provide unprecedented access to these processes *in vivo*. Cloning of these reporters was completed during this project and, when adulthood has been reached, fish will be screened to identify founder fish and fully characterised before experiments commence.

Although not discussed here, the important contribution of macrophages to cancer development is well accepted. Characterisation of macrophage recruitment, in addition to neutrophils, to developing PNCs is ongoing in the lab. Preliminary data shows macrophage recruitment at early stages of PNC development, similar in temporal response to neutrophil recruitment (data not shown). Moving forward, more comprehensive studies of both neutrophil and macrophage responses and their role in PNC initiation and development are planned, including the effect of metabolic alterations on leukocyte behaviour.

6.8 Final Conclusions.

The aim of this project was to investigate mitochondrial and metabolic alterations during cancer initiation. While the experiments described here are merely the tip of the iceberg in terms of fully understanding metabolic changes in PNCs, they clearly identify that alterations occur at very early stages of PNC initiation. The identification of a functionally-consequential hyper-fragmented mitochondrial phenotype in early PNCs and its importance for oncogenic processes places it as an ideal target for preventative interventions. While glycolytic studies are less conclusive, they prove that alterations are occurring in PNCs and provide justification for extensive metabolomic investigations in the future.

Supplemental Figures

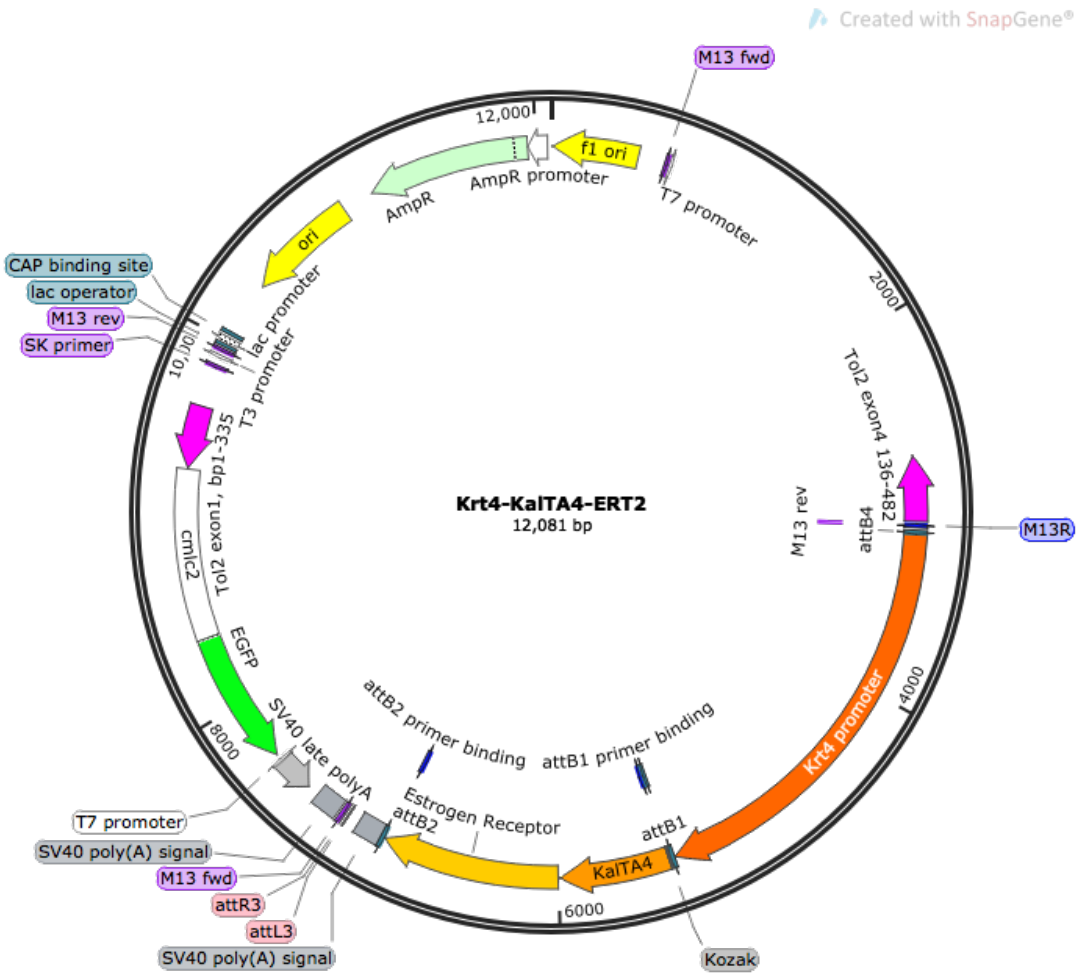

Supplemental Figure 1: Construct map for Krt4:KalTA4-ER^{T2} Construct used for generation of transgenic zebrafish line. Designed and constructed by Thomas Ramezani (Yi Feng, The University of Edinburgh).

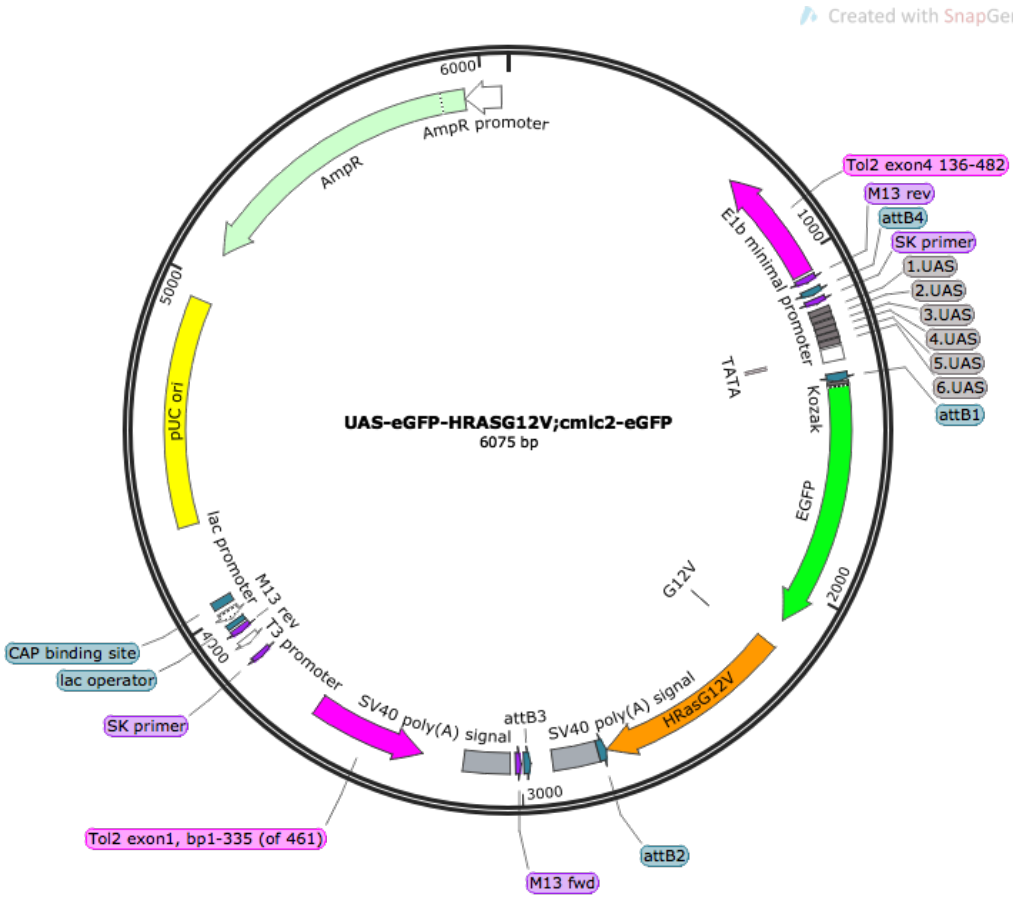

Supplemental Figure 2: Construct map for UAS:eGFP-HRAS^{G12V} Construct used for microinjection into the one-cell stage of Krt4:KalTA4-ER^{T2} zygotes. Designed and constructed by Thomas Ramezani (Yi Feng, The University of Edinburgh).

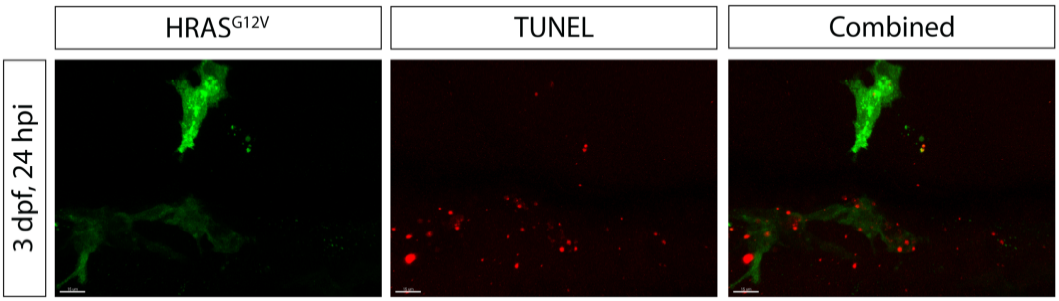

Supplemental Figure 3: TUNEL staining for apoptotic cell death. Representative images from a TUNEL assay for detection of apoptotic cell death in PNCs. Positive staining is achieved; however, some non-specific extra-nuclear staining is also observed. Also, PNC morphology appears altered as a result of proteinase treatment during the TUNEL protocol.

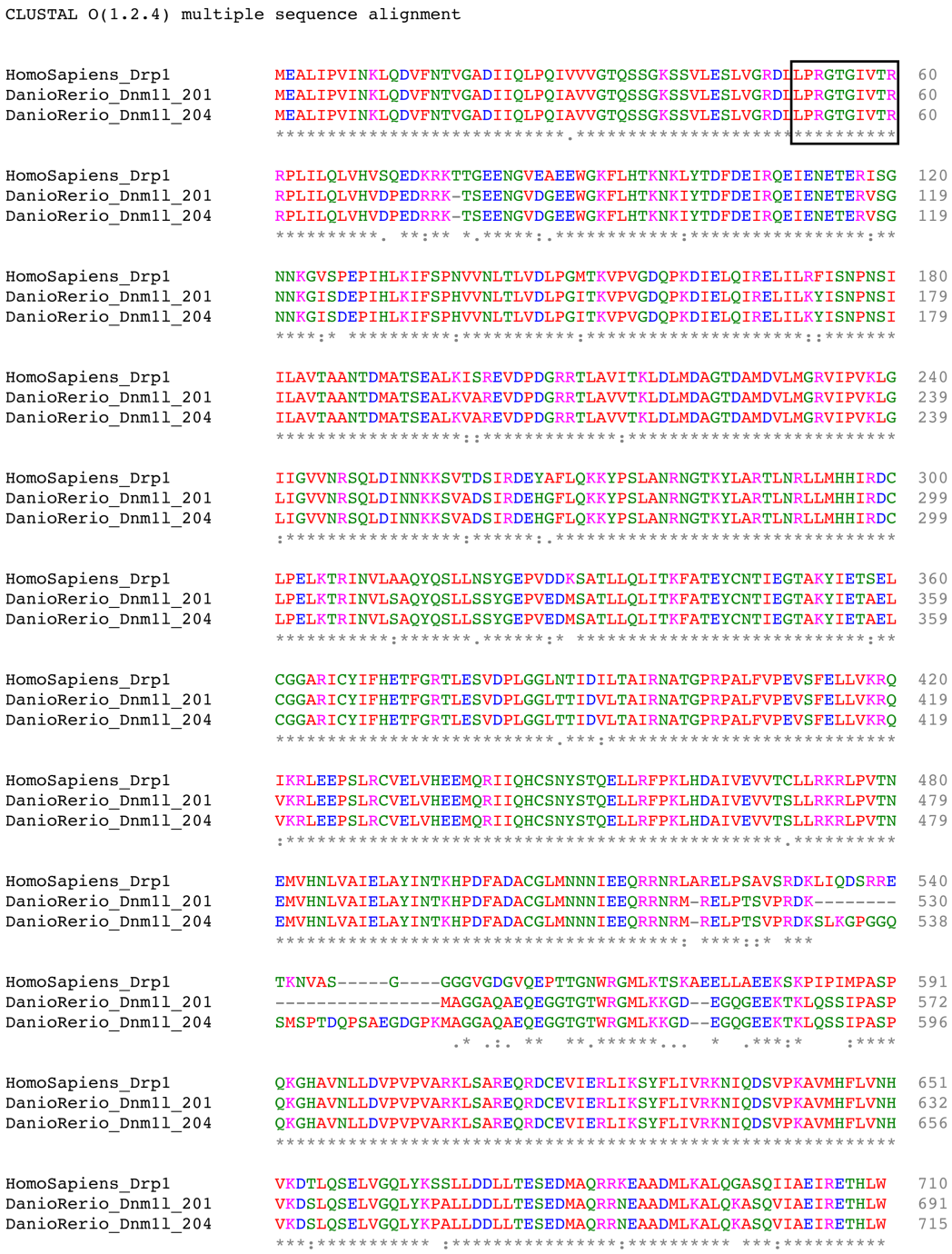

Supplemental Figure 4: Dnm1l is the zebrafish orthologue for human Dnm1. Clustal alignments for human Dnm1(Ensembl ENST00000452533.6) with two transcripts for zebrafish Dnm1l (Ensembl ENSDART00000006840.7 and Ensembl ENSDART00000173434.2, respectively). Ensembl reports 88.67 % homology between the human Dnm1 protein and zebrafish Dnm1l protein. The GTPase active region (aa 51-60, black box) shows 100 % conservation among all transcripts. This indicates that Dnm1l is indeed the zebrafish orthologue for human Dnm1.

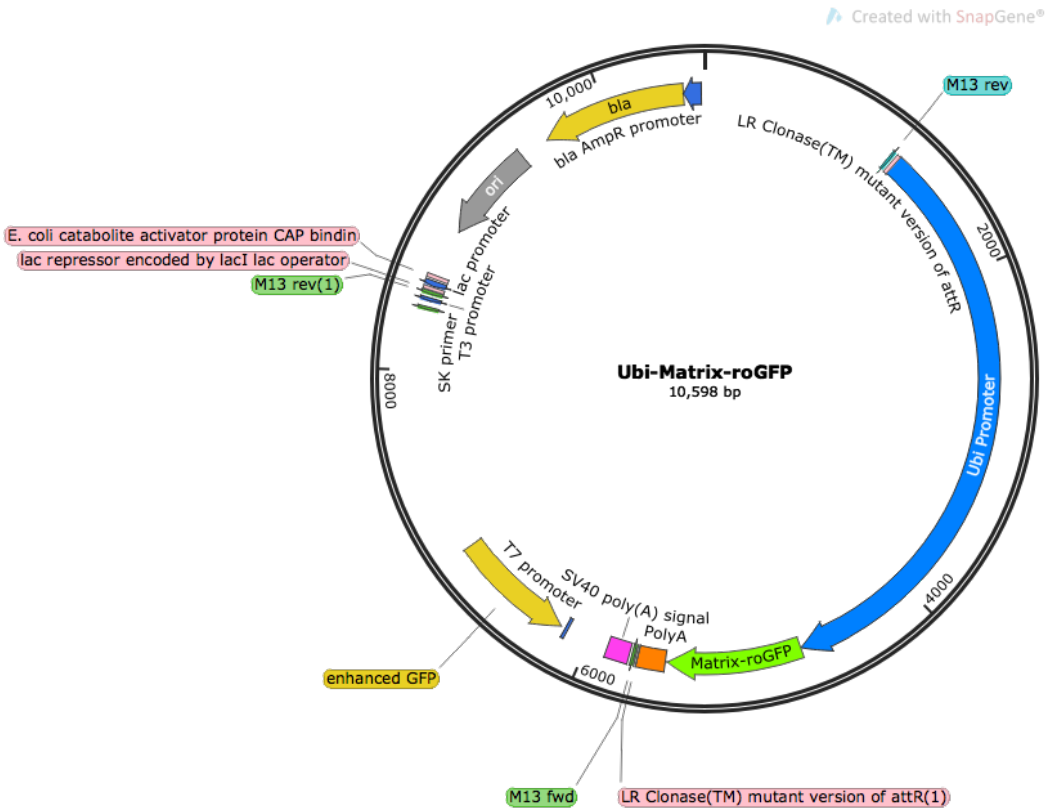

Supplemental Figure 5: Construct map for Ubi:Matrix-roGFP. Construct used for generation of transgenic zebrafish line.

8. Bibliography

[1] R. J. B. King and M. W. Robins, *Cancer Biology*, Third Edit. Pearson Education, 2006.

[2] American Cancer Society, "Cancer Facts and Figures 2018," *Am. Cancer Soc.*, pp. 1–71, 2018.

[3] "Cancer Research UK: Cancer Incidence Statistics." [Online]. Available: https://www.cancerresearchuk.org/health-professional/cancer-statistics/incidence#heading-Two. [Accessed: 29-Aug-2018].

[4] V. Vedham and M. Verma, "Cancer-Associated Infectious Agents and Epigenetic Regulation," in *Methods in molecular biology*, vol. 1238, 2015, pp. 333–354.

[5] "Cancer Research UK: Cancer Risk Statistics." [Online]. Available: https://www.cancerresearchuk.org/health-professional/cancer-statistics/risk#heading-One. [Accessed: 29-Aug-2018].

[6] J. M. P. Holly, L. Zeng, and C. M. Perks, "Epithelial cancers in the post-genomic era: should we reconsider our lifestyle?," *Cancer Metastasis Rev.*, vol. 32, no. 3–4, pp. 673–705, Dec. 2013.

[7] B. Alberts, A. Johnson, J. Lewis, M. Raff, K. Roberts, and P. Walter, *Molecular Biology of the Cell, 5th Edition*, 5th ed. Garland Science, 2007.

[8] "Cancer Research UK: Cancer Survival Statistics." [Online]. Available: https://www.cancerresearchuk.org/health-professional/cancer-statistics/survival. [Accessed: 29-Aug-2018].

[9] "CRUK Catching Cancer Early: A new frontier for early detection research." [Online]. Available: https://www.cancerresearchuk.org/funding-for-researchers/research-features/2017-06-20-catching-cancer-earlier-a-new-frontier-for-early-detection-research. [Accessed: 29-Aug-2018].

[10] "Cancer Research UK: Breast Cancer Screening." [Online]. Available: https://www.cancerresearchuk.org/about-cancer/breast-cancer/screening/breast-screening. [Accessed: 29-Aug-2018].

[11] "Cancer Research UK: Cervical Cancer Screening." [Online]. Available:

https://www.cancerresearchuk.org/about-cancer/cervical-cancer/getting-diagnosed/screening/about. [Accessed: 29-Aug-2018].

[12] "Cancer Research UK: Bowel Cancer Screening." [Online]. Available: https://www.cancerresearchuk.org/about-cancer/bowel-cancer/getting-diagnosed/screening. [Accessed: 29-Aug-2018].

[13] "Cancer Research UK: HPV and Cancer." [Online]. Available: https://www.cancerresearchuk.org/about-cancer/causes-of-cancer/infections-hpv-and-cancer/hpv-and-cancer. [Accessed: 29-Aug-2018].

[14] D. Hanahan and R. A. Weinberg, "The Hallmarks of Cancer.," *Cell*, vol. 100, no. 1, pp. 57–70, Jan. 2000.

[15] D. Hanahan and R. a Weinberg, "Hallmarks of cancer: The Next Generation.," *Cell*, vol. 144, no. 5, pp. 646–74, Mar. 2011.

[16] P. A. Futreal *et al.*, "A census of human cancer genes.," *Nat. Rev. Cancer*, vol. 4, no. 3, pp. 177–83, Mar. 2004.

[17] E. Porta-Pardo, L. Garcia-Alonso, T. Hrabe, J. Dopazo, and A. Godzik, "A Pan-Cancer Catalogue of Cancer Driver Protein Interaction Interfaces.," *PLoS Comput. Biol.*, vol. 11, no. 10, p. e1004518, Oct. 2015.

[18] F. Sanchez-Vega *et al.*, "Oncogenic Signaling Pathways in The Cancer Genome Atlas.," *Cell*, vol. 173, no. 2, p. 321–337.e10, Apr. 2018.

[19] P. C. Nowell, "The clonal evolution of tumor cell populations.," *Science (80-.).*, vol. 194, no. 4260, pp. 23–8, Oct. 1976.

[20] D. J. Ashley, "The two 'hit' and multiple 'hit' theories of carcinogenesis.," *Br. J. Cancer*, vol. 23, no. 2, pp. 313–28, Jun. 1969.

[21] A. G. Knudson, "Mutation and Cancer: Statistical Study of Retinoblastoma," 1971.

[22] C. Blanpain, "Tracing the cellular origin of cancer," *Nat. Cell Biol.*, vol. 15, no. 2, pp. 126–134, Feb. 2013.

[23] J. C. Y. Wang, "Good cells gone bad: the cellular origins of cancer," *Trends Mol. Med.*, vol. 16, no. 3, pp. 145–151, 2010.

[24] J. S. Flier, L. H. Underhill, and H. F. Dvorak, "Tumors: Wounds That Do Not

Heal," *N. Engl. J. Med.*, vol. 315, no. 26, pp. 1650–1659, Dec. 1986.

[25] T. D. Tlsty and P. W. Hein, "Know thy neighbor: Stromal cells can contribute oncogenic signals," *Curr. Opin. Genet. Dev.*, vol. 11, no. 1, pp. 54–59, 2001.

[26] T. D. Tlsty and L. M. Coussens, "Tumor Stroma and Regulation of Cancer Development," *Annu. Rev. Pathol. Mech. Dis*, vol. 1, pp. 119–50, 2006.

[27] A. van den Hooff, "Stromal Involvement In Malignant Growth," *Adv. Cancer Res.*, vol. 50, pp. 159–196, 1988.

[28] A. F. Olumi, G. D. Grossfeld, S. W. Hayward, P. R. Carroll, T. D. Tlsty, and G. R. Cunha, "Carcinoma-associated fibroblasts direct tumor progression of initiated human prostatic epithelium.," *Cancer Res.*, vol. 59, no. 19, pp. 5002–11, Oct. 1999.

[29] J. L. Camps *et al.*, "Fibroblast-mediated acceleration of human epithelial tumor growth in vivo.," *Proc. Natl. Acad. Sci. U. S. A.*, vol. 87, no. 1, pp. 75–9, Jan. 1990.

[30] M. Gleave, J. T. Hsieh, C. A. Gao, A. C. von Eschenbach, and L. W. Chung, "Acceleration of human prostate cancer growth in vivo by factors produced by prostate and bone fibroblasts.," *Cancer Res.*, vol. 51, no. 14, pp. 3753–61, Jul. 1991.

[31] P. Carmeliet and R. K. Jain, "Angiogenesis in cancer and other diseases," *Nature*, vol. 407, no. 6801, pp. 249–257, Sep. 2000.

[32] Y. Pylayeva-Gupta, E. Grabocka, and D. Bar-Sagi, "RAS oncogenes: weaving a tumorigenic web.," *Nat. Rev. Cancer*, vol. 11, no. 11, pp. 761–74, Nov. 2011.

[33] J. Cherfils and P. Chardin, "GEFs: Structural basis for their activation of small GTP-binding proteins," *Trends Biochem. Sci.*, vol. 24, no. 8, pp. 306–311, 1999.

[34] S. Donovan, K. M. Shannon, and G. Bollag, "GTPase activating proteins: Critical regulators of intracellular signaling," *Biochim. Biophys. Acta - Rev. Cancer*, vol. 1602, no. 1, pp. 23–45, 2002.

[35] M. F. Olson and R. Marais, "Ras protein signalling.," *Semin. Immunol.*, vol. 12, no. 1, pp. 63–73, Feb. 2000.

[36] K. Koera *et al.*, "K-ras is essential for the development of the mouse embryo.,"

Oncogene, vol. 15, no. 10, pp. 1151–1159, 1997.

[37] A. S. Dhillon, S. Hagan, O. Rath, and W. Kolch, “MAP kinase signalling pathways in cancer,” *Oncogene*, vol. 26, no. 22, pp. 3279–3290, May 2007.

[38] M. P. Wymann and L. Pirola, “Structure and function of phosphoinositide 3-kinases,” *Biochim. Biophys. Acta - Mol. Cell Biol. Lipids*, vol. 1436, no. 1–2, pp. 127–150, 1998.

[39] T. Kodaki, R. Woscholski, B. Hallberg, P. Rodriguez-Viciana Julian Downward, and P. J. Parker, “The activation of phosphatidylinositol 3-kinase by Ras,” *Curr. Biol.*, vol. 4, no. 9, pp. 798–806, 1994.

[40] P. Rodriguez-Viciana *et al.*, “Phosphatidylinositol-3-OH kinase direct target of Ras,” *Nature*, vol. 370, p. 527, Aug. 1994.

[41] G. G. Kelley, S. E. Reks, J. M. Ondrako, and A. V Smrcka, “Phospholipase Ce : a novel Ras effector,” *EMBO J.*, vol. 20, no. 4, pp. 743–754, 2001.

[42] R. M. F. Wolthuis, F. Zwartkruis, T. C. Moen, and J. L. Bos, “Ras-dependent activation of the small GTPase Ral,” *Curr. Biol.*, vol. 8, no. 8, pp. 471–474, 1998.

[43] K. Giehl, “Oncogenic Ras in tumour progression and metastasis.,” *Biol. Chem.*, vol. 386, no. 3, pp. 193–205, Mar. 2005.

[44] M. Malumbres and M. Barbacid, “RAS oncogenes: the first 30 years,” *Nat. Rev. Cancer*, vol. 3, no. 6, pp. 459–465, Jun. 2003.

[45] I. A. Prior, P. D. Lewis, and C. Mattos, “A comprehensive survey of Ras mutations in cancer.,” *Cancer Res.*, vol. 72, no. 10, pp. 2457–67, May 2012.

[46] COSMIC Database, “KRAS Gene - Somatic Mutations in Cancer.” [Online]. Available: https://cancer.sanger.ac.uk/cosmic/gene/analysis?ln=KRAS. [Accessed: 04-Sep-2018].

[47] COSMIC Database, “NRAS Gene - Somatic Mutations in Cancer.” [Online]. Available: https://cancer.sanger.ac.uk/cosmic/gene/analysis?ln=NRAS. [Accessed: 04-Sep-2018].

[48] COSMIC Database, “HRAS Gene - Somatic Mutations in Cancer.” [Online]. Available: https://cancer.sanger.ac.uk/cosmic/gene/analysis?ln=HRAS. [Accessed: 04-Sep-2018].

[49] S. A. Mccarthy, C. A. Pritchard, and J. A. Abraham, “Rapid induction of heparin-binding epidermal growth factor / diphtheria toxin receptor expression by Raf and Ras oncogenes,” *Genes Dev.*, vol. 9, pp. 1953–1964, 1995.

[50] L. M. Gangarosa, N. Sizemore, R. Graves-deal, S. M. Oldham, C. J. Der, and R. J. Coffey, “A Raf-independent Epidermal Growth Factor Receptor Autocrine Loop Is Necessary for Ras Transformation of Rat Intestinal Epithelial Cells,” *J. Biol. Chem.*, vol. 272, no. 30, pp. 18926–18931, 1997.

[51] A. Schulze, K. Lehmann, H. B. J. Jefferies, M. McMahon, and J. Downward, “Analysis of the transcriptional program induced by Raf in epithelial cells,” *Genes Dev.*, vol. 15, no. 8, pp. 981–994, 2001.

[52] K. Rosen, J. Rak, J. Jin, R. S. Kerbel, M. J. Newman, and J. Filmus, “Downregulation of the pro-apoptotic protein Bak is required for the ras-induced transformation of intestinal epithelial cells.,” *Curr. Biol.*, vol. 8, no. 24, pp. 1331–4, 1998.

[53] S. R. Datta *et al.*, “Akt phosphorylation of BAD couples survival signals to the cell- intrinsic death machinery,” *Cell*, vol. 91, no. 2, pp. 231–241, 1997.

[54] X. Fang *et al.*, “Regulation of BAD phosphorylation at serine 112 by the Ras-mitogen-activated protein kinase pathway,” *Oncogene*, vol. 18, no. 48, pp. 6635–6640, 1999.

[55] T. Kinoshita, T. Yokota, K. Arai, and A. Miyajima, “Regulation of Bcl-2 expression by oncogenic Ras protein in hematopoietic cells.,” *Oncogene*, vol. 10, no. 11, pp. 2207–12, Jun. 1995.

[56] L. Wu, Y. J. Nam, G. Kung, M. T. Crow, and R. N. Kitsis, “Induction of the apoptosis inhibitor ARC by Ras in human cancers,” *J. Biol. Chem.*, vol. 285, no. 25, pp. 19235–19245, 2010.

[57] J. Rak *et al.*, “Mutant ras Oncogenes Upregulate VEGF/VPF Expression : Implications for Induction and Inhibition of Tumor Angiogenesis,” *Cancer Res.*, vol. 55, pp. 4575–4581, 1995.

[58] C. Blancher, J. W. Moore, N. Robertson, and a L. Harris, “Effects of ras and von Hippel-Lindau (VHL) gene mutations on hypoxia-inducible factor (HIF)-1alpha,

HIF-2alpha, and vascular endothelial growth factor expression and their regulation by the phosphatidylinositol 3'-kinase/Akt signaling pathway.," *Cancer Res.*, vol. 61, no. 19, pp. 7349–7355, 2001.

[59] O. Kranenburg, M. F. B. G. Gebbink, and E. E. Voest, "Stimulation of angiogenesis by Ras proteins," *Biochim. Biophys. Acta - Rev. Cancer*, vol. 1654, no. 1, pp. 23–37, 2004.

[60] B. B. Ancrile, K. M. O. Hayer, and C. M. Counter, "Oncogenic Ras-Induced Expression of Cytokines: A New Target of Anti-Cancer Therapies," *Mol. Interv.*, vol. 8, no. 1, pp. 22–27, 2008.

[61] A. Sparmann and D. Bar-Sagi, "Ras-induced interleukin-8 expression plays a critical role in tumor growth and angiogenesis," *Cancer Cell*, vol. 6, no. 5, pp. 447–458, 2004.

[62] G. Yang *et al.*, "The chemokine growth-regulated oncogene 1 (Gro-1) links RAS signaling to the senescence of stromal fibroblasts and ovarian tumorigenesis," *Proc. Natl. Acad. Sci.*, vol. 103, no. 44, pp. 16472–16477, 2006.

[63] B. Ancrile, K. H. Lim, and C. M. Counter, "Oncogenic Ras-induced secretion of IL6 is required for tumorigenesis," *Genes Dev.*, vol. 21, no. 14, pp. 1714–1719, 2007.

[64] M. S. Pepper, "Role of the Matrix Metalloproteinase and Plasminogen Activator – Plasmin Systems in Angiogenesis on have," *Arter. Thromb Vasc Biol*, vol. 21, no. 7, pp. 1104–1117, 2001.

[65] R. C. O'Hagan and J. Heyer, "KRAS Mouse Models: Modeling Cancer Harboring KRAS Mutations.," *Genes Cancer*, vol. 2, no. 3, pp. 335–43, Mar. 2011.

[66] C. Guerra *et al.*, "Tumor induction by an endogenous K-ras oncogene is highly dependent on cellular context," *Cancer Cell*, vol. 4, no. 2, pp. 111–120, Aug. 2003.

[67] S. R. Hingorani *et al.*, "Preinvasive and invasive ductal pancreatic cancer and its early detection in the mouse.," *Cancer Cell*, vol. 4, no. 6, pp. 437–50, Dec. 2003.

[68] X. Chen *et al.*, "Endogenous expression of HrasG12V induces developmental

defects and neoplasms with copy number imbalances of the oncogene," *Proc. Natl. Acad. Sci.*, vol. 106, no. 19, pp. 7979–7984, May 2009.

[69] L. Chin *et al.*, "Essential role for oncogenic Ras in tumour maintenance," *Nature*, vol. 400, no. 6743, pp. 468–472, Jul. 1999.

[70] C. Santoriello *et al.*, "Kita driven expression of oncogenic HRAS leads to early onset and highly penetrant melanoma in zebrafish.," *PLoS One*, vol. 5, no. 12, p. e15170, 2010.

[71] D. M. Langenau *et al.*, "Effects of RAS on the genesis of embryonal rhabdomyosarcoma.," *Genes Dev.*, vol. 21, no. 11, pp. 1382–95, Jun. 2007.

[72] S. W. Park, J. M. Davison, J. Rhee, R. H. Hruban, A. Maitra, and S. D. Leach, "Oncogenic KRAS induces progenitor cell expansion and malignant transformation in zebrafish exocrine pancreas.," *Gastroenterology*, vol. 134, no. 7, pp. 2080–90, Jun. 2008.

[73] X. Le, D. M. Langenau, M. D. Keefe, J. L. Kutok, D. S. Neuberg, and L. I. Zon, "Heat shock-inducible Cre/Lox approaches to induce diverse types of tumors and hyperplasia in transgenic zebrafish," *Proc. Natl. Acad. Sci.*, vol. 104, no. 22, pp. 9410–9415, May 2007.

[74] T. Ramezani, D. W. Laux, I. R. Bravo, M. Tada, and Y. Feng, "Live Imaging of Innate Immune and Preneoplastic Cell Interactions Using an Inducible Gal4/UAS Expression System in Larval Zebrafish Skin," *J. Vis. Exp.*, no. 96, pp. 1–7, 2015.

[75] A. Boiteux and B. Hess, "Design of Glycolysis," *Philos. Trans. R. Soc. Lond. B. Biol. Sci.*, vol. 293, no. 1063, pp. 5–22, 1981.

[76] D. . Nelson and M. . Cox, *Lehninger Principles of Biochemistry*, Fifth. New York: Sarah Tenney, 2008.

[77] N. Kresge, R. D. Simoni, and R. L. Hill, "Otto Fritz Meyerhof and the elucidation of the glycolytic pathway.," *J. Biol. Chem.*, vol. 280, no. 4, pp. 124–127, 2005.

[78] J. E. Wilson, "Isozymes of mammalian hexokinase: structure, subcellular localization and metabolic function," *J. Exp. Biol.*, vol. 206, no. 12, pp. 2049–2057, 2003.

[79] J. V. Passonneau and O. H. Lowry, “The role of phosphofructokinase in metabolic regulation,” *Adv. Enzyme Regul.*, vol. 2, no. C, pp. 265–274, 1964.

[80] L. Hue and M. H. Rider, “Role of fructose 2, 6-bisphosphate in the control of glycolysis in mammalian tissues.,” *Biochem. J.*, vol. 245, no. 2, p. 313, 1987.

[81] W. J. Israelsen and M. G. Vander Heiden, “Pyruvate kinase: Function, regulation and role in cancer.,” *Semin. Cell Dev. Biol.*, vol. 43, pp. 43–51, Jul. 2015.

[82] R. A. Harris, M. M. Bowker-Kinley, B. Huang, and P. Wu, “Regulation of the activity of the pyruvate dehydrogenase complex,” *Adv. Enzyme Regul.*, vol. 42, pp. 249–259, 2002.

[83] L. Shi and B. P. Tu, “Acetyl-CoA and the Regulation of Metabolism: Mechanisms and COnsequences,” *Curr. Environ. Heal. Reports*, vol. 33, pp. 125–131, 2015.

[84] M. Adeva-Andany *et al.*, “Comprehensive review on lactate metabolism in human health,” *Mitochondrion*, vol. 17, pp. 76–100, 2014.

[85] M. Akram, “Citric Acid Cycle and Role of its Intermediates in Metabolism,” *Cell Biochem. Biophys.*, vol. 68, no. 3, pp. 475–478, 2014.

[86] J. P. Hosler, S. Ferguson-miller, and D. a Mills, “Energy Transduction: Proton Transfer Through the Respiratory Complexes,” *Annu Rev Biochem*, vol. 75, pp. 165–187, 2006.

[87] M. D. Brand and M. P. Murphy, “Control of electron flux through the respiratory chain in mitochondria and cells.,” *Biol. Rev. Camb. Philos. Soc.*, vol. 62, no. 2, pp. 141–93, 1987.

[88] OpenStax College, “Biology,” 2013.

[89] M. A. Bianchet, J. Hullihen, P. L. Pedersen, and L. M. Amzel, “The 2.8-A structure of rat liver F1-ATPase: configuration of a critical intermediate in ATP synthesis/hydrolysis.,” *Proc. Natl. Acad. Sci. U. S. A.*, vol. 95, no. 19, pp. 11065–70, Sep. 1998.

[90] V. Adam-Vizi and C. Chinopoulos, “Bioenergetics and the formation of mitochondrial reactive oxygen species,” *Trends Pharmacol. Sci.*, vol. 27, no. 12, pp. 639–645, 2006.

[91] C. Quijano, M. Trujillo, L. Castro, and A. Trostchansky, “Interplay between oxidant species and energy metabolism,” *Redox Biol.*, vol. 8, pp. 28–42, 2016.

[92] O. Warburg, “On the origin of cancer cells.,” *Science (80-.).*, vol. 123, no. 3191, pp. 309–14, Feb. 1956.

[93] P. S. Ward and C. B. Thompson, “Metabolic Reprogramming: A cancer hallmark even warburg did not anticipate.,” *Cancer Cell*, vol. 21, no. 3, pp. 297–308, Mar. 2012.

[94] S. S. Gambhir, “Molecular imaging of cancer with positron emission tomography,” *Nat. Rev. Cancer*, vol. 2, no. 9, pp. 683–693, Sep. 2002.

[95] K. B. Nolop *et al.*, “Glucose utilization in vivo by human pulmonary neoplasms.,” *Cancer*, vol. 60, no. 11, pp. 2682–9, Dec. 1987.

[96] G. Di Chiro, “Positron emission tomography using [18F] fluorodeoxyglucose in brain tumors. A powerful diagnostic and prognostic tool.,” *Invest. Radiol.*, vol. 22, no. 5, pp. 360–71, May 1987.

[97] K. Kubota *et al.*, “Differential diagnosis of lung tumor with positron emission tomography: a prospective study.,” *J. Nucl. Med.*, vol. 31, no. 12, pp. 1927–32, Dec. 1990.

[98] N. C. Gupta *et al.*, “Solitary pulmonary nodules: detection of malignancy with PET with 2-[F-18]-fluoro-2-deoxy-D-glucose.,” *Radiology*, vol. 184, no. 2, pp. 441–444, Aug. 1992.

[99] C. K. Hoh *et al.*, “Cancer detection with whole-body PET using 2-[18F]fluoro-2-deoxy-D-glucose.,” *J. Comput. Assist. Tomogr.*, vol. 17, no. 4, pp. 582–9, 1993.

[100] M. Kunkel *et al.*, “Overexpression of Glut-1 and increased glucose metabolism in tumors are associated with a poor prognosis in patients with oral squamous cell carcinoma,” *Cancer*, vol. 97, no. 4, pp. 1015–1024, Feb. 2003.

[101] J. Li, W. Xu, F. Kong, X. Sun, and X. Zuo, “Meta-analysis: Accuracy of 18FDG PET-CT for distant metastasis staging in lung cancer patients,” *Surg. Oncol.*, vol. 22, no. 3, pp. 151–155, Sep. 2013.

[102] A. M. Evens and L. Kostakoglu, “The role of FDG-PET in defining prognosis of Hodgkin lymphoma for early-stage disease.,” *Blood*, vol. 124, no. 23, pp. 3356–

64, Nov. 2014.

[103] L. Ceriani *et al.*, “Utility of baseline 18FDG-PET/CT functional parameters in defining prognosis of primary mediastinal (thymic) large B-cell lymphoma.,” *Blood*, vol. 126, no. 8, pp. 950–6, Aug. 2015.

[104] A. Annibaldi and C. Widmann, “Glucose metabolism in cancer cells,” *Curr. Opin. Clin. Nutr. Metab. Care*, vol. 13, no. 4, pp. 466–470, 2010.

[105] M. D. Hirschey *et al.*, “Dysregulated metabolism contributes to oncogenesis,” *Semin. Cancer Biol.*, vol. 35, 2015.

[106] E. Bustamante and P. L. Pedersen, “High aerobic glycolysis of rat hepatoma cells in culture: role of mitochondrial hexokinase.,” *Proc. Natl. Acad. Sci. U. S. A.*, vol. 74, no. 9, pp. 3735–9, Sep. 1977.

[107] E. Bustamante, H. P. Morris, and P. L. Pedersen, “Energy metabolism of tumor cells. Requirement for a form of hexokinase with a propensity for mitochondrial binding.,” *J. Biol. Chem.*, vol. 256, no. 16, pp. 8699–704, Aug. 1981.

[108] R. B. Robey and N. Hay, “Mitochondrial hexokinases, novel mediators of the antiapoptotic effects of growth factors and Akt,” *Oncogene*, vol. 25, no. 34, pp. 4683–4696, Aug. 2006.

[109] S. Mazurek, “Pyruvate kinase type M2: A key regulator of the metabolic budget system in tumor cells,” *Int. J. Biochem. Cell Biol.*, vol. 43, no. 7, pp. 969–980, Jul. 2011.

[110] J. Kim, I. Tchernyshyov, G. L. Semenza, and C. V. Dang, “HIF-1-mediated expression of pyruvate dehydrogenase kinase: A metabolic switch required for cellular adaptation to hypoxia,” *Cell Metab.*, vol. 3, no. 3, pp. 177–185, Mar. 2006.

[111] V. R. Fantin, J. St-Pierre, and P. Leder, “Attenuation of LDH-A expression uncovers a link between glycolysis, mitochondrial physiology, and tumor maintenance,” *Cancer Cell*, vol. 9, no. 6, pp. 425–434, Jun. 2006.

[112] A. Le *et al.*, “Inhibition of lactate dehydrogenase A induces oxidative stress and inhibits tumor progression.,” *Proc. Natl. Acad. Sci. U. S. A.*, vol. 107, no. 5, pp.

2037–42, Feb. 2010.

[113] I. P. M. Tomlinson *et al.*, “Germline mutations in FH predispose to dominantly inherited uterine fibroids, skin leiomyomata and papillary renal cell cancer,” *Nat. Genet.*, vol. 30, no. 4, pp. 406–410, Apr. 2002.

[114] B. E. Baysal *et al.*, “Mutations in SDHD, a mitochondrial complex II gene, in hereditary paraganglioma.,” *Science (80-.).*, vol. 287, no. 5454, pp. 848–51, Feb. 2000.

[115] D. W. Parsons *et al.*, “An Integrated Genomic Analysis of Human Glioblastoma Multiforme,” *Science (80-.).*, vol. 321, no. 5897, pp. 1807–1812, Sep. 2008.

[116] J. Balss, J. Meyer, W. Mueller, A. Korshunov, C. Hartmann, and A. von Deimling, “Analysis of the IDH1 codon 132 mutation in brain tumors,” *Acta Neuropathol.*, vol. 116, no. 6, pp. 597–602, Dec. 2008.

[117] C. Hartmann *et al.*, “Type and frequency of IDH1 and IDH2 mutations are related to astrocytic and oligodendroglial differentiation and age: a study of 1,010 diffuse gliomas,” *Acta Neuropathol.*, vol. 118, no. 4, pp. 469–474, Oct. 2009.

[118] H. Yang, Y. Xiong, and K. Guan, “Metabolic alteration in tumorigenesis.,” *Sci. China Life Sci.*, vol. 56, no. 12, pp. 1067–75, Dec. 2013.

[119] E. K. Oermann, J. Wu, K.-L. Guan, and Y. Xiong, “Alterations of metabolic genes and metabolites in cancer.,” *Semin. Cell Dev. Biol.*, vol. 23, no. 4, pp. 370–80, Jun. 2012.

[120] C. R. Justus, E. J. Sanderlin, and L. V Yang, “Molecular Connections between Cancer Cell Metabolism and the Tumor Microenvironment.,” *Int. J. Mol. Sci.*, vol. 16, no. 5, pp. 11055–86, Jan. 2015.

[121] M. G. Vander Heiden, L. C. Cantley, and C. B. Thompson, “Understanding the Warburg Effect: The Metabolic Requirements of Cell Proliferation,” *Science (80-.).*, vol. 324, no. 5930, pp. 1029–1033, May 2009.

[122] C. V Dang, “Links between metabolism and cancer.,” *Genes Dev.*, vol. 26, no. 9, pp. 877–90, May 2012.

[123] J. S. Flier, M. M. Mueckler, P. Usher, and H. F. Lodish, “Elevated levels of

glucose transport and transporter messenger RNA are induced by ras or src oncogenes.," *Science*, vol. 235, no. 4795, pp. 1492–5, Mar. 1987.

[124] C. Chen, N. Pore, A. Behrooz, F. Ismail-Beigi, and A. Maity, "Regulation of glut1 mRNA by Hypoxia-inducible Factor-1," *J. Biol. Chem.*, vol. 276, no. 12, pp. 9519–9525, Mar. 2001.

[125] R. Blum, J. Jacob-Hirsch, N. Amariglio, G. Rechavi, and Y. Kloog, "Ras inhibition in glioblastoma down-regulates hypoxia-inducible factor-1α, causing glycolysis shutdown and cell death," *Cancer Res.*, vol. 65, no. 3, pp. 999–1006, 2005.

[126] H. K. Kole, R. J. Resnick, M. Van Doren, and E. Racker, "Regulation of 6-phosphofructo-1-kinase activity in ras-transformed rat-1 fibroblasts," *Arch. Biochem. Biophys.*, vol. 286, no. 2, pp. 586–590, 1991.

[127] F. N. LOW, "Mitochondrial structure.," *J. Biophys. Biochem. Cytol.*, vol. 2, no. 4 Suppl, pp. 337–40, Jul. 1956.

[128] M. Brini, "Ca(2+) signalling in mitochondria: mechanism and role in physiology and pathology.," *Cell Calcium*, vol. 34, no. 4–5, pp. 399–405, 2003.

[129] S. Desagher and J. C. Martinou, "Mitochondria as the central control point of apoptosis.," *Trends Cell Biol.*, vol. 10, no. 9, pp. 369–77, Sep. 2000.

[130] S. Grandemange, S. Herzig, and J. C. Martinou, "Mitochondrial dynamics and cancer," *Semin. Cancer Biol.*, vol. 19, no. 1, pp. 50–56, 2009.

[131] H. A. L. Tuppen, E. L. Blakely, D. M. Turnbull, and R. W. Taylor, "Mitochondrial DNA mutations and human disease," *Biochim. Biophys. Acta - Bioenerg.*, vol. 1797, no. 2, pp. 113–128, 2010.

[132] S. A. Detmer and D. C. Chan, "Functions and dysfunctions of mitochondrial dynamics," *Nat. Rev. Mol. Cell Biol.*, vol. 8, no. 11, pp. 870–879, Nov. 2007.

[133] A. Y. Seo, A.-M. Joseph, D. Dutta, J. C. Y. Hwang, J. P. Aris, and C. Leeuwenburgh, "New insights into the role of mitochondria in aging: mitochondrial dynamics and more," *J. Cell Sci.*, vol. 123, no. 15, 2010.

[134] R. Rossignol, R. Gilkerson, R. Aggeler, K. Yamagata, S. J. Remington, and R. A. Capaldi, "Energy substrate modulates mitochondrial structure and oxidative capacity in cancer cells.," *Cancer Res.*, vol. 64, no. 3, pp. 985–93, Feb. 2004.

[135] H. Chen, A. Chomyn, and D. C. Chan, “Disruption of Fusion Results in Mitochondrial Heterogeneity and Dysfunction,” *J. Biol. Chem.*, vol. 280, no. 28, pp. 26185–26192, Jul. 2005.

[136] P. A. Parone *et al.*, “Preventing Mitochondrial Fission Impairs Mitochondrial Function and Leads to Loss of Mitochondrial DNA,” *PLoS One*, vol. 3, no. 9, p. e3257, Sep. 2008.

[137] D. G. Breckenridge, B.-H. Kang, D. Kokel, S. Mitani, L. A. Staehelin, and D. Xue, “Caenorhabditis elegans drp-1 and fis-2 Regulate Distinct Cell-Death Execution Pathways Downstream of ced-3 and Independent of ced-9,” *Mol. Cell*, vol. 31, no. 4, pp. 586–597, Aug. 2008.

[138] G. Twig *et al.*, “Fission and selective fusion govern mitochondrial segregation and elimination by autophagy,” *EMBO J.*, vol. 27, no. 2, pp. 433–446, Jan. 2008.

[139] C. Van den Bogert, P. Muus, C. Haanen, A. Pennings, T. E. Melis, and A. M. Kroon, “Mitochondrial biogenesis and mitochondrial activity during the progression of the cell cycle of human leukemic cells,” *Exp. Cell Res.*, vol. 178, no. 1, pp. 143–153, Sep. 1988.

[140] D. H. Margineantu, W. Gregory Cox, L. Sundell, S. W. Sherwood, J. M. Beechem, and R. A. Capaldi, “Cell cycle dependent morphology changes and associated mitochondrial DNA redistribution in mitochondria of human cell lines.,” *Mitochondrion*, vol. 1, no. 5, pp. 425–35, May 2002.

[141] M. Martínez-Diez, G. Santamaría, Á. D. Ortega, and J. M. Cuezva, “Biogenesis and Dynamics of Mitochondria during the Cell Cycle: Significance of 3’UTRs,” *PLoS One*, vol. 1, no. 1, p. e107, Dec. 2006.

[142] T. T. Renault *et al.*, “Mitochondrial shape governs BAX-induced membrane permeabilization and apoptosis,” *Mol. Cell*, vol. 57, no. 1, pp. 69–82, 2015.

[143] J. Ježek, K. F. Cooper, and R. Strich, “Reactive Oxygen Species and Mitochondrial Dynamics: The Yin and Yang of Mitochondrial Dysfunction and Cancer Progression.,” *Antioxidants (Basel, Switzerland)*, vol. 7, no. 1, Jan. 2018.

[144] M. D. Buck *et al.*, “Mitochondrial Dynamics Controls T Cell Fate through Metabolic Programming,” *Cell*, vol. 166, 2016.

[145] M. Noguchi and A. Kasahara, “Mitochondrial dynamics coordinate cell differentiation,” *Biochem. Biophys. Res. Commun.*, vol. 500, no. 1, pp. 59–64, 2018.

[146] T. Wai and T. Langer, “Mitochondrial Dynamics and Metabolic Regulation,” *Trends Endocrinol. Metab.*, vol. 27, no. 2, pp. 105–117, Feb. 2016.

[147] E. Smirnova, D. L. Shurland, S. N. Ryazantsev, and A. M. van der Bliek, “A human dynamin-related protein controls the distribution of mitochondria.,” *J. Cell Biol.*, vol. 143, no. 2, pp. 351–8, Oct. 1998.

[148] F. Legros, A. Lombès, P. Frachon, and M. Rojo, “Mitochondrial Fusion in Human Cells Is Efficient, Requires the Inner Membrane Potential, and Is Mediated by Mitofusins,” *Mol. Biol. Cell*, vol. 13, no. 12, pp. 4343–4354, Dec. 2002.

[149] S. Hoppins, “The regulation of mitochondrial dynamics,” *Curr. Opin. Cell Biol.*, vol. 29, pp. 46–52, 2014.

[150] D. L. Longo and S. L. Archer, “Mitochondrial Dynamics — Mitochondrial Fission and Fusion in Human Diseases,” *N. Engl. J. Med.*, vol. 369, no. 23, pp. 2236–2251, Dec. 2013.

[151] A. K. Lutz *et al.*, “Loss of Parkin or PINK1 Function Increases Drp1-dependent Mitochondrial Fragmentation,” *J. Biol. Chem.*, vol. 284, no. 34, pp. 22938–22951, Aug. 2009.

[152] S. Züchner *et al.*, “Mutations in the mitochondrial GTPase mitofusin 2 cause Charcot-Marie-Tooth neuropathy type 2A,” *Nat. Genet.*, vol. 36, no. 5, pp. 449–451, May 2004.

[153] A. Olichon *et al.*, “Effects of OPA1 mutations on mitochondrial morphology and apoptosis: Relevance to ADOA pathogenesis,” *J. Cell. Physiol.*, vol. 211, no. 2, pp. 423–430, May 2007.

[154] G. Arismendi-Morillo, “Electron microscopy morphology of the mitochondrial network in human cancer,” *Int. J. Biochem. Cell Biol.*, vol. 41, no. 10, pp. 2062–2068, Oct. 2009.

[155] A. Inoue-Yamauchi and H. Oda, “Depletion of mitochondrial fission factor DRP1 causes increased apoptosis in human colon cancer cells,” *Biochem.*

Biophys. Res. Commun., vol. 421, no. 1, pp. 81–85, Apr. 2012.

[156] J. Rehman *et al.*, "Inhibition of mitochondrial fission prevents cell cycle progression in lung cancer.," *FASEB J.*, vol. 26, no. 5, pp. 2175–86, May 2012.

[157] J. A. Kashatus *et al.*, "Erk2 phosphorylation of Drp1 promotes mitochondrial fission and MAPK-driven tumor growth.," *Mol. Cell*, vol. 57, no. 3, pp. 537–51, Mar. 2015.

[158] M. N. Serasinghe *et al.*, "Mitochondrial division is requisite to RAS-induced transformation and targeted by oncogenic MAPK pathway inhibitors," *Mol. Cell*, vol. 57, no. 3, pp. 521–537, 2015.

[159] R. L. K. Virchow, *Cellular pathology as based upon physiological and pathological histology ... / by Rudolf Virchow. Translated from the 2d ed. of the original by Frank Chance. With notes and numerous emendations, principally from MS. notes of the author*. Philadelphia : J. B. Lippincott, 1863.

[160] S. I. Grivennikov, F. R. Greten, and M. Karin, "Immunity, inflammation, and cancer.," *Cell*, vol. 140, no. 6, pp. 883–99, Mar. 2010.

[161] S. Wu *et al.*, "A human colonic commensal promotes colon tumorigenesis via activation of T helper type 17 T cell responses," *Nat. Med.*, vol. 15, no. 9, pp. 1016–1022, Sep. 2009.

[162] H. Takahashi, H. Ogata, R. Nishigaki, D. H. Broide, and M. Karin, "Tobacco Smoke Promotes Lung Tumorigenesis by Triggering IKKβ- and JNK1-Dependent Inflammation," *Cancer Cell*, vol. 17, no. 1, pp. 89–97, Jan. 2010.

[163] S. I. Grivennikov and M. Karin, "Inflammation and oncogenesis: a vicious connection.," *Curr. Opin. Genet. Dev.*, vol. 20, no. 1, pp. 65–71, Feb. 2010.

[164] M. Karin, "Nuclear factor-κB in cancer development and progression," *Nature*, vol. 441, no. 7092, pp. 431–436, May 2006.

[165] H. Yu, M. Kortylewski, and D. Pardoll, "Crosstalk between cancer and immune cells: role of STAT3 in the tumour microenvironment," *Nat. Rev. Immunol.*, vol. 7, no. 1, pp. 41–51, Jan. 2007.

[166] B. Ancrile, K.-H. Lim, and C. M. Counter, "Oncogenic Ras-induced secretion of IL6 is required for tumorigenesis," *Genes & Dev.*, vol. 21, no. 14, pp. 1714–

1719, Jul. 2007.

[167] F. R. Greten *et al.*, “IKKβ Links Inflammation and Tumorigenesis in a Mouse Model of Colitis-Associated Cancer,” *Cell*, vol. 118, no. 3, pp. 285–296, Aug. 2004.

[168] S. Maeda, H. Kamata, J.-L. Luo, H. Leffert, and M. Karin, “IKKβ Couples Hepatocyte Death to Cytokine-Driven Compensatory Proliferation that Promotes Chemical Hepatocarcinogenesis,” *Cell*, vol. 121, no. 7, pp. 977–990, Jul. 2005.

[169] S. Grivennikov *et al.*, “IL-6 and Stat3 Are Required for Survival of Intestinal Epithelial Cells and Development of Colitis-Associated Cancer,” *Cancer Cell*, vol. 15, no. 2, pp. 103–113, Feb. 2009.

[170] J. Bollrath *et al.*, “gp130-Mediated Stat3 Activation in Enterocytes Regulates Cell Survival and Cell-Cycle Progression during Colitis-Associated Tumorigenesis,” *Cancer Cell*, vol. 15, no. 2, pp. 91–102, Feb. 2009.

[171] J. Wyckoff *et al.*, “A Paracrine Loop between Tumor Cells and Macrophages Is Required for Tumor Cell Migration in Mammary Tumors,” *Cancer Res.*, vol. 64, no. 19, pp. 7022–7029, Oct. 2004.

[172] S. Goswami *et al.*, “Macrophages Promote the Invasion of Breast Carcinoma Cells via a Colony-Stimulating Factor-1/Epidermal Growth Factor Paracrine Loop,” *Cancer Res.*, vol. 65, no. 12, pp. 5278–5283, Jun. 2005.

[173] I. Mishalian, R. Bayuh, L. Levy, L. Zolotarov, J. Michaeli, and Z. G. Fridlender, “Tumor-associated neutrophils (TAN) develop pro-tumorigenic properties during tumor progression.,” *Cancer Immunol. Immunother.*, vol. 62, no. 11, pp. 1745–56, Nov. 2013.

[174] T. Chanmee, P. Ontong, K. Konno, and N. Itano, “Tumor-Associated Macrophages as Major Players in the Tumor Microenvironment,” *Cancers (Basel).*, vol. 6, pp. 1670–1690, 2014.

[175] S. J. Roberts *et al.*, “Characterizing tumor-promoting T cells in chemically induced cutaneous carcinogenesis,” *Proc. Natl. Acad. Sci.*, vol. 104, no. 16, pp. 6770–6775, Apr. 2007.

[176] D. G. DeNardo *et al.*, “CD4+ T Cells Regulate Pulmonary Metastasis of Mammary Carcinomas by Enhancing Protumor Properties of Macrophages,” *Cancer Cell*, vol. 16, no. 2, pp. 91–102, Aug. 2009.

[177] K. E. de Visser, L. V. Korets, and L. M. Coussens, “De novo carcinogenesis promoted by chronic inflammation is B lymphocyte dependent,” *Cancer Cell*, vol. 7, no. 5, pp. 411–423, May 2005.

[178] S. Ostrand-Rosenberg and S. Rosenberg, “Immune surveillance: a balance between protumor and antitumor immunity,” *Curr. Opin. Genet. Dev.*, vol. 18, pp. 11–18, 2008.

[179] J. S. Flier, L. H. Underhill, and H. F. Dvorak, “Tumors: Wounds That Do Not Heal,” *N. Engl. J. Med.*, vol. 315, no. 26, pp. 1650–1659, Dec. 1986.

[180] K. Goetze, S. Walenta, M. Ksiazkiewicz, L. A. Kunz-Schughart, and W. Mueller-Klieser, “Lactate enhances motility of tumor cells and inhibits monocyte migration and cytokine release,” *Int. J. Oncol.*, vol. 39, no. 2, pp. 453–463, Aug. 2011.

[181] K. Fischer *et al.*, “Inhibitory effect of tumor cell-derived lactic acid on human T cells.,” *Blood*, vol. 109, no. 9, pp. 3812–9, May 2007.

[182] E. Gottfried *et al.*, “Tumor-derived lactic acid modulates dendritic cell activation and antigen expression.,” *Blood*, vol. 107, no. 5, pp. 2013–21, Mar. 2006.

[183] C. J. Hall *et al.*, “Immunoresponsive Gene 1 Augments Bactericidal Activity of Macrophage-Lineage Cells by Regulating β-Oxidation-Dependent Mitochondrial ROS Production,” *Cell Metab.*, vol. 18, no. 2, pp. 265–278, 2013.

[184] A. Sica, T. Schioppa, A. Mantovani, and P. Allavena, “Tumour-associated macrophages are a distinct M2 polarised population promoting tumour progression: Potential targets of anti-cancer therapy,” *Eur. J. Cancer*, vol. 42, no. 6, pp. 717–727, 2006.

[185] R. Ostuni, F. Kratochvill, P. J. Murray, and G. Natoli, “Macrophages and cancer: from mechanisms to therapeutic implications,” *Trends Immunol.*, vol. 36, pp. 229–239, 2015.

[186] T. L. Putoczki *et al.*, “Interleukin-11 Is the Dominant IL-6 Family Cytokine during Gastrointestinal Tumorigenesis and Can Be Targeted Therapeutically,” *Cancer Cell*, vol. 24, no. 2, pp. 257–271, Aug. 2013.

[187] M. Chittezhath *et al.*, “Molecular Profiling Reveals a Tumor-Promoting Phenotype of Monocytes and Macrophages in Human Cancer Progression,” *Immunity*, vol. 41, no. 5, pp. 815–829, Nov. 2014.

[188] Z. G. Fridlender *et al.*, “Polarization of tumor-associated neutrophil phenotype by TGF-beta: ‘N1’ versus ‘N2’ TAN.,” *Cancer Cell*, vol. 16, no. 3, pp. 183–94, Sep. 2009.

[189] J. Jablonska, S. Leschner, K. Westphal, S. Lienenklaus, and S. Weiss, “Neutrophils responsive to endogenous IFN-β regulate tumor angiogenesis and growth in a mouse tumor model,” *J. Clin. Invest.*, vol. 120, no. 4, pp. 1151–1164, Apr. 2010.

[190] M. R. Galdiero, E. Bonavita, I. Barajon, C. Garlanda, A. Mantovani, and S. Jaillon, “Tumor associated macrophages and neutrophils in cancer.,” *Immunobiology*, vol. 218, no. 11, pp. 1402–10, Nov. 2013.

[191] N. Gungor *et al.*, “Genotoxic effects of neutrophils and hypochlorous acid,” *Mutagenesis*, vol. 25, no. 2, pp. 149–154, Mar. 2010.

[192] Y. Feng, C. Santoriello, M. Mione, A. Hurlstone, and P. Martin, “Live imaging of innate immune cell sensing of transformed cells in zebrafish larvae: parallels between tumor initiation and wound inflammation.,” *PLoS Biol.*, vol. 8, no. 12, p. e1000562, Jan. 2010.

[193] Y. Feng, S. Renshaw, and P. Martin, “Live imaging of tumor initiation in zebrafish larvae reveals a trophic role for leukocyte-derived PGE_2.,” *Curr. Biol.*, vol. 22, no. 13, pp. 1253–9, Jul. 2012.

[194] G. Streisinger, C. Walker, N. Dower, D. Knauber, and F. Singer, “Production of clones of homozygous diploid zebra fish (Brachydanio rerio).,” *Nature*, 1981.

[195] J. P. Briggs, “The zebrafish: a new model organism for integrative physiology.,” *Am. J. Physiol. Regul. Integr. Comp. Physiol.*, 2002.

[196] G. J. Lieschke and P. D. Currie, “Animal models of human disease: zebrafish

swim into view," *Nat. Rev. Genet.*, vol. 8, no. 5, pp. 353–367, May 2007.

[197] M. Westerfield, *The zebrafish book: A guide for the laboratory use of zebrafish (Danio rerio).*, 4th ed. Univ. of Oregon Press, 2000.

[198] C. M. Bennett *et al.*, "Myelopoiesis in the zebrafish, Danio rerio.," *Blood*, vol. 98, no. 3, pp. 643–51, 2001.

[199] D. Traver *et al.*, "The Zebrafish as a Model Organism to Study Development of the Immune System," *Adv. Immunol.*, vol. 81, pp. 254–330, 2003.

[200] W. Driever *et al.*, "A genetic screen for mutations affecting embryogenesis in zebrafish.," *Development*, vol. 123, pp. 37–46, Dec. 1996.

[201] P. Haffter *et al.*, "The identification of genes with unique and essential functions in the development of the zebrafish, Danio rerio.," *Development*, vol. 123, pp. 1–36, Dec. 1996.

[202] C. M. McCallum, L. Comai, E. A. Greene, and S. Henikoff, "Targeted screening for induced mutations," *Nat. Biotechnol.*, vol. 18, no. 4, pp. 455–457, Apr. 2000.

[203] A. Nasevicius and S. C. Ekker, "Effective targeted gene 'knockdown' in zebrafish," *Nat. Genet.*, vol. 26, no. 2, pp. 216–220, Oct. 2000.

[204] K. Kawakami, "Transgenesis and gene trap methods in zebrafish by using the Tol2 transposable element.," *Methods Cell Biol.*, vol. 77, pp. 201–22, 2004.

[205] R. T. Peterson, B. A. Link, J. E. Dowling, and S. L. Schreiber, "Small molecule developmental screens reveal the logic and timing of vertebrate development," *Proc. Natl. Acad. Sci.*, vol. 97, no. 24, pp. 12965–12969, Nov. 2000.

[206] R. T. Peterson *et al.*, "Chemical suppression of a genetic mutation in a zebrafish model of aortic coarctation," *Nat. Biotechnol.*, vol. 22, no. 5, pp. 595–599, May 2004.

[207] H. M. Stern *et al.*, "Small molecules that delay S phase suppress a zebrafish bmyb mutant.," *Nat. Chem. Biol.*, vol. 1, no. 7, pp. 366–70, Dec. 2005.

[208] R. D. Murphey, H. M. Stern, C. T. Straub, and L. I. Zon, "A Chemical Genetic Screen for Cell Cycle Inhibitors in Zebrafish Embryos," *Chem. Biol. Drug Des.*,

vol. 68, no. 4, pp. 213–219, Oct. 2006.

[209] R. M. White *et al.*, “DHODH modulates transcriptional elongation in the neural crest and melanoma,” *Nature*, vol. 471, no. 7339, pp. 518–522, Mar. 2011.

[210] G. B. Pliss, M. A. Zabezhinski, A. S. Petrov, and V. V Khudoley, “Peculiarities of N-nitramines carcinogenic action.,” *Arch. Geschwulstforsch.*, vol. 52, no. 8, pp. 629–34, 1982.

[211] R. White, K. Rose, and L. Zon, “Zebrafish cancer: the state of the art and the path forward,” *Nat. Rev. Cancer*, vol. 13, no. 9, pp. 624–636, Aug. 2013.

[212] D. M. Langenau *et al.*, “Myc-induced T cell leukemia in transgenic zebrafish.,” *Science (80-.).*, vol. 299, no. 5608, pp. 887–90, Feb. 2003.

[213] E. E. Patton *et al.*, “BRAF mutations are sufficient to promote nevi formation and cooperate with p53 in the genesis of melanoma.,” *Curr. Biol.*, vol. 15, no. 3, pp. 249–54, Feb. 2005.

[214] M. Dovey, R. M. White, and L. I. Zon, “Oncogenic NRAS Cooperates with p53 Loss to Generate Melanoma in Zebrafish,” *Zebrafish*, vol. 6, no. 4, pp. 397–404, Dec. 2009.

[215] C. J. Ceol *et al.*, “The histone methyltransferase SETDB1 is recurrently amplified in melanoma and accelerates its onset.,” *Nature*, vol. 471, no. 7339, pp. 513–7, Mar. 2011.

[216] C. K. Kaufman *et al.*, “A zebrafish melanoma model reveals emergence of neural crest identity during melanoma initiation.,” *Science*, vol. 351, no. 6272, p. aad2197, Jan. 2016.

[217] L. A. Rudner *et al.*, “Shared acquired genomic changes in zebrafish and human T-ALL.,” *Oncogene*, vol. 30, no. 41, pp. 4289–96, Oct. 2011.

[218] D. W. Laux, L. Kelly, I. Ribeiro, T. Ramezani, and Y. Feng, *Live imaging the earliest host innate immune response to preneoplastic cells using a zebrafish inducible KalTA4-ERT2/UAS system*, vol. 138. Elsevier Ltd, 2016.

[219] N. Yamamoto *et al.*, “Measurement of Glucose Uptake in Cultured Cells,” in *Current Protocols in Pharmacology*, vol. 55, no. 1, Hoboken, NJ, USA: John Wiley & Sons, Inc., 2011, p. 12.14.1-12.14.22.

[220] I. Zaimenko, J. Lisec, U. Stein, and W. Brenner, “Approaches and techniques to characterize cancer metabolism in vitro and in vivo,” *Biochim. Biophys. Acta - Rev. Cancer*, vol. 1868, no. 2, pp. 412–419, 2017.

[221] I. Agilent Technologies, “Seahorse XF e Extracellular Flux Analyzers: The World’s most advanced metabolic analyzers,” 2016.

[222] I. Agilent Technologies, “Agilent Seahorse XF Cell Mito Stress Test Kit: A Complete Profile of Mitochondrial Function,” 2016.

[223] I. Agilent Technologies, “Agilent Technologies Agilent Seahorse XF Glycolysis Stress Test Kit,” 2017.

[224] M. O. Yuneva *et al.*, “The metabolic profile of tumors depends on both the responsible genetic lesion and tissue type.,” *Cell Metab.*, vol. 15, no. 2, pp. 157–70, Feb. 2012.

[225] H. Xie *et al.*, “Targeting lactate dehydrogenase--a inhibits tumorigenesis and tumor progression in mouse models of lung cancer and impacts tumor-initiating cells.,” *Cell Metab.*, vol. 19, no. 5, pp. 795–809, May 2014.

[226] K. Sellers *et al.*, “Pyruvate carboxylase is critical for non–small-cell lung cancer proliferation,” *J. Clin. Invest.*, vol. 125, no. 2, pp. 687–698, Feb. 2015.

[227] S. Hayashi *et al.*, “A novel application of metabolomics in vertebrate development,” *Biochem. Biophys. Res. Commun.*, vol. 386, no. 1, pp. 268–272, Aug. 2009.

[228] E. S. Ong, C. F. Chor, L. Zou, and C. N. Ong, “A multi-analytical approach for metabolomic profiling of zebrafish (Danio rerio) livers,” *Mol. BioSyst.*, vol. 5, no. 3, pp. 288–298, Feb. 2009.

[229] S.-M. Huang, F. Xu, S. H. Lam, Z. Gong, and C. N. Ong, “Metabolomics of developing zebrafish embryos using gas chromatography- and liquid chromatography-mass spectrometry,” *Mol. Biosyst.*, vol. 9, no. 6, p. 1372, May 2013.

[230] V. Dunet, C. Rossier, A. Buck, R. Stupp, and J. O. Prior, “Performance of 18F-fluoro-ethyl-tyrosine (18F-FET) PET for the differential diagnosis of primary brain tumor: a systematic review and Metaanalysis.,” *J. Nucl. Med.*, vol. 53, no.

2, pp. 207–14, Feb. 2012.

[231] A. Chalkidou, D. B. Landau, E. W. Odell, V. R. Cornelius, M. J. O'Doherty, and P. K. Marsden, "Correlation between Ki-67 immunohistochemistry and 18F-fluorothymidine uptake in patients with cancer: A systematic review and meta-analysis.," *Eur. J. Cancer*, vol. 48, no. 18, pp. 3499–513, Dec. 2012.

[232] H. Jadvar, "Positron emission tomography in imaging evaluation of staging, restaging, treatment response, and prognosis in prostate cancer," *Abdom. Radiol.*, vol. 41, no. 5, pp. 889–898, May 2016.

[233] I. Grassi *et al.*, "The clinical use of PET with (11)C-acetate.," *Am. J. Nucl. Med. Mol. Imaging*, vol. 2, no. 1, pp. 33–47, 2012.

[234] M. M. Santoro, "Zebrafish as a model to explore cell metabolism.," *Trends Endocrinol. Metab.*, vol. 25, no. 10, pp. 546–54, Oct. 2014.

[235] V. V Belousov *et al.*, "Genetically encoded fluorescent indicator for intracellular hydrogen peroxide," *Nat. Methods*, vol. 3, no. 4, pp. 281–286, Apr. 2006.

[236] K. Santhakumar *et al.*, "A Zebrafish Model to Study and Therapeutically Manipulate Hypoxia Signaling in Tumorigenesis," *Cancer Res.*, vol. 72, no. 16, pp. 4017–4027, Aug. 2012.

[237] G. B. Waypa *et al.*, "Hypoxia triggers subcellular compartmental redox signaling in vascular smooth muscle cells.," *Circ. Res.*, vol. 106, no. 3, pp. 526–35, Feb. 2010.

[238] A. San Martín, S. Ceballo, I. Ruminot, R. Lerchundi, W. B. Frommer, and L. F. Barros, "A Genetically Encoded FRET Lactate Sensor and Its Use To Detect the Warburg Effect in Single Cancer Cells," *PLoS One*, vol. 8, no. 2, 2013.

[239] A. San Martín *et al.*, "Imaging mitochondrial flux in single cells with a FRET sensor for pyruvate.," *PLoS One*, vol. 9, no. 1, p. e85780, Jan. 2014.

[240] J. Berg, Y. P. Hung, and G. Yellen, "A genetically encoded fluorescent reporter of ATP:ADP ratio," *Nat. Methods*, vol. 6, no. 2, pp. 161–6, Jan. 2009.

[241] M. Tantama, J. Ramón Martínez-Franc¸ois, R. Mongeon, and G. Yellen, "Imaging energy status in live cells with a fluorescent biosensor of the

intracellular ATP-to-ADP ratio," *Nat. Commun.*, vol. 4, p. 2550, 2013.

[242] Y. P. Hung, J. G. Albeck, M. Tantama, and G. Yellen, "Imaging cytosolic NADH-NAD(+) redox state with a genetically encoded fluorescent biosensor.," *Cell Metab.*, vol. 14, no. 4, pp. 545–54, Oct. 2011.

[243] D. Balciunas *et al.*, "Harnessing a High Cargo-Capacity Transposon for Genetic Applications in Vertebrates," *PLoS Genet.*, vol. 2, no. 11, p. e169, 2006.

[244] C. Hall, M. V. Flores, T. Storm, K. Crosier, and P. Crosier, "The zebrafish lysozyme C promoter drives myeloid-specific expression in transgenic fish.," *BMC Dev. Biol.*, vol. 7, p. 42, 2007.

[245] R. Marín-Juez, M. Rovira, D. Crespo, M. van der Vaart, H. P. Spaink, and J. V Planas, "GLUT2-mediated glucose uptake and availability are required for embryonic brain development in zebrafish.," *J. Cereb. blood flow Metab.*, vol. 35, no. 1, pp. 74–85, Jan. 2015.

[246] M. Distel, M. F. Wullimann, and R. W. Köster, "Optimized Gal4 genetics for permanent gene expression mapping in zebrafish.," *Proc. Natl. Acad. Sci. U. S. A.*, vol. 106, no. 32, pp. 13365–70, Aug. 2009.

[247] Y. Takasaki, J. S. Deng, and E. M. Tan, "A nuclear antigen associated with cell proliferation and blast transformation.," *J. Exp. Med.*, vol. 154, no. 6, pp. 1899–909, Dec. 1981.

[248] R. Bravo, R. Frank, P. A. Blundell, and H. Macdonald-Bravo, "Cyclin/PCNA is the auxiliary protein of DNA polymerase-δ," *Nature*, vol. 326, no. 6112, pp. 515–517, Apr. 1987.

[249] W. L. Richards, M. K. Song, H. Krutzsch, R. P. Evarts, E. Marsden, and S. S. Thorgeirsson, "Measurement of cell proliferation in microculture using hoechst 33342 for the rapid semiautomated microfluorimetric determination of chromatin DNA," *Exp. Cell Res.*, vol. 159, no. 1, pp. 235–246, 1985.

[250] R. A. Blaheta, M. Franz, M. K. H. Auth, H. J. C. Wenisch, and B. H. Markus, "A rapid non-radioactive fluorescence assay for the measurement of both cell number and proliferation," *J. Immunol. Methods*, vol. 142, no. 2, pp. 199–206, Sep. 1991.

[251] A. Salic and T. J. Mitchison, “A chemical method for fast and sensitive detection of DNA synthesis in vivo,” *Proc. Natl. Acad. Sci.*, vol. 105, no. 7, pp. 2415–2420, Feb. 2008.

[252] M. van Engeland, L. J. Nieland, F. C. Ramaekers, B. Schutte, and C. P. Reutelingsperger, “Annexin V-affinity assay: a review on an apoptosis detection system based on phosphatidylserine exposure.,” *Cytometry*, vol. 31, no. 1, pp. 1–9, Jan. 1998.

[253] Y. Gavrieli, Y. Sherman, and S. A. Ben-Sasson, “Identification of Programmed Cell Death In Situ via Specific Labeling of Nuclear DNA Fragmentation,” *J. Cell Biol.*, vol. 119, no. 3, pp. 493–501, 1992.

[254] J. Yuan, S. Shaham, S. Ledoux, H. M. Ellis, and H. R. Horvitz, “The C. elegans cell death gene ced-3 encodes a protein similar to mammalian interleukin-1β-converting enzyme,” *Cell*, vol. 75, no. 4, pp. 641–652, Nov. 1993.

[255] M. O. Hengartner, “The biochemistry of apoptosis,” *Nature*, vol. 407, no. 6805, pp. 770–776, Oct. 2000.

[256] S. Elmore, “Apoptosis: A Review of Programmed Cell Death,” *Toxicol. Pathol.*, vol. 35, pp. 495–516, 2007.

[257] S. Mazumder, D. Plesca, and A. Almasan, “Caspase-3 Activation is a Critical Determinant of Genotoxic Stress-Induced Apoptosis,” in *Apoptosis and Cancer*, Totowa, NJ: Humana Press, 2008, pp. 13–21.

[258] C. B. Kimmel, W. W. Ballard, S. R. Kimmel, B. Ullmann, and T. F. Schilling, “Stages of embryonic development of the zebrafish.,” *Dev. Dyn.*, vol. 203, no. 3, pp. 253–310, 1995.

[259] H. S. Huitfeldt, A. Heyden, O. P. F. Clausen, E. V. Thrane, D. Roop, and S. H. Yuspa, “Altered regulation of growth and expression of differentiation-associated keratins in benign mouse skin tumors,” *Carcinogenesis*, vol. 12, no. 11, pp. 2063–2067, 1991.

[260] T. Tamura, S. Said, W. Lu, and D. Neufeld, “Specificity of Tunel Method Depends on Duration of Fixation,” *Biotech. Histochem.*, vol. 75, no. 4, pp. 197–200, Jan. 2000.

[261] N. Taguchi, N. Ishihara, A. Jofuku, T. Oka, and K. Mihara, “Mitotic phosphorylation of dynamin-related GTPase Drp1 participates in mitochondrial fission.,” *J. Biol. Chem.*, vol. 282, no. 15, pp. 11521–9, Apr. 2007.

[262] M. Liesa, M. Palacín, and A. Zorzano, “Mitochondrial Dynamics in Mammalian Health and Disease,” *Physiol. Rev.*, vol. 89, no. 3, pp. 799–845, Jul. 2009.

[263] D. Senft and Z. A. Ronai, “Regulators of mitochondrial dynamics in cancer,” *Curr. Opin. Cell Biol.*, vol. 39, no. Table 1, pp. 43–52, 2016.

[264] A. Cassidy-Stone *et al.*, “Chemical inhibition of the mitochondrial division dynamin reveals its role in Bax/Bak-dependent mitochondrial outer membrane permeabilization.,” *Dev. Cell*, vol. 14, no. 2, pp. 193–204, Feb. 2008.

[265] G. T. Hanson *et al.*, “Investigating mitochondrial redox potential with redox-sensitive green fluorescent protein indicators.,” *J. Biol. Chem.*, vol. 279, no. 13, pp. 13044–53, Mar. 2004.

[266] P. Niethammer, C. Grabher, A. T. Look, and T. J. Mitchison, “A tissue-scale gradient of hydrogen peroxide mediates rapid wound detection in zebrafish,” *Nature*, vol. 459, no. 7249, pp. 996–999, Jun. 2009.

[267] F. Hirschhaeuser, U. G. A. Sattler, and W. Mueller-Klieser, “Lactate: a metabolic key player in cancer.,” *Cancer Res.*, vol. 71, no. 22, pp. 6921–5, Nov. 2011.

[268] B. M. Heckman-Stoddard, A. DeCensi, V. V. Sahasrabuddhe, and L. G. Ford, “Repurposing metformin for the prevention of cancer and cancer recurrence,” *Diabetologia*, vol. 60, no. 9, pp. 1639–1647, 2017.

[269] B. J. Quinn, H. Kitagawa, R. M. Memmott, J. J. Gills, and P. A. Dennis, “Repositioning metformin for cancer prevention and treatment,” *Trends Endocrinol. Metab.*, vol. 24, no. 9, pp. 469–480, 2013.

[270] W. Pendergrass, N. Wolf, and M. Pool, “Efficacy of MitoTracker Green™ and CMXRosamine to measure changes in mitochondrial membrane potentials in living cells and tissues,” *Cytom. Part A*, vol. 61, no. 2, pp. 162–169, Oct. 2004.

[271] B. Xiao, X. Deng, W. Zhou, and E.-K. Tan, “Flow Cytometry-Based Assessment of Mitophagy Using MitoTracker,” *Front. Cell. Neurosci.*, vol. 10, p. 76, Mar. 2016.

[272] K. D. Stackley, C. C. Beeson, J. J. Rahn, and S. S. L. Chan, “Bioenergetic profiling of zebrafish embryonic development,” *PLoS One*, vol. 6, no. 9, 2011.

[273] Y. Gibert, S. L. McGee, and A. C. Ward, “Metabolic profile analysis of zebrafish embryos.,” *J. Vis. Exp.*, no. 71, p. e4300, Jan. 2013.

[274] S. S. Korshunov, V. P. Skulachev, and A. A. Starkov, “High protonic potential actuates a mechanism of production of reactive oxygen species in mitochondria,” *FEBS Lett.*, vol. 416, no. 1, pp. 15–18, Oct. 1997.

[275] J. E. Bestman, K. D. Stackley, J. J. Rahn, T. J. Williamson, and S. S. L. Chan, “The cellular and molecular progression of mitochondrial dysfunction induced by 2,4-dinitrophenol in developing zebrafish embryos.,” *Differentiation*, vol. 89, no. 3–4, pp. 51–69, Jan. 2015.

[276] B. . Hames and N. . Hooper, *Instant Notes: Biochemistry*, Second Edi. Oxford: Bios Scientific Publishers Ltd., 2000.

[277] D. Fraher, A. Sanigorski, N. A. Mellett, P. J. Meikle, A. J. Sinclair, and Y. Gibert, “Zebrafish Embryonic Lipidomic Analysis Reveals that the Yolk Cell Is Metabolically Active in Processing Lipid,” *Cell Rep.*, vol. 14, no. 6, pp. 1317–1329, Feb. 2016.

[278] K. E. Sant and A. R. Timme-Laragy, “Zebrafish as a Model for Toxicological Perturbation of Yolk and Nutrition in the Early Embryo,” *Curr. Environ. Heal. Reports*, vol. 5, no. 1, pp. 125–133, Feb. 2018.

[279] P. G. Lloyd, C. D. Hardin, and M. Sturek, “Examining glucose transport in single vascular smooth muscle cells with a fluorescent glucose analog.,” *Physiol. Res.*, vol. 48, no. 6, pp. 401–10, 1999.

[280] C. Mosimann, C. K. Kaufman, P. Li, E. K. Pugach, O. J. Tamplin, and L. I. Zon, “Ubiquitous transgene expression and Cre-based recombination driven by the ubiquitin promoter in zebrafish.,” *Development*, vol. 138, no. 1, pp. 169–77, Jan. 2011.

[281] T. Wilson and J. W. Hastings, “Bioluminescence,” *Annu. Rev. Cell Dev. Biol.*, vol. 14, no. 1, pp. 197–230, Nov. 1998.

[282] S. Liu and S. D. Leach, “Zebrafish Models for Cancer,” *Annu. Rev. Pathol. Mech.*

Dis, vol. 6, pp. 71–93, 2011.

[283] M. C. Mione and N. S. Trede, “The zebrafish as a model for cancer.,” *Dis. Model. Mech.*, vol. 3, no. 9–10, pp. 517–23, 2010.

[284] C. M. Freisinger and A. Huttenlocher, “Live imaging and gene expression analysis in zebrafish identifies a link between neutrophils and epithelial to mesenchymal transition.,” *PLoS One*, vol. 9, no. 11, p. e112183, 2014.

[285] C. Michailidou, M. Jones, P. Walker, J. Kamarashev, A. Kelly, and A. F. L. Hurlstone, “Dissecting the roles of Raf- and PI3K-signalling pathways in melanoma formation and progression in a zebrafish model.,” *Dis. Model. Mech.*, vol. 2, no. 7–8, pp. 399–411, 2009.

[286] S. Phane Berghmans *et al.*, “tp53 mutant zebrafish develop malignant peripheral nerve sheath tumors,” *PNAS*, vol. 102, no. 2, pp. 407–412, 2005.

[287] R. Di Micco *et al.*, “Oncogene-induced senescence is a DNA damage response triggered by DNA hyper-replication,” *Nature*, vol. 444, no. 7119, pp. 638–642, Nov. 2006.